

7-21-2009

Heterogeneity effects on flow and transport within a shallow fluvial aquifer

Nicholas Engdahl

Follow this and additional works at: https://digitalrepository.unm.edu/eps_etds

Recommended Citation

Engdahl, Nicholas. "Heterogeneity effects on flow and transport within a shallow fluvial aquifer." (2009).
https://digitalrepository.unm.edu/eps_etds/27

This Thesis is brought to you for free and open access by the Electronic Theses and Dissertations at UNM Digital Repository. It has been accepted for inclusion in Earth and Planetary Sciences ETDs by an authorized administrator of UNM Digital Repository. For more information, please contact disc@unm.edu.

Nicholas B. Engdahl

Candidate

Earth and Planetary Sciences

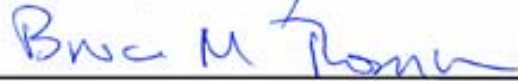
Department

This thesis is approved, and it is acceptable in quality and form for publication:

Approved by the Thesis Committee:

 _____, Chairperson

 _____

 _____

**HETEROGENEITY EFFECTS ON FLOW AND TRANSPORT
WITHIN A SHALLOW FLUVIAL AQUIFER**

BY

NICHOLAS B. ENGDAHL

**B.A., EARTH AND PLANETARY SCIENCE,
UNIVERSITY OF NEW MEXICO, 2006**

THESIS

Submitted in Partial Fulfillment of the
Requirements for the Degree of

**Master of Science
Earth and Planetary Science (Hydrogeology)**

The University of New Mexico
Albuquerque, New Mexico

May, 2009

© 2009, Nicholas B. Engdahl

**HETEROGENEITY EFFECTS ON FLOW AND TRANSPORT
WITHIN A SHALLOW FLUVIAL AQUIFER**

BY

NICHOLAS B. ENGDAHL

ABSTRACT OF THESIS

Submitted in Partial Fulfillment of the
Requirements for the Degree of

**Master of Science
Earth and Planetary Science (Hydrogeology)**

The University of New Mexico
Albuquerque, New Mexico

May, 2009

Heterogeneity effects on flow and transport within a shallow fluvial aquifer

by

Nicholas B. Engdahl

B.A., Earth and Planetary Science, University of New Mexico, 2006

Abstract

The effects of aquifer heterogeneity on flow and transport are considered numerically at two scales using high resolution groundwater models. Heterogeneity effects on river loss were evaluated at the kilometer scale using stochastic, geostatistical models with grid cells on the order of several meters. It was found that river loss decreased directly with an increase in the extent of heterogeneity and that homogeneous approximations resulted in increased loss estimates. Heterogeneity effects on transport were simulated at the scale of several meters using a homogeneous approximation, traditional geostatistical models and a new integrated method of aquifer characterization. The integrated method combines geophysics and geostatistics to create a more realistic approximation of subsurface features. Using grid cells of several centimeters, transport was simulated for multiple heterogeneity realizations in three directions through the models to evaluate potential anisotropy of the transport rates. The resulting breakthrough curves for the homogeneous and traditional geostatistical models showed no directional anisotropy but the integrated models showed anisotropic behavior consistent with the bedding direction as well as non-Fickian transport rates.

Table of contents

Heterogeneity effects on flow and transport within a shallow fluvial aquifer.....	1
An introduction.....	1
References.....	5
Chapter 1	
Heterogeneity Effects on River Loss within a Transition Probability Framework	6
1.0 - Introduction	6
1.1 - Background.....	8
2.0 - Transition Probability Simulation	11
2.1 - Hydrofacies Distribution and Model Development	12
2.2 - Stochastic Groundwater Flow Simulation.....	17
3.0 - Model Results and Discussion.....	21
4.0 - Summary and Conclusions.....	26
Acknowledgements.....	27
References.....	29
Tables.....	33
Figures.....	34
Chapter 2	
An integrated approach to shallow aquifer characterization: combining geophysics and geostatistics.....	43
1.0 - Introduction	43
2.0 - Previous Work	44

2.1 – Aquifer characterization	46
2.2 – Transition Probability Based Indicator Geostatistics.....	47
2.3 – Ground Penetrating Radar	48
3.0 – Integrated Characterization.....	50
3.1 – Depositional Region Growing Routine.....	50
3.2 – 3-D Region Grouping Routine.....	52
3.3 – Geostatistical Filling.....	54
4.0 – Example Application	56
4.1 – Data Collection	57
4.2 – Pre-Processing	58
4.3 – Geostatistical simulation.....	60
5.0 – Results.....	61
6.0 - Conclusions	63
Acknowledgments	64
References.....	65
Tables.....	68
Figures.....	69
Chapter 3	
Anisotropic transport rates in heterogeneous porous media.....	76
1.0 - Introduction	76
2.0 - Model development.....	79
2.1 - Transition Probability Geostatistics	80
2.2 - Integrated Geophysical/Geostatistical modeling.....	81

2.3 – Heterogeneity Modeling	83
2.4 - Numerical Flow and Transport Modeling	84
3.0 - Results and discussion	86
4.0 – Conclusions.....	89
Acknowledgements.....	91
References.....	92
Tables.....	97
Figures.....	98
Heterogeneity effects on flow and transport within a shallow fluvial aquifer.....	106
Final conclusions	106
Appendices.....	109

Heterogeneity effects on flow and transport within a shallow fluvial aquifer

Nicholas B. Engdahl

An introduction

Accurate characterization of subsurface heterogeneities is essential to our understanding of flow and transport [*Dominico and Schwartz, 1998; Sophocleous, 2002; Fleckenstein et al., 2006*]. Far too often, heterogeneity is neglected for no reason beyond the difficulty of describing complex subsurface geometries from sparse data sources. The convenience and ease of use of a homogeneous or overly simplified heterogeneous model appears to have overshadowed the inaccuracies inherent in the model for many mainstream applications. Despite the numerous papers written on understanding and incorporating multi-scale geologic heterogeneities into models, it is still remarkably easy to find a study that relies on a purely random hydraulic conductivity (K) field or a purely homogeneous, unrealistic model domain.

The consensus of the present day groundwater community seems to be that we will never be able to exactly recreate the subsurface stratigraphy within the computer and many appear to have taken this consensus as justification to abandon the pursuit of realistic models. Although we will never recreate the subsurface, we can, and should, always be looking for ways to improve our representations of aquifers. This charge also implies that the most modern and advanced tools and methods available should be explored at every possible juncture. Particularly important are shallow aquifers since they are more easily accessible to a wider variety of tools than deep aquifers, cost less to

collect the primary data, and can provide an analog to deeper aquifers when the systems are believed to be similar.

Within the commonly used finite difference framework, the assumption of a representative elementary volume (REV) is necessary at some scale but the influence of heterogeneities within the REV is neglected. Herein is a collection of three papers which investigate some of the limitations of modeling based on the scale at which heterogeneity is assumed. The three papers, each separate chapter, focus on two scales of heterogeneity: a moderately sized REV, and a high resolution REV where a single cell of the moderate scale model (the first chapter in this collection) comprises the entire model domain on the high resolution model (the second and third chapters in this collection).

The first chapter, *Heterogeneity effects on river loss within a transition probability framework*, investigates the inaccuracies introduced by homogeneous simulations in the context of groundwater/surface water interaction along the Rio Grande in the southern portion of Albuquerque, NM. The scale of the heterogeneous groundwater model used in this paper is roughly the same size as a single grid cell within a previous, regional scale model of the area constructed by *McAda and Barroll* [2002]. The heterogeneity model constructed in this paper was constructed almost entirely from existing data that otherwise may have never been used. This illustrates a common occurrence that data required for the construction of such a heterogeneity model often exist, if one is willing to look for them and apply the data in an appropriate manner. The results of this paper highlight some of the consequences that can arise from oversimplification of a model, including oversimplification of the river bed. The results of the stochastic groundwater models show the dependence of river loss on river stage

and also the dependence on heterogeneity shown by the log transformed variance of the K field. The results were compared to previous models [McAda and Barroll, 2002], and to a field study conducted along the same reach of the Rio Grande [Veenhuis, 2002].

The second chapter, *An integrated approach to aquifer characterization: combining geophysics and geostatistics*, moves from the scale of hundreds of meters to the scale of only a few meters. A method is introduced for investigating the heterogeneities within the scale of a single model cell of the first paper. This scale is nearly impossible to investigate in field studies and has received little treatment beyond the theoretical realm. Since this scale is much smaller than many groundwater models an integrated method for aquifer characterization was developed. The integrated method (InMod) uses complementary methods of geophysical and geostatistical aquifer characterization techniques to build a more realistic model which is capable of preserving some basic but fundamentally important sedimentary features. The REV of the final models produced with this method was approximately 6 cm. The integrated model realizations closely honor the measured geostatistics of the study site, preserve crosscutting relations and consistently have higher variance than models produced by the same measured geostatistics alone. This implies that the models are able to incorporate a greater degree of heterogeneity.

The third chapter, *Anisotropic transport rates in heterogeneous porous media*, investigates the influence of previously unresolved heterogeneities on transport. This paper uses the method introduced in the second paper of this collection to construct a series of groundwater flow models to evaluate the directional effects sedimentary structures may have on contaminant transport. Two other methods for aquifer

characterization were also considered, one using more traditional geostatistical methods, the transition probability [Carle, 1996], and two homogeneous models. Three orientations of the flow path across the direction of bedding were simulated using MODFLOW-2000 [Harbaugh *et al.*, 2000] for flow modeling and RWHET [LaBolle, 2006] for particle tracking and transport simulation. The paper highlights the importance of sedimentary structures, which are frequently ignored in many models, by comparing the transport behavior of the three model types. When modeling transport with a homogeneous approximation, even one that is set to be the arithmetic or geometric mean K value of a heterogeneous model, the simulated transport does not match the classically expected behavior.

This collection also contains supplemental data and literature for the three chapters. Appendix A to this volume contains a general user's manual for the integrated modeling program (InMod) outlined in the second chapter. The programs and routines described in appendix A are highly customizable, and the manual outlines the steps and generalized theoretical development of the integrated modeling routine. The programming language used for the integrated modeling code is FORTRAN 95 and potential users will need to be familiar with the language to modify portions of the code for their particular application. Appendix B contains the categorical logs used for geostatistical modeling of the six boreholes used for the integrated modeling studies. Appendix C contains the site layout and actual GPR lines used in the integrated modeling and transport simulations and appendix D contains a hard copy printout of the FORTRAN 95 code used for the primary routine of the integrated modeling routine, though the electronic source code may be obtained from the author..

The three papers and appendices of this collection are written with the intent of advancing research and stimulating interest into the details of the effects of heterogeneity and the assumption of homogeneity. The work herein represents the combined efforts of many individuals, which are acknowledged in the various chapters, but the author is especially grateful for the assistance and support of Gary Weissmann, Eric Vogler, and Nedra Bonal in the preparation of these manuscripts.

References

- Carle, S.F. (1999), T-PROGS: Transition probability geostatistical software, users manual version 2.1., 84 pp., University of California, Davis, CA.
- Dominico, P.A., and Schwartz, F.W., (1998), *Physical and Chemical Hydrogeology*, 2nd edition, 506 pp., John Wiley and Sons, New York, New York.
- Fleckenstein, J.H., Niswonger, R.G., and Fogg, G.E. (2006), River/aquifer interactions, geologic heterogeneity, and low-flow management, *Ground Water*, 44(4), 837-852.
- Harbaugh, A.W., Banta, E.R., Hill, M.C., and McDonald, M.G. (2000), MODFLOW-2000, the U.S. Geological Survey modular ground-water model – user guide to modularization concepts and the ground-water flow process, *Open-File Report 00-92*, 107 pp., U.S. Geological Survey.
- LaBolle, E.M. (2006), RWHet: random walk particle model for simulating transport in heterogeneous permeable media, user's manual and program documentation, Version 3.2, 27 pp.
- McAda, D.P., and Barroll, P. (2002), Simulation of ground-water flow in the middle Rio Grande basin between Cochiti and San Acacia, New Mexico, *Water-Resources Investigations Report 02-4200*, 81 pp., U.S. Geological Survey.
- Sophocleous, M. (2002), Interactions between groundwater and surface water: the state of the science, *Hydrogeology Journal*, 10, 52-67.
- Veenhuis, J. E. (2002), Summary of flow loss between selected cross sections on the Rio Grande in and near Albuquerque, New Mexico, *Water-Resources Investigations Report 02-4131*, 30 pp., U.S. Geological Survey.

Heterogeneity Effects on River Loss within a Transition Probability Framework

Nicholas B. Engdahl, Eric T. Vogler, and Gary S. Weissmann

1.0 - Introduction

Consideration of aquifer heterogeneity effects on groundwater/surface water interaction can assist in more accurate estimations of surface water flow loss. These effects are especially important in the arid southwest United States where management and accounting of surface water flows are important in order to meet state water demands and interstate-compact agreements. Many modeling studies that include river/aquifer interactions have been focused on questions of regional scale water management and use [Onta *et al.*, 1991; Reichard, 1995; Wang *et al.*, 1995; Konrad, 2006]. For such efforts, the motivation to understand river/aquifer interaction is municipal planning and water balance [Fleckenstein *et al.*, 2006], but many models rely on what may be interpreted as an oversimplification of the heterogeneity within the study area. A general overview of groundwater/surface water interaction methods and studies can be found in Sophocleous [2002] and Woessner [2000]. River/aquifer interactions have been described in many different contexts at several scales. Cardenas and Wilson [2006a, 2006b, 2007] evaluated small-scale features using a high-resolution, finite element model to quantify the interaction of a laminar water column and triangular bedforms using homogeneous bed material. Assumptions of homogeneity can be reasonable and are unavoidable in certain applications; however, streambeds are commonly oversimplified in many models [Cardenas and Zlotnik, 2003]. The interaction between an alluvial aquifer system and

river is influenced by the spatial arrangement of hydrofacies at the interface between the river and the underlying aquifer [Woessner, 2000]. Fleckenstein *et al.* [2004] presented groundwater/surface water interaction in heterogeneous porous media in the context of flow restoration and aquifer recharge. They showed that even small improvements in the accuracy of describing the subsurface heterogeneity reduce model uncertainty associated with river/aquifer interaction, and estimates of the exchange of water between the interconnected systems can be computed [Fleckenstein *et al.*, 2004]. This description of the heterogeneity near the river interface, as in Proce *et al.* [2004], becomes a necessary step in quantifying river/aquifer exchange beyond the small scale.

The accuracy of results for many modeling applications is limited by the difficulty of characterizing subsurface heterogeneity with commonly sparse data sets. Numerous techniques have been developed to recreate geologic heterogeneity, but all generally fall into one of three categories: descriptive, process imitating, or structure imitating [Koltermann and Gorelick, 1996]. Several examples of each category are described in Koltermann and Gorelick [1996]. Transition probability based indicator geostatistics is a structure imitating method that has been shown to honor actual data and recreate plausible subsurface geometric configurations with a reasonable degree of realism [Carle and Fogg, 1996; Weissmann and Fogg, 1999; Weissmann *et al.*, 1999].

In this work we present an application of transition probability geostatistical methods to quantify the effects of heterogeneity on groundwater/surface water interaction. This task is done by describing the subsurface geology from relatively sparse data, by interpolating the data into three dimensions using transition probability geostatistics, by stochastically modeling the groundwater/surface water interactions, and

evaluating the model results and the uncertainty associated with the results. The simulated interaction of groundwater and surface water is expressed as a function of river stage and the degree of heterogeneity within the aquifer in order to quantify the influence of the spatial arrangement of hydrofacies within the exchange zone.

1.1 - Background

The Rio Grande, in central New Mexico, is the primary source of surface water to the region (Figure 1). The river flows across its own deposits, which overlie a regional aquifer system supplying the greater Albuquerque area [*Bartolino and Cole, 2002*]. Parts of the Rio Grande have been identified as gaining reaches [*Winograd, 1959*], but most of the river course in New Mexico has been shown to be losing water to the aquifer [*Moore and Anderholm, 2002*].

The river deposits are mostly unconsolidated alluvial fill ranging in particle size from clay to boulders, but in the Albuquerque reach, flood control (in the form of a major dam 60 km upstream from the study site) and channelization have restricted the maximum mobile particle size to pebbles, although larger clasts may be present at depth [*Hawley and Haase, 1992; Bartolino and Cole, 2002*]. In the 1930s, riverside drains were installed to intercept leakage from the Rio Grande for agricultural management and land use reasons related to lowland flooding. The hydraulic consequences of channelization and drain installation were not investigated in great detail, and regular monitoring of hydraulic heads was not conducted until several decades afterward, when a need to quantify the interactions of the system was first identified [*Rankin, 2007*].

To help provide the data needed to understand the interactions of the Rio Grande, in 2003 the U.S. Geological Survey (USGS) began installing a series of nested piezometers along the Albuquerque reach to provide hydraulic data necessary to describe the groundwater/surface water interaction. This paper focuses on the earliest installed piezometers near the Rio Bravo Bridge.

The piezometer nests were oriented roughly in a straight line normal to the high flow channel in two transects. Piezometers were installed using direct push technology with a Geoprobe®. During piezometer installation at the Rio Bravo Bridge crossing nearly continuous cores were collected at seven piezometer locations (Figure 1). These cores provide information for understanding the subsurface lithology, vertical and lateral lithofacies distribution, and the degree of heterogeneity at the site. Each piezometer nest consists of two to three piezometers completed and screened at different depths. At all nests, a shallow-screened piezometer was completed at a depth of several meters to monitor the fluctuations of the phreatic surface. For nests with three piezometers, one deep piezometer was completed at approximately 18 m, and in most cases, an intermediate-depth piezometer was completed approximately half-way between the shallow and deep screened intervals depending on the ability to complete a piezometer within those intervals. The transects span from both banks to the riverside drains (Figure 1). Piezometers were installed next to the river, near the drains, and within the riparian corridor known as the bosque, which separates the river from the drains.

The piezometers in the first transect, installed 60 m upstream of the Rio Bravo bridge, were supplemented with a surface water gage that was installed along the west bank of the Rio Grande at the stilling well of a discontinued USGS monitoring station

about 5 m east of the near-river piezometer nest. The riverside drains in the first transect were also instrumented with pressure transducers near the two piezometer nests adjacent to the drains. The second transect of piezometers, installed approximately 150 m upstream from the first transect, was installed several months after the first transect. Pressure transducers were installed in both riverside drains in the second transect, similar to the first transect, but no surface water gage was installed in the main channel.

Continuous groundwater elevation data for the Rio Bravo piezometer network and stage data collected in the river and drains are available from January 2004 through the present (2008) at the USGS New Mexico project website (<http://nm.water.usgs.gov/bosque.html>) [Rankin, 2007] and the USGS National Water Information System (<http://waterdata.usgs.gov/nwis/>). Hourly hydraulic-head measurements were made and recorded using dedicated submersible pressure transducers with integrated data loggers.

Rio Grande channel profiles along both transects are very similar. The west bank abruptly drops off into a deep and narrow section of channel that grades upward to a wide shallow channel towards the east. The combination of groundwater and surface water monitoring in the double transect configuration has created a detailed data set to evaluate river/aquifer interactions within an unconsolidated alluvial-aquifer setting in New Mexico. Several other double transects, some not maintained by the USGS, exist along the Rio Grande but the longest, most continuous data record to our knowledge has come from the Rio Bravo site [Rankin, 2007].

Previous studies have investigated groundwater/surface water interaction along the Rio Grande, including Kernodle *et al.* [1995] and Kernodle [1998]. McAda and

Barroll [2002] simulated regional groundwater flow within the Rio Grande Basin and estimated loss from the river to be approximately 1.84 m³/s. *Veenhuis* [2002] used field measurements to estimate loss at selected cross sections on the Rio Grande and calculated a value of 2.46 m³/s through the Albuquerque corridor. These studies provide a basis for comparison with the results of our model.

2.0 - Transition Probability Simulation

To model the distribution of hydrofacies at the site, we used the transition probability geostatistics method [*Carle and Fogg*, 1996]. Details of transition probability theory have been given by *Carle and Fogg* [1996, 1997], *Carle et al.* [1998], *Weissmann et al.* [1999], *Weissmann and Fogg* [1999], and *Ritzi* [2000], but a very brief overview is presented here.

For the case of spatial variability of the subsurface, categories may be defined as exclusive units such as lithofacies, soil types [*Goovaerts*, 1994], or hydrofacies, as used here. Indicators or indicator variables are used to describe the presence or absence of a particular hydrofacies at a particular location. In general, an indicator variable $I_k(x)$ can be defined by

$$I_k(x) = \begin{cases} 1, & \text{if category } k \text{ is present at } x \\ 0, & \text{otherwise} \end{cases}, \quad (1)$$

where the category k represents a particular hydrofacies at location x [*Carle*, 1999].

Indicator hydrofacies may be selected from several sources of spatial information in relation to subsurface heterogeneity such as core logs, soil surveys, geophysical data, and other observed data types. To calculate the transition probability of one hydrofacies being adjacent to itself or another hydrofacies at a specific location x , a developed hydrofacies data set may be sampled at a fixed lag interval (h). Transition probability $t_{jk}(h)$ in one dimension is defined as

$$t_{jk}(h) = \Pr \{k \text{ present at } x+h | j \text{ present at } x \}, \quad (2)$$

where j and k are two indicator hydrofacies [Carle, 1999]. If hydrofacies j is said to be at location x , then $t_{jk}(h)$ is the likelihood of finding hydrofacies k at some variable separation or lag distance h from position x [Carle and Fogg, 1996].

In practice, application of the transition probability method is very similar to the methods outlined in *Deutsch and Journel* [1998] for indicator variogram computation, fitting, and simulation. The transition probability is substituted for the widely known indicator semivariogram and is then used in a sequential indicator simulation to generate plausible schemes, or realizations, of subsurface hydrofacies configurations within the study area [Carle, 1999].

2.1 - Hydrofacies Distribution and Model Development

Core recovery at the study site was approximately 60 % of the total depth cored. Intervals lost during recovery were geologically interpolated based on the character of the surrounding material during the transition probability modeling in order to fill in missing sections. The cumulative length of core represented is approximately 92 m for the purposes of model construction. Four separate hydrofacies were identified from

inspection of recovered core on the basis of lithology (Table 1). Hydrofacies 1 is a mud to silty sand dominated unit referred to herein as the mud hydrofacies. Hydrofacies 2 is a fine sand dominated unit and hydrofacies 3 is a coarse sand dominated unit, collectively making up the sand hydrofacies. Hydrofacies 4 is referred to as coarser than sand (or gravel) and represents the *Wentworth* [1922] scale classification of grains larger than 2 mm. Volumetrically, the coarse sand hydrofacies was the most extensive, followed by fine sand, mud, and coarser than sand, respectively (Figure 2).

Creation of a transition probability model begins by translating the interpreted core into a categorized data file of indicator hydrofacies, similar to the GEOEAS format of *Deutsch and Journal* [1998]. Two methods are commonly used for describing indicator variables: hard weighting and soft weighting. Hard-weighted indicator variables allow a data set to be described based on the presence or absence of the variable at some location, as described by equation (1). The indicator method of soft weighting is an expansion of the GEOEAS format by which any number of indicator variables may be present at one location in space such that the hydrofacies proportions sum to one [*Carle*, 1999], as in

$$\sum i(x)_{ij\dots n} = \{i(x)_i + i(x)_j \dots + i(x)_n\} = 1, \quad (3)$$

where $i(x)_n$ is the relative proportion of each possible hydrofacies, denoted by the subscripts i, j, \dots, n , at location x . This method is useful when describing any location that may not fit precisely into only one of the selected categorical variables.

Interpreted core data were input into the TPROGS software package [Carle, 1999] as a discrete lag model for the vertical direction using the soft weighting option from equation 3, which is supported in the latest version of the TPROGS package. Soft weights were implemented when the discrete sampling interval landed on a contact between hydrofacies or when a discrete sampling location was interpreted to be a combination of two hydrofacies. Where the lithologic selection was clear, the interval was hard conditioned at a probability of one (1) for the corresponding hydrofacies. Transition probabilities between hydrofacies were measured in the vertical direction at all lags, and a Markov chain model was fit to the measured data (Figure 3).

Lateral model parameters were developed using the interpreted core data, volumetric proportions of hydrofacies, and mean hydrofacies lengths that were measured from aerial photographs and a National Biological Survey wetland survey [Roelle and Hagenbuck, 1994] that described the distribution of sediment at the surface similarly to Weissmann *et al.* [1999]. The mean lengths in the lateral directions for all hydrofacies were estimated by measuring the major and semi-major axis lengths of depositional regions thought to correspond to each hydrofacies from the wetland survey. For the sand hydrofacies (hydrofacies 2 and 3), depositional mean lengths are expected to be similar to the geometry of modern sand bars along the river. To supplement the wetland survey data, additional mean lengths were measured from aerial photographs showing the position of sand bars along the Rio Grande over the last three decades (<http://seamless.usgs.gov/>).

Individual depositional events were not easily identifiable for the mud hydrofacies because the deposits were laterally continuous at the land surface within the study area.

The lateral extent of the mud hydrofacies was approximated in the field using terraces within the study site as length constraints to supplement the wetland survey and aerial photograph data sets.

Large surface exposures of gravel or lag deposits were not visible at the site. Some emplaced gravel deposits were observed with a mud matrix surrounding the gravel and were measured as accurately as possible by hand in the field, but gravel deposits with no matrix were observed in the core. Because gravel is deposited during high flow events, it can be assumed that the gravel deposits will be no more laterally continuous than the deposits of the coarse sand hydrofacies [Weissmann *et al.*, 1999]. The estimated mean lengths for the gravel hydrofacies were established using measured distances at the study site and perceived mean lengths measured from aerial photographs of nearby river sections within 1.5 km that did contain exposed gravel. Both sets of measurements were subject to the constraint imposed by the mean length of the coarse sand hydrofacies, and any measurements beyond those limits were discarded.

The supplemental data provided enough information to generate a model of hydrofacies spatial variability similar to Weissmann *et al.* [1999] for the lateral directions, with reasonably good agreement with the calculated probabilities. We assume that hydrofacies have similar juxtaposition relations in positive and negative directions along any lateral orientation [Weissmann *et al.*, 1999]; therefore, lateral transition rates were computed under the assumption that the transition rates in the positive and negative lag directions were equivalent, referred to by Carle [1999] as symmetric probabilities. TPROGS also allows for the selection of a background category that fills in space not occupied by the other hydrofacies, defined here to coincide with hydrofacies 2. This

category does not require specified transition rates and is computed as the difference between the prescribed transition rates and unity. These assumptions allow a reduction in the number of transition rates required to generate a model of spatial variability (Figure 4).

Three-dimensional realizations of the subsurface configuration were created using the SIS module of TPROGS. Thirty realizations were initially created for the purpose of stochastic modeling by varying the random seed of the SIS module. Visual inspection of the realizations revealed certain similarities, such as similar geometric elements and the amount of noise within the image. Ultimately, 6 realizations were found to capture most of the variability of the 30 realizations. These six realizations are thought to be representative of the likely range of variability within the hydraulic conductivity (K) distributions of the model area, and the remaining realizations were discarded prior to stochastic simulation because of time constraints and to improve computational efficiency. A base-case homogeneous model also was constructed using a single K value of 13.72 m/d (45 ft/d) from *McAda and Barroll* [2002] to provide a comparison to previous studies, and a homogeneous model calibrated to the observed heads at the study site was constructed for each simulated river stage. Several models in the past have defined the riverbed conductance to be less than the surrounding aquifer, but here we only consider a purely homogeneous case where the riverbed and aquifer are assigned the same K value.

2.2 - Stochastic Groundwater Flow Simulation

Simulation of groundwater flow and flow loss from the Rio Grande at the study site was done with a numerical, three-dimensional finite difference model, using MODFLOW-2000 [Harbaugh *et al.*, 2000]. The model domain is oriented north-south along the river course of the Rio Grande and spans the piezometer double transect at the Rio Bravo Bridge crossing (Figure 5). The model is discretized as a 100-row, 150-column, and 100-layer model grid using 1,047,300 active out of 1,500,000 total grid cells. Except for model layer 1, the uniform dimension of each grid cell is 5, 12, and 0.3 m in the east-west, north-south, and vertical directions, respectively. These dimensions allowed the highest possible model resolution based on the computational limits of the programs used for simulation. Model layer 1 thickness was increased from 0.3 to 3 m to allow for differences in the phreatic surface elevations and to prevent model cells from becoming flooded or going dry. Groundwater flow and flow loss were simulated from the river at each river stage using a steady-state approximation. The steady-state approximation is justified by the rapid groundwater level equilibrium (less than 1 hour) observed when the study area experiences a hydrologic stress such as an abrupt increase in river stage.

Boundary conditions used in the model were selected to most closely match the physical system, incorporating specific observed conditions in the surface water stage and groundwater head record. Specified head (Dirichlet) boundaries were used to simulate the riverside drains with a corresponding gradient interpolated from riverside drain stage gages. Specified head boundary conditions also are imposed on the northern and southern model boundaries by interpolating observed groundwater elevations from double transect piezometers for selected river stage conditions (table 2). The boundaries

are located approximately 500 m up- and down gradient from the monitoring area to minimize boundary effects on river loss in the double transect area. Nested piezometer data from the site indicate that the deepest water being monitored within the study area experiences nearly horizontal flow with a negligible vertical component. Therefore, no-flow conditions were used for the base of the model corresponding to the bottom of layer 100 at a depth of approximately 30 m below land surface, where only horizontal groundwater flow was observed. The model base depth also coincides with the bottom of the alluvium, which contains the shallow aquifer identified by *Roark* [2001]. Similarly, the phreatic surface is simulated as a no-flow boundary where the Dupuit assumption is invoked. A head dependent flux (Cauchy) boundary condition is used to simulate loss or gain from the river. The head dependent flux boundary is simulated here using the RIVER package of MODFLOW-2000 [*Harbaugh et al.*, 2000], as

$$Q_n = \frac{K_n A_n}{D_n} (H_n - h_n) \quad (4)$$

where Q_n is the simulated river loss (+) or gain (-) per boundary cell n ; K_n is the hydraulic conductivity of riverbed material; D_n is the thickness of the riverbed; A_n is the area of the riverbed for cell n ; h_n is the calculated groundwater hydraulic head; and H_n is the prescribed surface water stage. As a further measure to avoid boundary condition effects, river loss was only monitored in the area between the two transects. This measurement is hereafter referred to as reach loss.

The river is in direct hydraulic contact with the underlying aquifer, as indicated by sediment characteristics and the observed head data. To simulate the direct hydraulic

contact, K of the riverbed was assigned to be the simulated hydrofacies value for the corresponding grid cell from transition probability realizations, and the riverbed thickness was set equal to unity. To arrive at total flow loss from the river between the double transects, individual cell losses from equation (4) are summed over the prescribed observation area using the MODFLOW-2000 observation package [Banta, 2000].

Evapotranspiration (ET) rates and zones were assigned in model layer 1 to correspond to observed types and relative density of vegetation along the river in the study area. Vegetation observed in the model area ranges from cottonwood (*Populus Wislizeni*) forest, saltcedar (*Tamarix*), and various willow (*Salix*) species, to access roads routinely mowed for weed control, and grassy regions along the river edge. The MODFLOW 2000 [Harbaugh *et al.*, 2000] evapotranspiration segment package was used to simulate ET where different ET rates were assigned to the corresponding vegetation type zones, along with zone-specific ET extinction depth, where the extinction depth corresponds to the depth of the phreatic surface where ET ceases to occur. ET rates for the weed-controlled access area, willow or grassy, saltcedar, and cottonwood zones used in the model are 0.0002, 0.0025, 0.0045, and 0.0070 mm/d, respectively [Cleverly *et al.*, 2002; Nagler *et al.*, 2005]. The corresponding extinction depths for these zones are 0.1, 0.3, 2.0, and 5.0 m, respectively [McAda and Barroll, 2002; Cleverly *et al.*, 2002; Nagler *et al.*, 2005].

The resulting finite-difference numerical scheme was solved using the preconditioned conjugate gradient package solver [Hill, 1990]. Point targets for groundwater hydraulic head observation were placed in model layers corresponding to

the piezometer screened intervals. The data used for the calibration targets were the head measurements in the piezometers at the time of the selected river and drain stages.

The range of allowable K values for each hydrofacies was determined from *Domenico and Schwartz* [1990] and *Hornberger et al.* [1998] for the corresponding grain sizes (Table 1). Initial modeling indicated that the extreme portions of the K ranges consistently resulted in nonconvergence of the model, thus, the allowable K values were later restricted to maximize computational efficiency. The K values for each hydrofacies were selected for each set of model runs by a random algorithm with a uniform probability distribution. The algorithm enforced the hierarchical order of hydrofacies (i.e., K value for hydrofacies 1 is less than hydrofacies 2; 2 is less than 3...etc.). Identical K values were used in each of the six TPROGS realizations to compare the results of different subsurface configurations, which were independently modeled by MODFLOW-2000. The model package consisted of a series of programs written to automatically vary model parameters, log model results, and control MODFLOW-2000. The model package was run on several different processors simultaneously and occasionally generated duplicate sets of K values because of rounding. Statistical analysis indicated that the duplicates were near normally distributed and had no substantial effect on the mean of the distribution. To avoid any unforeseen effects, the duplicates were discarded as nonunique values for final analysis.

A series of five different river/drain stage configurations were selected for analysis, representing high, moderate, and low flows of the Rio Grande (Table 2). Initial analysis of the surface water data indicated no temporal correlation between the stage of the river and the stage of the engineered riverside drain structures. The engineered nature

of the riverside drain flows limited our analysis only to conditions observed during the period of record, and no other conditions were used for flow loss modeling purposes.

The number of simulations was set by trial and error to be high enough that the statistical distribution of results reached a stationary mean but was kept low enough to minimize model run time. With these considerations, the model package was run at least 1000 times for each of the 5 river stages using the 6 hydrofacies realizations. After completely running one stage, the model package was recompiled, boundary conditions were modified to reflect a different observed flow regime, and the model was restarted under the revised stage conditions. All input parameters and output data associated with each model run (K values, river loss, etc...) were automatically logged by the model package, and as such, no external calibration or parameter estimation code was required (see *Hill et al.* [2000]).

3.0 - Model Results and Discussion

All stochastic modeling results for the Rio Grande and riverside drain stages were compared to observed groundwater levels from the piezometer network to address the plausibility of each associated K realization and corresponding K value occurring at the site. The root mean squared errors (RMS) of simulated to observed groundwater elevations for all simulated reach losses corresponding to each combination of river and riverside drain stages are shown in Figure 6. Overall, RMS increases with decreasing loss, suggesting a lower boundary to reach loss. The lowest RMS values occur for observed and simulated river stages of 1501.23 (Figure 6b) and 1501.39 m. These simulations correspond to the smaller hydraulic gradient between the river and the east

riverside drain of 0.005 m/m (Table 2). However, the variability of error shown in Figure 6 increases with both river stage and simulated loss.

The arithmetic mean hydraulic conductivity (\bar{K}) and arithmetic mean log transformed hydraulic conductivity (\bar{Y} , $Y=\ln(K)$) of each K field for each TPROGS realization were determined volumetrically for each hydrofacies. Simulated reach losses compared to \bar{Y} for each stage are shown in Figure 7. Simulated reach loss increases with increasing \bar{Y} as expected from equation (4). Similar to the error results in Figure 6, with increasing river stage, more variability is observed in the distribution of reach loss as a function of \bar{Y} .

The degree of heterogeneity of each subsurface realization was quantified by calculating the variance of the K (σ^2_K) and Y (σ^2_Y) fields. Most σ^2_Y values are less than 2, placing this system into the category of weakly to moderately heterogeneous [Sarris and Paleologos, 2004]. There was a weak relation between σ^2_K and \bar{K} at all river stages, with considerable scatter but a positive trend. This relation is due to restrictions placed on ranges of K used because the variance of the distribution is very sensitive to erratic, high values [Isaaks and Srivastava, 1989], and high variance can only be achieved at higher \bar{K} values. To determine the effect of the degree of heterogeneity on reach loss, simulations were performed where \bar{K} was held constant at 9.7 m/d with a single stage value of 1501.23 m (Figure 8). Resulting simulations indicated a negative relation between river loss and σ^2_Y , because greater σ^2_Y corresponds to greater volumetric proportions of lower K hydrofacies. This relation suggests that for a given \bar{K} , the greater the degree of heterogeneity within a fluvial sedimentary environment, such as the one investigated in this study, the less the resulting loss from surface water will be for a

given surface water stage. Scatter in the data may be explained by the variations in the spatial arrangement of the hydrofacies from different subsurface realizations.

Stochastic modeling results indicate that the mean reach loss values increase with increasing stage (Figure 9). During periods of high flow associated with reservoir releases, snowmelt runoff, and monsoon season streamflow, reach loss can range from approximately 350 to 650 m³/d within the reach studied (Figure 9d). The uncertainty in reach loss also increases with increasing stage and is expressed as an increase in the distribution of the results. Note that the 1 σ range of plausible reach loss values shown in Figure 9d for a stage of 1502.21 m does not overlap the simulated 1 σ range of reach loss values for stages of 1501.04 and 1501.23 m (Figures 9a and 9b).

An effective K was determined for each simulated stage, using a homogeneous model. During this process, the K values were allowed to vary beyond limitations placed on the stochastic K field realizations on the basis of observed and computed hydrofacies distribution. The homogeneous, effective hydraulic conductivity was defined as the K value that produced the smallest cumulative deviation from the measured head values, as expressed by the RMS error (Table 2). The stochastic effective K values were defined as the mean K value of the stochastic model for each stage that produced the smallest RMS error. Homogeneous effective K values at all stages were considerably higher than the mean of the stochastically determined effective K values by onehalf to one order of magnitude (Table 2).

Overall the mean reach loss indicated the expected positive relation to stage with a nearly linear relation shown in Figure 10a. The error associated with this relation is shown by one standard deviation (1 σ) error bars from the stochastic simulations of reach

loss. The homogeneous, effective K simulations were not strongly related to river stage (Figure 10b). The river stages and simulated reach loss span most of the normal flow conditions of the Rio Grande, based on USGS streamflow records (<http://waterdata.usgs.gov/nwis/>). Large flood events could produce reach loss values outside of the 1σ range, but such events are unlikely because of the regulated operation of the Rio Grande [Richard *et al.*, 2005].

The stochastic flow loss simulations indicated consistent trends in reach loss when compared to the hydraulic gradient, whereas homogeneous flow loss results were not as strongly related to the hydraulic gradient. The differences between the stochastic and homogeneous effective K indicate that the use of a homogeneous K for applications at the regional scale may result in an overestimation of reach loss from what may appear to be a good set of effective parameters. The inclusion of a smaller K value for riverbed conductance may be a simple way to greatly improve homogeneous loss estimates.

Analysis of the stochastically determined effective K values indicated that the minimum RMS error results were consistently generated when the K values for hydrofacies 3 and 4 were similar (Figure 11a). This statement is valid at all stages for the stochastic model results. In contrast, the homogeneous effective K behaved erratically and was largely dependent on river stage (Figure 11a), similar to the behavior for the homogeneous effective K when comparing loss and stage (Figure 10). The consistent results of the heterogeneous representation of the deposits indicates that, despite the weak degree of heterogeneity, not accounting for some degree of heterogeneity could result in an overestimation of loss for this system. Furthermore, when compared solely on the basis of RMS error, the effective stochastic and homogeneous parameters are nearly

identical, but a substantially higher K is required to provide the same fits as the stochastic results (Figure 11b). Regional scale models have traditionally used a single K value of 13.72 m/d. A set of homogeneous simulations run using such values indicated moderate agreement with measured values in terms of the RMS error (Figure 11b) but the loss values of those results were also erratic, similar to Figure 10b.

Understanding the cause of the differences between the measured and observed heads is inhibited by a lack of data about the distribution of the flux out of and into the river, or even out of the riverside drains because no piezometer nests were located beyond the model space outside of the riverside drains. Detailed instrumentation of the riverside drains with nested piezometers could indicate if they are in fact the primary structure controlling the local hydraulic gradient, and similar instrumentation within and near the river channel could help clarify the exchange of water between the river and aquifer.

Most parameters evaluated for this study indicated normal or nearly normal statistical distributions as seen in Figure 9 and as such may be approximated by their mean. Within the study area, a \bar{K} value of 3.9 m/d provides results with the lowest overall, simulated RMS error. This value was estimated by the lowest cumulative RMS error of all the river stages using a single homogeneous \bar{K} for all the simulated stages. When compared against the range of \bar{K} , the suggested value represents a minimum error sill in the results that is consistent for all stages, though RMS error increased directly with stage. This value is suggested for use in modeling applications seeking a homogeneous approximation of small scale regions directly along the Rio Grande within close proximity of the study area. However, caution should be exercised for use in a

regional scale model because this value of \bar{K} may not sufficiently capture any spatial (compositional or grain size) variability that may exist in the fluvial deposits over a large areal extent.

For comparison to previous studies, the loss simulated of the stochastic models was normalized to the monitoring area. The studies of *Veenhuis* [2002] and *McAda and Barroll* [2002] were also normalized to the river area used to estimate loss. The loss per unit area calculated by the stochastic model was only 40% of that estimated by *McAda and Barroll* [2002] and 35% of the median estimates of *Veenhuis* [2002]. The disagreement is likely due to different scales of the studies because it is unlikely that a relatively small-scale stochastic model of one specific area is representative of all heterogeneities of the Rio Grande through the Albuquerque basin. However, the loss estimated by *McAda and Barroll* [2002] and the loss estimated by this stochastic approach both fall within the 1σ uncertainty in the field based estimates of *Veenhuis* [2002], indicating that the results of both numerical studies are physically plausible. Though the results are physically plausible, this stochastic groundwater modeling paper only presents a reasonable representation of the system being modeled. Within this stochastic model, as with all groundwater models, uncertainty does exist and this representation may not match the actual, physical configuration of hydrofacies or the hydrologic processes within the study site.

4.0 - Summary and Conclusions

A transition probability framework was used to test the effects of aquifer heterogeneity on reach loss. Stochastic modeling indicated that the primary control on

reach loss is the \bar{K} value of the realization. A relation between \bar{K} and σ_K^2 indicates that the degree of heterogeneity also influences loss. However, because the volumetric distribution of hydrofacies between realizations is virtually constant, heterogeneity does not cause as great of an influence as the \bar{K} value. A strong relation between river stage and reach loss was observed for all realizations. This relation is a direct result of the incorporation of Darcy's law in equation (4) and is expressed as an operating curve for estimating reach loss in the study area as a function of stage within a 1σ range. In this constant transition probability framework for weakly to moderately heterogeneous porous media, the volumetric proportions of the individual hydrofacies within the channel appear to have a greater influence on reach loss than the spatial arrangement of the same hydrofacies.

An evaluation of effective K values indicated that using a homogeneous approximation can result in residuals comparable to a stochastic evaluation, but the conditions to achieve such results can require substantially higher K values, resulting in a larger estimation of reach loss. Inclusion of some minimal heterogeneity in the form of reduced riverbed conductance may reduce possible overestimation of flow loss. The most compelling evidence for the higher accuracy of the stochastic results comes from consistent performance at all stages, whereas the homogeneous approximation is highly sensitive to fluctuations in stage.

Acknowledgements

This work was supported by the U.S. Army Corps of Engineers. The authors would also like to acknowledge Dale Rankin of the U.S. Geological Survey for his

assistance in the compilation of the field data and access to the collection of core samples. The authors would also like to thank Barbara Bekins and Doug McAda of the U.S. Geological Survey for helpful reviews of this manuscript.

References

- Bartolino, J.R., and Cole, J.C. (2002), Ground-water resources of the Middle Rio Grande Basin, New Mexico, *Circular 1222*, 77 pp., U.S. Geological Survey.
- Banta, E.R. (2000), MODFLOW-2000, the U.S. Geological Survey Modular Ground-Water Model; documentation of packages for simulating evapotranspiration with a segmented function (ETS1) and drains with return flow (DRT1), *Open File Report 2000-466*, 209 pp., U.S. Geological Survey.
- Cardenas, M.B., and Wilson, J.L. (2006a), The influence of ambient groundwater discharge on exchange zones induced by current-bedform interactions, *Journal of Hydrology*, 331(1-2), 103-109.
- Cardenas, M.B., and Wilson, J.L. (2006b), Hydrodynamics of coupled flow above and below a sediment-water interface with triangular bedforms, *Advances in Water Resources*, 30(3), 301-313.
- Cardenas, M.B., and Wilson, J.L. (2007), Exchange across a sediment-water interface with ambient groundwater discharge, *Journal of Hydrology*, 346, 69-80.
- Cardenas, M.B., and Zlotnik, V.A. (2003), Three-dimensional model of modern channel bend deposits, *Water Resources Research*, 39(6), 1141, doi:10.1029/2002WR001383.
- Carle, S.F., and Fogg, G.E. (1996), Transition probability-based indicator geostatistics, *Mathematical Geology*, 28(4), 453-476.
- Carle, S.F., and Fogg, G.E. (1997), Modeling spatial variability with one and multidimensional continuous-lag markov chains, *Mathematical Geology*, 29(7), 891-918.
- Carle, S.F., LaBolle, E.M., Weissmann, G.S., Van Brocklin, D., and Fogg, G.E. (1998), Conditional simulation of hydrofacies architecture: a transition probability/markov approach. in *Hydrogeologic models of sedimentary aquifers, concepts in hydrogeology and environmental geology no. 1*, edited by G.S. Fraser, and J.M., Davis, (SEPM) Society for Sedimentary Geology Special Publication, pp. 147-170.
- Carle, S.F. (1999), T-PROGS: Transition probability geostatistical software, users manual version 2.1., 84 pp., University of California, Davis, CA.
- Cleverly, J.R., Dahm, C.N., Thibault, J.R., Gilroy, D.J., and Coonrod, J.E. (2002), Seasonal estimates of actual evapo-transpiration from tamarix ramosissima stands

- using three-dimensional eddy covariance, *Journal of Arid Environments*, 52, 181-197.
- Deutsch, C.V., and Journel, A.G. (1998), *GSLIB – Geostatistical Software Library Users Guide*, 384 pp., Oxford University Press, New York, NY.
- Domenico, P.J., and Schwartz, F.W. (1990) *Physical and Chemical Hydrogeology*, 582 pp., John Wiley and Sons.
- Fleckenstein, J.H., Niswonger, R.G., and Fogg, G.E. (2006), River/aquifer interactions, geologic heterogeneity, and low-flow management, *Ground Water*, 44(4), 837-852
- Fleckenstein, J., Anderson, M., Fogg, G., and Mount, J. (2004), Managing surface water-groundwater to restore fall flows in the Cosumnes river, *Journal of Water Resources Planning and Management*, 130(4), 301-310.
- Goovaerts, P., (1994), Comparison of CoIK, IK, mIK performances for modeling conditional probabilities of categorical variables, in *Geostatistics for the Next Century*, edited by R. Dimitrakopoulos, pp. 18-29, Kluwer Academic Publ., Dordrecht.
- Hawley, J.W., and Haase, C.S. (compilers) (1992), Hydrogeologic framework of the northern Albuquerque Basin, *Open-File Report 387*, New Mexico Bureau of Mines and Mineral Resources.
- Harbaugh, A.W., Banta, E.R., Hill, M.C., and McDonald, M.G. (2000), MODFLOW-2000, the U.S. Geological Survey modular ground-water model – user guide to modularization concepts and the ground-water flow process, *Open-File Report 00-92*, 107 pp., U.S. Geological Survey.
- Hill, M.C. (1990), PRECONDITIONED CONJUGATE-GRADIENT 2 (PCG2), a computer program for solving ground-water flow equations, *Water Resources Investigations Report 90-4048*, 43 pp., U.S. Geological Survey.
- Hill, M.C., Banta, E.R., Harbaugh, A.W., and Anderman, E.R. (2000), MODFLOW-2000, the U.S. Geological Survey modular ground-water model; user guide to the observation, sensitivity, and parameter-estimation processes and three post-processing programs, *Open-File Report 00-184*, 209 pp., U.S. Geological Survey
- Hornberger, G.M., Raffensperger, J.P., Wiberg, P.L., and Eshleman, K.N. (1998), *Elements of Physical Hydrology*, 312 pp., The Johns Hopkins University Press.
- Isaaks, E.H., and Srivastava, R.M. (1989), *An Introduction to Applied Geostatistics*, 592 pp., Oxford University Press, New York, NY.

- Kernodle, J.M., McAda, D.P., and Thorn, C.R. (1995), Simulation of ground-water flow in the Albuquerque Basin, central New Mexico, with projections to 2020, *Water-Resources Investigations Report 94-4251*, 114 pp., U.S. Geological Survey.
- Kernodle, J.M. (1998), Simulation of ground-water flow in the Albuquerque Basin, central New Mexico, 1901-95, with projections to 2020, *Open File Report 96-209*, 55 pp., U.S. Geological Survey.
- Koltermann, C.E., and Gorelick, S.M. (1996), Heterogeneity in sedimentary deposits: a review of structure-imitating, process-imitating, and descriptive approaches, *Water Resources Research*, 32(9), 2617–2658.
- Konrad, C.P. (2006), Longitudinal hydraulic analysis of river/aquifer exchanges, *Water Resources Research*, 42, W08425.
- McAda, D.P., and Barroll, P. (2002), Simulation of ground-water flow in the middle Rio Grande basin between Cochiti and San Acacia, New Mexico, *Water-Resources Investigations Report 02-4200*, 81 pp., U.S. Geological Survey.
- Moore, S.J., and Anderholm, S.K. (2002), Spatial and temporal variations in streamflow, dissolved solids, nutrients, and suspended sediment in the Rio Grande Valley study unit, Colorado, New Mexico and Texas, 1993-95, *Water-Resources Investigations Report 02-4224*, 52 pp., U.S. Geological Survey.
- Nagler, P.L., Cleverly, J.R., Glenn, E., Lampkin, D., Huete, A., and Wan, Z. (2005), Predicting riparian evapotranspiration from MODIS vegetation indices and meteorological data, *Remote Sensing of Environment*, 94, 17-30.
- Onta, P.R., Dasgupta, A., and Harboe, R. (1991), Multistep planning model for conjunctive use of surface-water and ground-water resources, *Journal of Water Resources Planning and Management*, 117(4), 662–678.
- Proce, C.J., Ritzi, R.W., Dominic, D.F., and Dai, Z. (2004), Modeling multiscale heterogeneity and aquifer interconnectivity, *Ground Water*, 42(3), 658-670.
- Rankin, D.R. (2007), Data Collection at Selected Cross Sections on the Rio Grande, accessed on August 20, 2007 at URL: <http://nm.water.usgs.gov/bosque.html>
- Reichard, E.G. (1995), Groundwater-surface water management with stochastic surface water supplies—a simulation optimization approach, *Water Resources Research*, 31(11), 2845–2865.
- Richard, G.A., Julien, P.U., and Baird, D.C. (2005), Statistical analysis of lateral migration of the Rio Grande, New Mexico, *Geomorphology*, 71, 139-155.

- Ritzi, R.W. (2000) Behavior of indicator variograms and transition probabilities in relation to the variance in lengths of hydrofacies, *Water Resources Research*, 36(11), 3375-3381.
- Roark, D.M. (2001), Estimation of hydraulic characteristics in the Santa Fe Group aquifer system using computer simulations of river and drain pulses in the Rio Bravo study area, near Albuquerque, New Mexico, *Water-Resources Investigations Report 01-4069*, 52 pp., U.S. Geological Survey.
- Roelle, J.E. and Hagenbuck, W.W. (1994), *Surface Cover Maps of the Rio Grande Floodplain from Velarde to Elephant Butte Reservoir, New Mexico*, 57 pp., U.S. Geological Survey, Ft. Collins, CO..
- Sarris, T.S. and Paleologos, E.K. (2004), Numerical investigation of the anisotropic hydraulic conductivity behavior in heterogeneous porous media, *Stochastic Environmental Research and Risk Assessment*, 18, 188-197.
- Sophocleous, M. (2002), Interactions between groundwater and surface water: the state of the science, *Hydrogeology Journal*, 10, 52-67.
- Veenhuis, J. E. (2002), Summary of flow loss between selected cross sections on the Rio Grande in and near Albuquerque, New Mexico, *Water-Resources Investigations Report 02-4131*, 30 pp., U.S. Geological Survey.
- Wang, C.C., Mortazavi, B., Liang, W.K., Sun, N.Z., and Yeh, W.W.G. (1995), Model development for conjunctive use study of the San Jacinto Basin, California, *Water Resources Bulletin*, 31(2), 227-241.
- Wentworth, C. K. (1922), A scale of grade and class terms for clastic sediments, *Journal of Geology*, 30, 377-392.
- Weissmann, G.S., Carle, S.F., and Fogg, G.E. (1999), Three-dimensional hydrofacies modeling based on soil surveys and transition probability geostatistics, *Water Resources Research*, 35(6), 1761-1770.
- Weissmann, G.S., and Fogg, G.E. (1999), Multi-scale alluvial fan heterogeneity modeled with transition probability geostatistics in a sequence stratigraphic framework, *Journal of Hydrology*, 226(1-2), 48-65.
- Winograd, I.J. (1959), Ground water conditions and geology of Sunshine Valley and western Taos County, New Mexico, *Technical Report 12*, 70 pp., New Mexico State Engineer.
- Woessner, W.W. (2000), Stream and fluvial plain ground water interactions: rescaling hydrogeologic thought, *Ground Water*, 38(3), 423-429, doi:10.1111/j.1745-6584.2000.tb00228.x.

Tables

Table 1. Hydrofacies descriptions based on recovered core samples with the corresponding, published K value ranges

Hydrofacies	Unit	Mean Wentworth Size ¹ (mm)	Published K range ^{2,3} (m/d)	Volumetric Fraction (%)
1	Mud	0.0039 – 0.0625	$5.0 \times 10^{-4} - 1.0 \times 10^0$	12.2
2	Fine sand	0.0625 – 0.3	$1.0 \times 10^{-3} - 1.5 \times 10^1$	33.8
3	Coarse sand	0.3 – 2.0	$1.0 \times 10^{-2} - 5.0 \times 10^1$	45.9
4	Coarser than sand	> 2.0	$5.0 \times 10^{-1} - 1.0 \times 10^3$	8.1

¹ - Wentworth (1922)

² - Domenico and Schwartz (1990)

³ - Hornberger et al. (1998)

Table 2. River and drain stages for each simulation set with effective hydraulic conductivity and associated RMS error for stochastic and homogeneous results. Letters a,b,c, and d correspond to Figures 6, 7, and 9, K_{eff} denotes effective hydraulic conductivity, and loss refers to total reach loss.

Simulation	River Stage (m)	Drain Stage (m)		Hydraulic Gradient (m/m)		Homogeneous			Stochastic		
		East	West	East	West	K_{eff} (m/d)	RMS (m)	Loss (m ³ /d)	K_{eff} (m/day)	RMS (m)	Loss (m ³ /d)
1 (a)	1501.04	1499.40	1500.11	0.007	0.011	29.30	0.33	2518.00	3.60	0.33	243.19
2 (b)	1501.23	1499.95	1500.88	0.005	0.004	17.70	0.12	1101.00	4.48	0.13	267.21
3	1501.39	1500.10	1500.40	0.005	0.012	29.30	0.14	3230.00	4.64	0.14	329.12
4 (c)	1501.74	1499.02	1499.92	0.011	0.021	15.80	0.21	1485.00	3.82	0.21	360.71
5 (d)	1502.21	1499.51	1500.10	0.011	0.025	32.30	0.32	6950.00	3.46	0.30	500.67

Figures

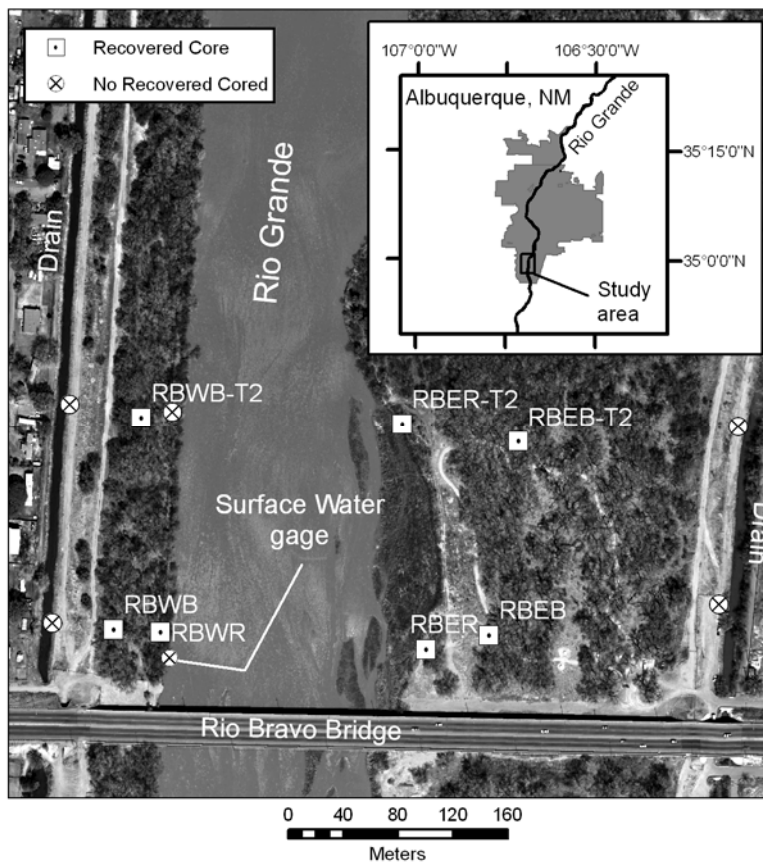


Figure 1. Site location near the south end of Albuquerque, NM. Piezometer nests with recovered core are indicated by squares and the nests not cored are shown as circles.

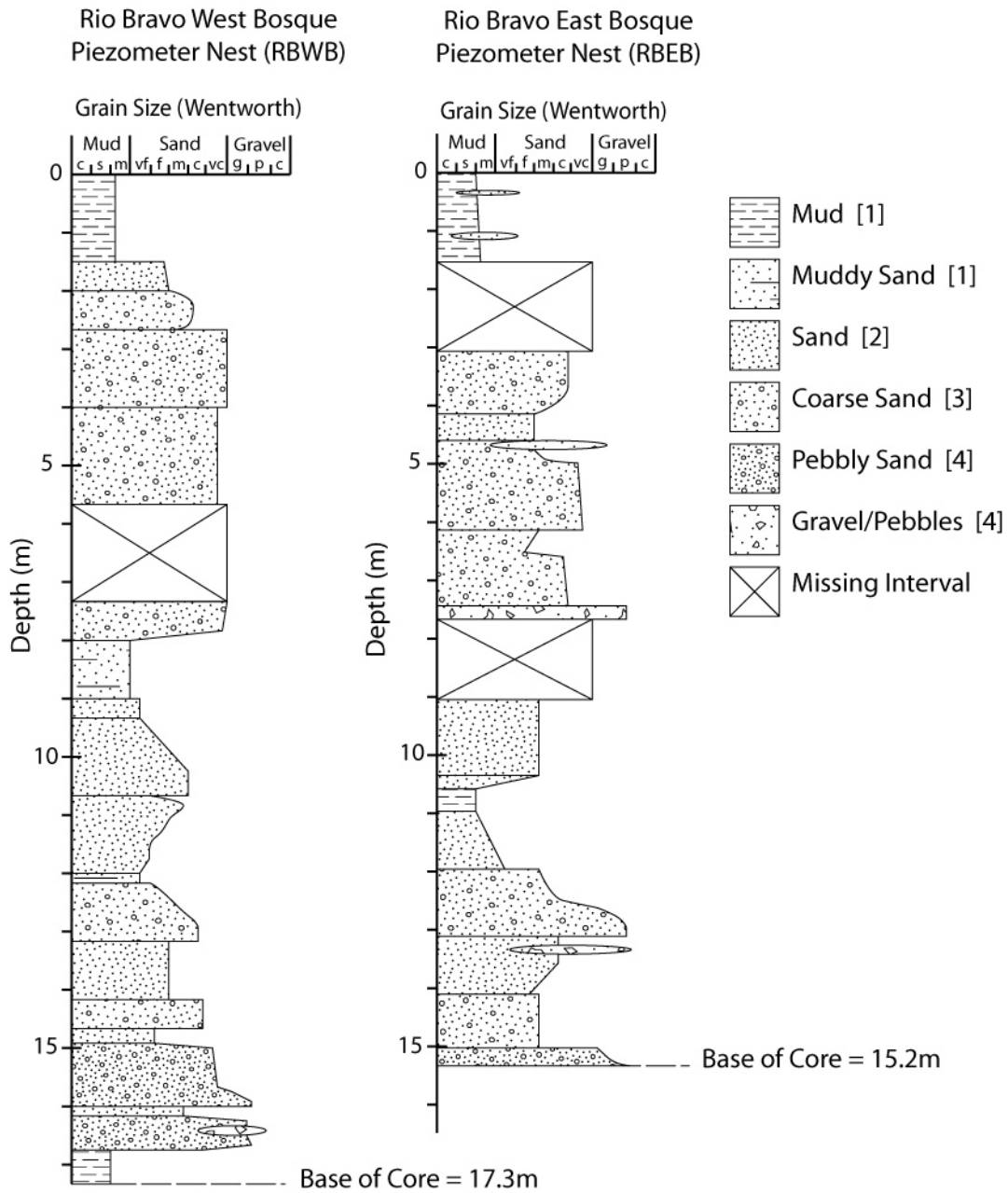


Figure 2. Stratigraphic column of subsurface lithology at the Rio Bravo West Bosque (RBWB) and Rio Bravo East Bosque (RBEb) piezometer nests. Shading indicates overall grain size description used for hydrofacies classification (Table 1) and position along the horizontal is mean grain size at the corresponding depth below land surface.

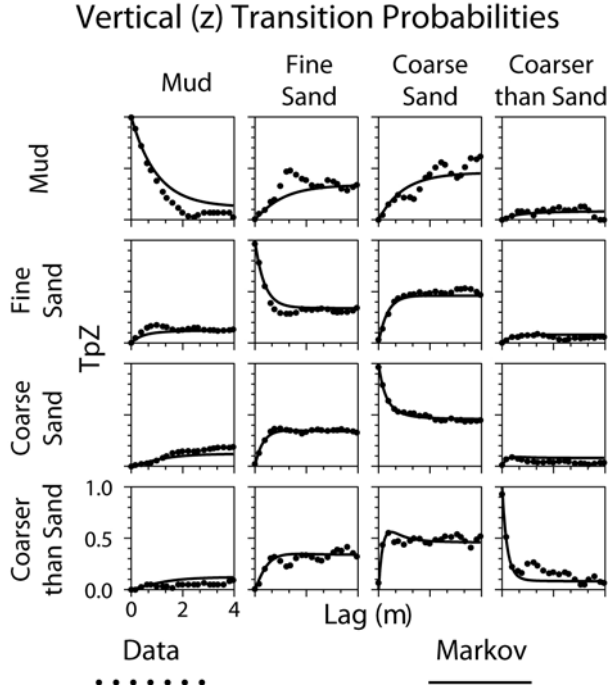


Figure 3. Vertical transition probability matrix for the Rio Bravo site. Markov fits indicate the modeled, continuous lag transition probabilities used for simulation.

$$Tp_x = \begin{bmatrix} l=26.5m & b & 0.31 & 0.16 \\ b & l=40m & b & b \\ s & b & l=35m & 0.34 \\ s & b & s & l=10m \end{bmatrix} \quad Tp_y = \begin{bmatrix} l=75m & b & 0.3 & 0.08 \\ b & l=160m & b & b \\ s & b & l=160m & 0.34 \\ s & b & s & l=30m \end{bmatrix}$$

Figure 4. Lateral transition rate matrices (Tp) for the x and y model directions at the Rio Bravo site. Mean hydrofacies lengths (l) are given as the diagonal entries, b indicates a background category, and s indicates a symmetric probability.

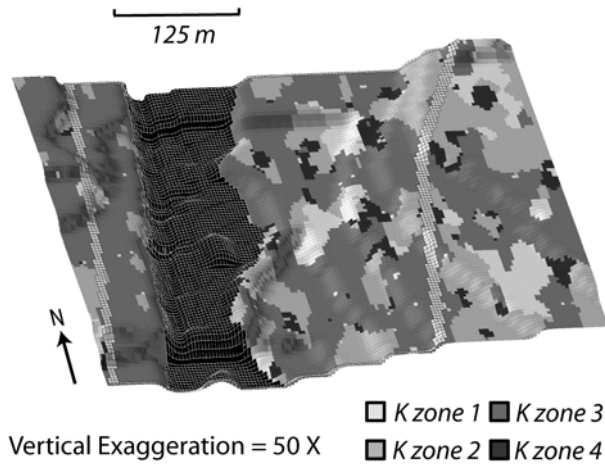


Figure 5. 3-D perspective view of model layer one top elevations showing hydrofacies categories from one of the six TPROGS realizations. White gridded areas represent constant head boundaries and black gridded areas represent river zones. The sharp dropoff of the channel bottom can be seen along the west bank.

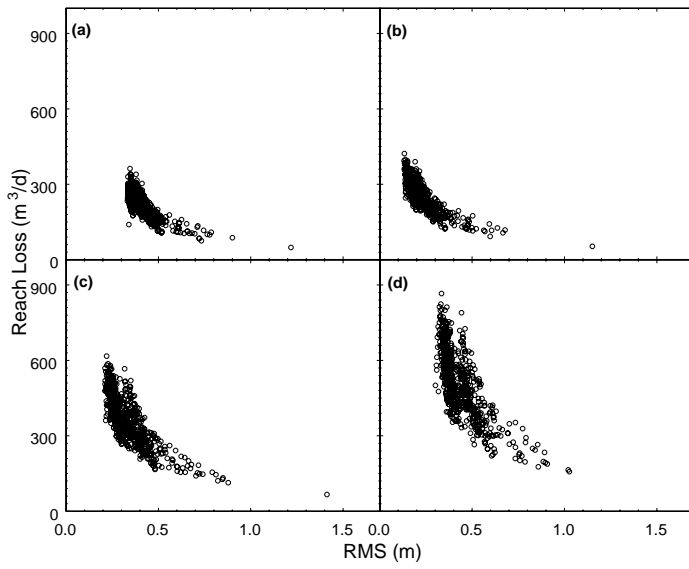


Figure 6. Simulated reach loss compared to RMS for river stage (a) 1501.04, (b) 1501.23, (c) 1501.74, and (d) 1502.21m.

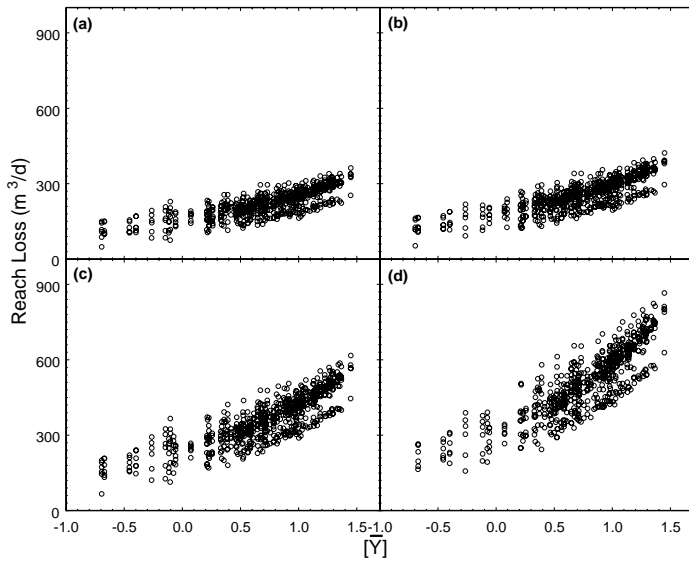


Figure 7. Simulated reach loss as a function of \bar{Y} ($Y=\ln(K)$) for river stage (a) 1501.04, (b) 1501.23, (c) 1501.74, and (d) 1502.21m.

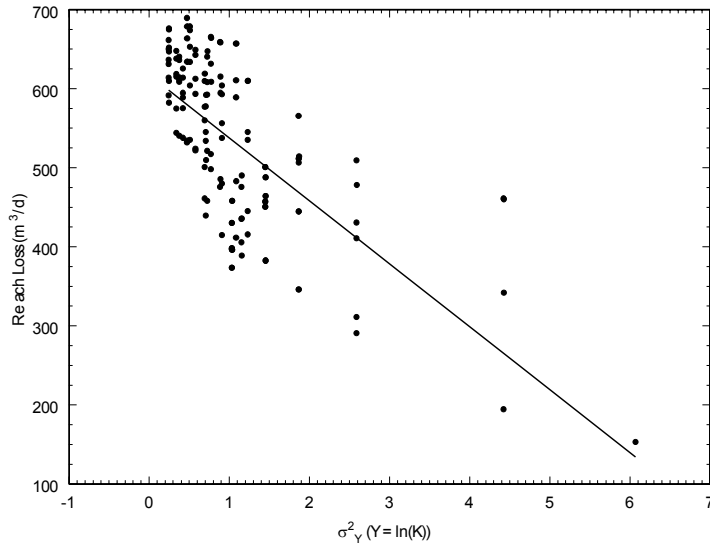


Figure 8. The effect of variance on reach loss. Here $\bar{K} = 9.7$ m/d and river stage was set to 1501.23 m.

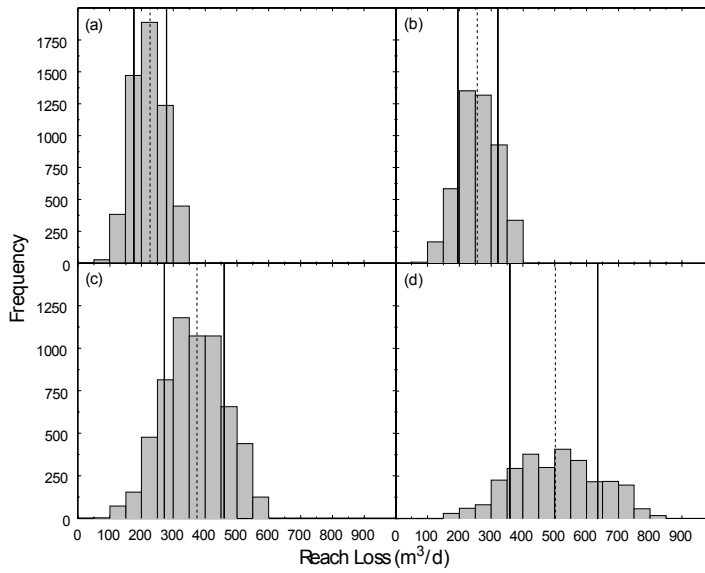


Figure 9. Histogram of reach loss for all stochastic model results for river stage **(a)** 1501.04, **(b)** 1501.23, **(c)** 1501.74, and **(d)** 1502.21 m and the effect of stage on mean reach loss (dotted line) and one standard deviation range of uncertainty (solid lines).

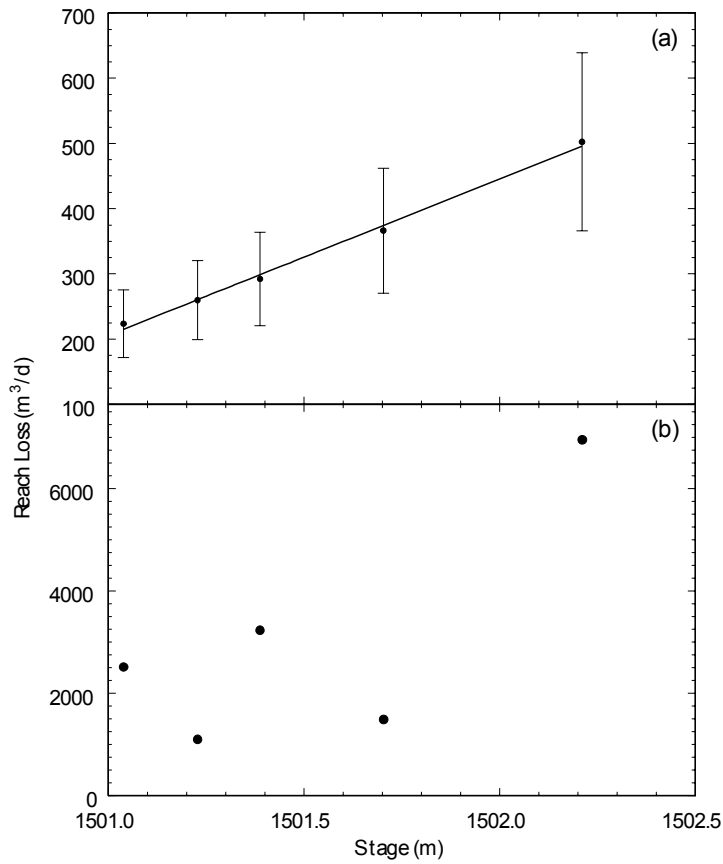


Figure 10. Reach loss as a function of stage for **(a)** stochastic K realizations, and **(b)** homogeneous effective K distributions. Error bars denote one standard deviation.

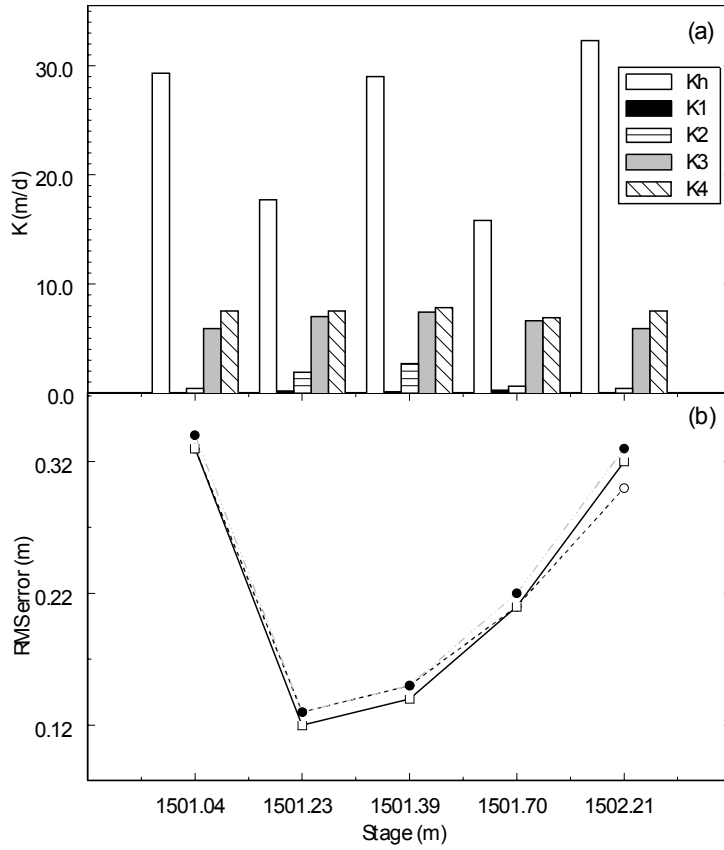


Figure 11. (a) Bar plot of homogeneous effective K_h and mean of stochastically determined effective K distributions for each individual hydrofacies (1-4) and (b) RMS error values at each stage for the homogeneous, 13.72 m/d simulation (solid circles), homogeneous effective parameters (squares) and stochastic effective parameters (open circles).

An integrated approach to shallow aquifer characterization: combining geophysics and geostatistics

Nicholas B. Engdahl, Gary S. Weissmann, and Nedra D. Bonal

1.0 - Introduction

Despite the many methods now available for subsurface characterization, few are able to realistically simulate depositional features, such as cross beds and erosional surfaces [Koltermann and Gorelick, 1996]. Such features are commonly referred to as unresolved heterogeneities that are typically accounted for in modeling through the use of dispersion parameters. They have also been suggested as possible contributors to anomalous transport behavior and preferential flow path formation [Cardenas and Zlotnik, 2003; Levy and Berkowitz, 2003; Zheng and Gorelick, 2003; Cortis et al., 2004; Close et al., 2004], however the precise influence of these heterogeneities is largely unknown. Many of the software packages currently available for heterogeneity modeling (e.g. GSLIB, FLUVSIM, and TPROGS) do not account for process-based geologic tendencies and rely on oversimplifications of subsurface geometry [Bridge and Hyndman, 2004]. For many moderate to large scale applications (tens to thousands of meters), these simplifications are understandable to some extent, they allow for the construction of a groundwater model that can provide a reasonable estimate of a system's behavior but fail to yield much insight towards smaller scale processes.

A major limitation to most flow and transport modeling efforts at the moderately small scale (several meters) is the quality of a heterogeneity model built from insufficient subsurface data. Most characterizations are based on one of two types of data: physical

data (e.g. sediment samples and driller's logs) and geophysical data (e.g. seismic surveys, ground penetrating radar, and DC resistivity arrays). Physical datasets usually consist of sparse point data and provide a sample or record of the actual lithology with depth at the sampling point. Many physical characterizations are interpolated into three dimensions using geostatistical techniques which honor geologic trends and spatial distributions but are not necessarily representative of the actual configuration of the subsurface deposits [Koltermann and Gorelick, 1996]. The sampling density required to provide accurate three dimensional recreations at the moderately small scale from physical data is neither practical nor cost effective [Deutsch, 2002]. Conversely, shallow geophysical techniques can provide a relatively dense dataset but resolution and depth are limited by the equipment used and site specific conditions [Knight *et al.*, 1997; Neal, 2004]. Additionally, interpretation of geophysical data is often non-unique.

Herein is presented a method which combines each scheme for an integrated approach to shallow aquifer characterization. The following example of our integrated approach utilizes geophysics to delineate the major sedimentary structures within the subsurface which are then "filled in" with geostatistically simulated hydrofacies assignments using a dynamic automated routine. The model generated by the dynamic code closely honors the statistical distribution of sediment within the subsurface and preserves the geometry of sedimentary structures.

2.0 - Previous Work

Ground penetrating radar (GPR) as a hydrologic tool has been growing rapidly in recent years [Knight *et al.*, 1997; Neal, 2004; Annan, 2005]. Most GPR studies in this

category focus on determining the sedimentary or hydraulic character of a portion of the subsurface. Broadly, there have been two approaches to this problem: delineation of subsurface features, and determination of aquifer properties.

GPR has been tested as a method for the direct estimation of aquifer properties, such as hydraulic conductivity, and several studies have shown promising links between hydraulic and dielectric properties [*Rea and Knight, 1997; Novakovic et al., 2002; Kowalsky et al., 2004; Lesmes and Friedman, 2005*]. More often, GPR is used as a tool to map or delineate subsurface features like channel deposits (e.g. *Lunt et al., 2004a; Bersezio et al., 2007*). Such work formed the basis for the concept of radarfacies, those portions of the GPR data having similar electromagnetic response [*Huggenberger, 1993; Regli et al., 2002*]. Radarfacies may be extensive units or simply a recognized pattern of reflections guiding data interpretation. From the radarfacies concept, GPR was used to identify a hierarchy of regions within the subsurface (e.g. *Barrash and Clemo, 2002; Rubin et al., 2006; Bersezio et al., 2007*). These regions define portions of the subsurface that formed under different flow conditions, or those having different lithologies, and can have several smaller regions grouped into a larger region in a hierarchy. This allows more resolution in some cases but many times, the space within the hierarchical regions has been assumed homogeneous or classified on the basis of lithofacies instead of hydrofacies.

The use of GPR and geostatistics together has largely been descriptive where variogram analysis has been used to describe GPR data (e.g. *Rea and Knight, 1998*). The integrated method presented in this paper combines elements of hierarchical GPR studies

with geostatistical simulation in automated fashion. This allows individual regions to be delineated but does not force the interior of the regions to be homogeneous.

A crucial part of the integrated approach presented in this paper is a region growing algorithm. Many such algorithms have been used in other scientific applications but in the earth sciences, growing algorithms are used mostly in image processing. Growing algorithms are used frequently in the processing and segmentation of synthetic aperture radar (SAR and InSAR) such as *Lira and Frulla* [1997], and *Xu and Cumming* [1999]. *Mehnert and Jackway* [1997] present a seeded region growing algorithm that is applied to watershed delineation. Region growing algorithms have also been used extensively in medical applications such as *Revol-Muller et al.* [2002] and *Wan and Higgins* [2003]. Many other example of region growing algorithms exist though most of the published algorithms rely on complex mathematics and statistical operations but the method presented here is, by comparison, very simple.

2.1 – Aquifer characterization

Aquifer characterization, for this study, is defined as a quantitative description of the subsurface in terms of hydraulically important parameters such as hydraulic conductivity (K), permeability (k), or any other applicable quantity. Such parameters are frequently assumed for individual lithofacies since real data are often unavailable. Oftentimes, an entire aquifer is approximated as a homogeneous mass using the ensemble average of a parameter, usually K , to describe flow [*Bridge and Hyndman*, 2004]. More realistic, heterogeneous characterizations will typically use physical or geophysical data to condition the model to account for subsurface variability [*Koltermann and Gorelick*,

1996]. These models require detailed subsurface information, which is usually very difficult to obtain, and employ a process of interpretation, statistical description, interpolation and simulation to create a virtual, multidimensional representation of the system being modeled.

2.2 – Transition Probability Based Indicator Geostatistics

Geostatistics are a set of descriptive and simulation tools to aide in modeling a spatially referenced system [*Journel and Huijbregts*, 1978]. Often, geostatistics are used in hydrogeologic studies to describe a sparse dataset, such as lithology from driller's logs, for the purposes of generating a plausible field of hydraulic conductivities (e.g. *Weissmann and Fogg*, 1999; *Ritzi*, 2000; *Fleckenstein et al.*, 2006; *Rubin et al.*, 2006). The resulting simulations can then be used for groundwater flow and transport modeling. Many options for model development are available to the practitioner depending on the desired result and available data. The most common tools include variogram analysis, kriging, and simulation. Examples of each tool are found in *Deutsch and Journel* [1998] and will not be reviewed here.

Transition Probability geostatistics (TPROGS) provides an expansion of the traditional variogram fitting and sequential indicator simulation (SIS) technique. Details of TPROGS are given by *Carle and Fogg* [1996, 1997] and *Carle* [1999]. The transition probability is the likelihood of finding one particular hydrofacies juxtaposed beside another at some separation (lag) distance. This type of analysis is similar to the traditional variogram method of description and simulation but the semi-variogram is replaced by the Markov chain model for the simulation process. The measured transition probabilities

are fit using a Markov chain model which is then utilized by a 1, 2 or 3 dimensional sequential indicator simulation that generates plausible hydrofacies configurations. By changing the random seed, any number of realizations can be generated for a particular Markov chain model; all are equally probable and honor the actual data and the Markov chain model can be constructed to preserve fining upward tendencies and depositional anisotropy [Carle and Fogg, 1996; Weissmann and Fogg, 1999]. This approach, however, is unable to simulate depositional structures such as cross beds.

2.3 – Ground Penetrating Radar

Ground penetrating radar as a geophysical tool has been growing in popularity over the last decade and numerous papers have been written on its uses and applications (refer to section 1.2). Only a brief overview with some of the relevant points is presented here. See Neal [2004] and *Sensors & Software* [1999] for details on theory, acquisition, and processing of GPR and Annan [2005] for geologic applications specific to sedimentology.

GPR uses electromagnetic energy as a probe into the dielectric properties of the subsurface. Several studies have shown a promising relationship between dielectric and hydraulic properties but this is a complex relationship that is still being developed [Rea and Knight, 1998]. Most surveys, including those used for this study, are reflection surveys. In a reflection survey, a radar wave is transmitted into the ground and continuous reflections from the subsurface materials produce a return signal with different amplitude than that of the original signal. Round trip travel time of each wave is measured, and this travel time can be converted to depth using the radar wave velocity.

GPR allows the user to compile a large, moderately high resolution dataset over a relatively short period of time.

For the popular common-offset reflection method, a transmitter and receiver are used in tandem and are kept a fixed distance apart as dictated by the frequency of the antennas and site characteristics [*Sensors & Software*, 1999] and the data at the current point is collected. Both transmitter and receiver are then moved a specified distance along the survey line, the next data are collected and the process repeats for the remainder of the line. Data interpretation can be difficult and is often highly subjective but interpretations based on grain size contrasts have recently identified bounding surfaces from GPR data (e.g. *Barrash and Clemo*, 2002; *Regli et al.*, 2002; *Lunt et al.*, 2004a; *Bersezio et al.*, 2007).

One restriction of GPR is a tradeoff between depth and resolution. A higher frequency will typically give better resolution at the cost of penetration depth. Resolution can be measured in terms of the minimum resolvable structure (MRS) size which is defined as $\frac{1}{4}$ of the wavelength of the GPR signal and is sensitive to both the antenna frequency and wave velocity through the ground [*Neal*, 2004]. Wave velocity can be approximated by using empirical values for various media or velocity can be determined for a site by using the common midpoint GPR method, discussed in *Neal* [2004]. In many cases, the MRS resolution is sufficient to capture details of interest but objects smaller than the MRS are effectively lost.

3.0 – Integrated Characterization

The integrated approach presented here initially utilizes conditioning data in the form of lithology from drill core and identified bounding surfaces. Here, bounding surfaces are interpreted to be erosional contacts within a sequence of fluvial deposits. Previously, the bounding surface between two deposits has been recognized as the boundary between the probability density functions describing the hydraulic properties of the deposit [Ritzi, 2000]. Conceptually, these features mark the beginning of a depositional unit and the maximum preserved extent of sediments associated with each unit. In this study we identify bounding surface locations using GPR data (details in section 4). The code described in this section uses bounding surfaces to delineate sedimentologic units via a region growing routine. It then fills these regions with lithologic/hydrologic character using transition probability geostatistics conditioned on drill core lithology.

3.1 – Depositional Region Growing Routine

The volumes between bounding surfaces are interpreted to be individual periods of deposition. To identify these regions/volumes, the bounding surface conditioning data for this method are treated as a set of indicator variables

$$I_B(h_{x,y,z}) = \begin{cases} 1, & \text{if } h_{x,y,z} \text{ is a bounding surface} \\ 0, & \text{if otherwise} \end{cases} \quad (1)$$

where I_B is the bounding surface indicator variable at position h given by the Cartesian model coordinates x, y, z (Figure 1). Specific methods for selecting the bounding surfaces

are given later in our example application (section 4). The spatial limits of the model are treated as assumed bounding surfaces but are not formally assigned as indicator variables. The conditioning data used herein are a collection of 2-D slices of bounding surfaces within the study area that are combined to generate a 3-D representation of sedimentary regions which are identified and grouped by a basic growing algorithm written in FORTRAN 95.

The algorithm begins searching in 2-D within the y - z plane in the lowest model layer at the northernmost location (location 2 in Figure 1). From the initial point, the algorithm moves vertically upward through the model layers until a cell satisfying the indicator condition is found or the model top is encountered. If no bounding surface points are identified in a given column the algorithm advances to the next column along y and repeats the search. Once a bounding surface point is found, the algorithm begins to search downward to compute the height of the current bounding surface above the next lowest surface or model base layer (Figure 2). To advance, the algorithm self-centers at the mean height within the current column and takes one step in the positive y direction. Vertical searching is conducted at the new location to compute the limits of the new column and the process continues. The terminal point of a region contained between bounding surfaces is identified when the height of the surface goes to zero or the limit of the model is reached. When all columns and points of the bounded region are identified they are assigned a group number and the algorithm begins searching for the next ungrouped location to serve as the new initial location. As the regions grow, the algorithm continuously checks for abrupt increases or decreases in height. These occurrences can indicate the abrupt pinching out of a depositional unit and can be

encountered within the model. Any change in height exceeding the threshold set by the user is treated as a terminal point and the growth of the region is stopped.

After all regions within a 2-D model slice have been identified, some basic checking is conducted. Any regions that are smaller than user defined limits are assimilated into the next group in the negative y direction (Figure 2) or the largest adjacent group if near the upper y limit of the model. Once a slice is checked the algorithm advances in the strike direction (Figure 1) to the next y - z plane of the model for processing or, if operating in the 2-D mode, the routine switches to geostatistical filling. The individual 2-D slices are combined into volumes during the execution of a hydrofacies assignment routine.

3.2 – 3-D Region Grouping Routine

From the group assignments the filling routine determines the limits (2-D or 3-D) and size of each region. Here, only the three dimensional case is presented but simplified procedures can be used for 2-D models. For 3-D processing, the individual 2-D slices are combined to create depositional volumes. As a basis for matching, the filling routine computes geometric characteristics of each region within each y - z slice. Currently, the routine finds the minimum and maximum y and z values of the region, the total count of cells within the region, the center of mass or centroid of the region and the aspect ratio, defined here as the ratio of length to height. The 2-D center of mass is computed within the routine as

$$C(r)_y = \left[\sum_{i=a}^b (h-h_o) i \right] \times \frac{1}{n} \quad (2)$$

$$C(r)_z = \left[\sum_{i=a}^b \sum_{j=h_0}^h j \right] \times \frac{1}{n} \quad (3)$$

where C is the centroid point of region r in the direction of the subscripts y and z , a and b are the minimum and maximum limits in the y direction, i is position in the y direction, j is position in the z direction, h_0 and h are the minimum and maximum heights in the i th column, and n is the total cell count within the region. The form of equations 2 and 3 were selected to be complimentary to the already stepwise movement of the routine and assume the coordinate system of the integrated model. Due to the sometimes awkward geometries of bounding surfaces it is possible for the z direction centroid point to be located outside the region. In this case, the z centroid is shifted to the vertical midpoint of the region in the y centroid column to avoid exceeding the limits of the region during matching. The aspect ratio of a region within the model is computed as

$$AR(r) = \frac{(y_{\max} - y_{\min})}{(z_{\max} - z_{\min})} \quad (4)$$

where AR is the aspect ratio of region r and the y and z terms represent the minimum and maximum limits of the region, in the y - z plane. Using the centroid, aspect ratio and cell count the algorithm attempts to match each region in one column (slice in the y - z plane) with the adjacent column. The algorithm checks the geometric parameters of the region in the next column at the centroid point of the first column. If the parameters in the second

column are within the prescribed limits, the grouping is accepted and the process continues using the region in the newly grouped column as the starting parameters. If the parameter matching limits are exceeded the adjacent column is not grouped and the routine ends grouping for the selected three dimensional region. The growth conditions may be modified to include any logical rules based on geometric parameters that may be suited to the application at hand. As with the region identification process, the grouping process is continued until all model cells are matched and the final result is a fully three dimensional set of volumes representing individual depositional units.

When selecting grid resolution, it is important to consider the maximum resolution allowable by the GPR data. The method presented here only applies when the GPR resolution is on the order of the size (thickness) of the bounding surfaces and is unlikely to produce realistic results if bounding surfaces are much smaller than the GPR resolution.

3.3 – Geostatistical Filling

Identification of individual sedimentation regions will allow a more confident use of a single set of stationary geostatistics to describe the subsurface variability within each unit. To accomplish this, the filling routine of this method requires a pool of at least one but up to 99 categorical subsurface realizations. The realization(s) may be generated by any method suited to the application, including sequential Gaussian simulations (SGS), the sequential indicator simulation (SIS) routine of the Geostatistical Software Library (GSLIB) [*Deutsch and Journel, 1998*], or TPROGS, so long as the grid size and resolution match that of the bounding surface data. From the depositional units identified

from the bounding surfaces, the processing routine selects a starting region and determines the 3-D limits of the region. These limits define a rectangular volume which dictates the window size to be used in geostatistical filling. If the simulations are not conditioned, the routine randomly selects a subsurface realization from the pool and randomly shifts the rectangular representation of the selected region somewhere within the bounds of the realization (Figure 3). The hydrofacies categories within the subsurface realization are inserted into their corresponding locations within the bounding surface model through a lookup routine. The next unfilled region is then selected and the process repeats for the remainder of the regions until the entire model is constructed. This filling scheme assumes that the geostatistics of each unit are stationary but that the location of any unconditioned unit within a geostatistical realization is unknown. The random moving window scheme allows for depositional position to be represented as a random variable. If data are available to support use of a different set of statistics for different unit types, the algorithm can select from a subset of realizations that specifically use these different statistics.

An exception to this filling routine was created to incorporate conditioning data in the geostatistical realizations. These points coincide with the data collected at the study site, referred to hereafter as hard conditioned regions, and represent the actual subsurface lithology at the sampling locations. Such locations were enforced in the final filling routine by abandoning the random moving window for those regions. The cells within a region containing hard conditioned data were filled with cells corresponding to their exact position within the geostatistical realizations but the particular realization used for filling was still selected randomly from the pool. This preserves the known hydrofacies

locations but allows for some degree of uncertainty in the areas surrounding the conditioning points.

A further, dynamic capability of this method is the use of rules, based on the geometry of the depositional units, to constrain filling conditions. Using a set of rules similar to those of the growing algorithm, depositional regions may be filled from a set of geostatistics suited to a particular geometry. For example, regions having particularly low aspect ratios may be known to have geostatistical properties that vary significantly from large aspect ratio regions. By defining a threshold aspect ratio, small aspect ratio regions can be filled from a different set of geostatistical realizations than large aspect ratio regions (e.g. different lithofacies). This can provide an additional degree of non-stationarity within the simulated subsurface model.

The combination of the depositional region identification routine, the 3-D geometric matching routine, and the moving window filling routine make up the integrated modeling package we shall refer to as “InMod”.

4.0 – Example Application

The following example outlines the process of utilizing InMod for subsurface categorization. Here, the conditioning is based on GPR data and core as described earlier but the conditioning data could also be generated from scale photographs, lidar scans of an outcrop analog, well logs, data collected by trenching, or other methods depending on the available data. A flowchart of this application of InMod is shown in Figure 4.

4.1 – Data Collection

GPR data were collected on an active channel bar on the Rio Grande at a site located 100m north of the Rio Bravo Bridge crossing in Albuquerque, NM (Figure 5a). Data collection was conducted prior to snowmelt runoff and coincided with the lowest annual flow conditions of the river. The study site location was selected to minimize several sources of interference that are frequently encountered in GPR surveys [*Close et al.*, 2004]. The selected site had little to no dip and was extremely flat. A terrestrial lidar scan of the surface, conducted immediately after GPR data collection, confirmed that the maximum relief of the bar was approximately half that of the minimum resolvable structure. As such, surface elevation corrections were not applied to the individual traces. To minimize water table interference, the GPR site was located on the lowest channel bar surface with a depth to water of only a few centimeters. At this location, three sources of GPR interference (the air wave, ground wave and water table reverberation effect) were essentially combined into one interval allowing for more of the GPR energy to enter the saturated portion of the bar.

Data collection was initially conducted in a roughly North to South path subparallel to the river flow direction and parallel to the flow direction over the bar. All data were collected with the common offset method on a PulseEKKO 100 recording system using 200 MHz antennas [*Sensors and Software Inc.*, Mississauga, Ontario]. Eleven 16-m long GPR lines were collected in the long direction, spaced apart at an interval of 0.5m (Figure 5b). A series of tie lines were also collected perpendicular to the main lines. Eight of these lines were collected at 2.0m spacing along the dip direction of the site. For all GPR surveys, the antennae were separated by the manufacturers

recommended distance of 0.5m apart and moved along the survey lines in 0.1m increments.

Core recovery for subsurface characterization at the site was not sufficient for confident description prior to the start of spring runoff. Some shallow hand cores were recovered and photographed immediately after the GPR survey but detailed sampling was not possible. Several months later, after high flows had subsided, we were able to core at the study site using a GeoprobeTM. Portions of the study site had been reworked by the river and the north-western most corner had been completely reclaimed by the river. Some of the original reference marks were found under 2 cm of new sediment and allowed precise location of the core within the model space. Core from six locations within the center most portion of the study area were recovered to individual depths of 2.5 m (Figure 5b). Core recovery was approximately 51 % of the total depth cored resulting in a total of 7.4 meters of core to be used for geostatistical description with the assumption that the top of each core coincides with the minimum depth cored of each interval. Missing intervals were not manually interpolated as this is an integral component of TPROGS.

4.2 – Pre-Processing

The GPR data were initially processed using the ReflexW analysis and interpretation package [Sandmeier Software, 2006]. Based on the estimated wave velocity (0.06 m/ns) through the study unit from published values of similar deposits [Neal, 2004], the minimum resolvable structure (MRS) was determined to be approximately 0.06m. The amplitudes of the 11 GPR lines were interpolated into a three

dimensional model at the MRS resolution by inverse distance weighting of the signals into the space between the original GPR lines giving a final model space of 83 by 268 cells in the strike (columns) and dip (rows) directions respectively. Part of the data were masked by the water table reverberation effect and were disregarded, leaving approximately 3.5m of usable depth which translated into 144 model layers (Figure 6a).

Erosional contacts or bounding surfaces were identified in a manner where only the peaks of the signal were used to identify bounding surfaces (Figure 6b). GPR data can be extremely noisy and difficult to interpret [Annan, 2005]. In zero offset GPR surveys, the peaks of a reflected GPR wave generally represent the strongest difference in the local dielectric response of the subsurface. Significant background noise can fundamentally alter the amplitude of the reflected peaks but we propose that it is unlikely that a peak will be completely masked by noise. As with most GPR studies, the amplitudes of the data were altered by standard data migration techniques including scaling with a moving window, mean subtracting routine (Dewow) and applying an Automatic Gain Compensation (AGC) filter. An AGC normalizes the GPR signal by its inverse and consequently the original amplitudes are lost, though the locations of the peaks are not likely to be masked [Vandenberghe and van Overmeeren, 1999]. The peaks in the data could then be treated as the local extremes in electromagnetic response, which are believed to correspond, at least partially, to erosional contacts or bounding surfaces.

Bounding surfaces on individual GPR lines were identified by visually inspecting the peaks on each of the 83 dip direction filtered traces (Figure 6, top). Manual processing was selected due to the many difficulties associated with automated

delineation of complex, multilayered geometries. The peaks of the GPR data were input into the ArcINFO package [Environmental Systems Research Institute, Inc., Redlands, CA] as non-projected point data in relative model coordinates (row, column and layer numbers). For each column of the model, points determined to not be associated with a bounding surface were discarded and the remaining bounding surfaces were interpolated onto the model grid (Figure 6, bottom).

4.3 – Geostatistical simulation

The geostatistical realizations for region filling were compiled from inspection of the core recovered from the site. Three hydrofacies were selected for geostatistical simulations: 1. coarse material containing gravel to coarse sand; 2. moderate grain sizes from moderately coarse to medium fine sand; 3. fine grained material including fine sand to clay. The volumetric distribution of hydrofacies was dominated by hydrofacies 2, followed by hydrofacies 3, and finally hydrofacies 1, each having 55, 26, and 19 % of the total, recovered volume respectively.

Transition probabilities were measured from the categorized core data from the study site. The Markov chain model used to fit the vertical transition probabilities slightly exaggerates the probability sills of the measured transition probabilities. This is believed to largely be a result of the missing interval between the bottom of the shallow cores and the top of the deeper cores. The volumetric distribution of hydrofacies and mean lengths are thought to be representative of the subsurface at the study site and a decision was made to honor the volumetric proportions over the measured probabilities. The lateral

models were developed from the distribution of hydrofacies observed on the surface of the study site and nearby locations in a manner similar to *Weissmann et al.* [1999].

Markov chain models were created using embedded transition probabilities within the TPROGS geostatistical package [*Carle, 1999*] (Figure 7). Thirteen three dimensional realizations were generated from the Markov chain models to be used as the pool of realizations for the filling routine of InMod. The number of realizations to be used in the pool can be somewhat arbitrary but was made high enough to capture the expected variability of the subsurface at the study site.

Five additional subsurface realizations were generated from the Markov chain models to provide a comparison of InMod realizations to a more standard TPROGS method. These additional realizations were not used in the construction of the integrated models.

The GPR identified bounding surfaces and the geostatistical realizations were input into the growing algorithm to develop hydrofacies maps. The threshold value for all geometric matching parameters was set to plus or minus fifty percent of the current region based on observations of the GPR data. The three dimensional mode of the growing algorithm and filling routine were used to generate five possible subsurface configurations.

5.0 – Results

The subsurface configurations generated by the conditioned filling routine of InMod exhibit features that are geologically expected within a fluvial environment at the scale of this study (Figure 8). The realizations may initially appear to have few

differences to many geostatistical methods but crosscutting relationships and truncated beds are visible on closer inspection. Further, the volumetric distribution of hydrofacies within the final integrated models is consistent both with the measured proportions and the volumetric proportions created by TPROGS simulations. The realizations generated by InMod contain fewer laterally continuous features than the TPROGS geostatistical realizations. This is due to the nature of the seasonal flows that created the shallow deposits being simulated which can create small channel scours not captured by the geostatistics but visible in the GPR data. The study site sees significantly more seasonal and annual variability than the main stem channel and should not be expected to have a large number of laterally continuous features in the strike direction of the model. Elongate features in the dip direction are also consistent with features observed on the surface of the study site at the surface and in the GPR data.

For comparison to the raw geostatistical realizations, values were assigned for the hydraulic conductivity (K) of each hydrofacies. K of 1 m/day was assigned for the sand hydrofacies (2) and it is assumed that the coarse and fine hydrofacies each deviate from the sand by an order of magnitude (0.1 and 10 m/day, hydrofacies 3 and 1 respectively). Comparisons were accomplished using the arithmetic and geometric mean K values and the variance computed from each mean (table 1). For the integrated models, the mean K is observed to be slightly higher than the mean K of all the TPROGS models, though it is within 7 and 3 % for the arithmetic and geometric means respectively. The realizations created with InMod are 36 % higher in the arithmetic variance and 15 % higher in the geometric variance than the transition probability models. The higher variance indicates that more heterogeneities are captured using InMod. A groundwater flow and transport

model constructed with InMod may have the potential to generate more realistic transport behavior than is observed in more simplistic models.

The transition probability of the InMod realizations was compared to the measured probabilities used to generate the pool of realizations used in the filling scheme (Figure 9). Significant variability was expected and observed in the measured probabilities of the integrated models but the Markov chain model used to fit the original probabilities reasonably approximates the observed geostatistics in the integrated models.

6.0 - Conclusions

We developed a collection of algorithms (InMod) that combine geostatistics and geophysics to create a model of subsurface variability that is able to take advantage of the strengths of each method. The approach uses GPR to identify individual depositional events which are automatically identified by a growing algorithm. The regions are filled with hydrofacies assignments from a pool of geostatistical realizations generated by any number of methods. The area used for filling is selected to match exactly the geometry of each depositional region as identified in the GPR data and is inserted into the integrated model by a lookup routine. The growing algorithm and filling routine may be conditioned to function on any set of rules based on measurable geometric properties. The resulting models are comparable to traditional geostatistical models in their mean values and volumetric hydrofacies proportions while having a higher variance. The simulated cross cutting relationships and sharp juxtaposition between depositional events preserved using this method may help to quantify the influence of cross beds and other sedimentary structures on flow and transport problems.

Acknowledgments

The authors would like to thank the New Mexico Institute of Mining and Technology, Department of Geophysics for the use of their GPR system, Fred Gebhardt and Dale Rankin of the US Geological Survey New Mexico Water Science center for their assistance in the collection of the sample cores, and Chris Engdahl and Amy Williams for their assistance in the collection of the GPR data used in this study.

References

- Annan, A.P. (2005), GPR methods for hydrogeological studies, in *Hydrogeophysics* (ed. Y. Rubin and S.S. Hubbard), pp. 185-213.
- Barrash, W. and Clemo, T. (2002), Hierarchical geostatistics and multifacies systems: Boise Hydrogeophysical Research site, Boise, Idaho, *Water Resources Research*, 38(11), 1196.
- Bersezio, R., Giudici, M., and Mele, M. (2007), Combining sedimentological and geophysical data for high-resolution 3-D mapping of fluvial architectural elements in the Quaternary Po plain (Italy), *Sedimentary Geology*, 202, 230-248.
- Bridge, J.J. and Hyndman, D.W. (editors) (2004), Aquifer Characterization, in *Aquifer Characterization* (ed. Bridge and Hyndman) , SEPM special publication No. 80, pp. 1-2.
- Cardenas, M.B. and Zlotnik, V.A. (2003), Three-dimensional model of modern channel bend deposits, *Water Resources Research*, 39(6), 1141.
- Carle, S. F., and Fogg, G.E. (1996), Transition Probability-Based Indicator Geostatistics, *Mathematical Geology*, 28(4), 453-476.
- Carle, S.F., and Fogg, G.E. (1997), Modeling spatial variability with one and multidimensional continuous-lag markov chains, *Mathematical Geology*, 29(7), 891-918.
- Carle, S.F. (1999), *T-PROGS: Transition probability geostatistical software, users manual version 2.1.*, Davis, CA: University of California, Davis, 84 pp.
- Close, M.E., Nobes, D.C., and Pang L. (2004), Presence of Preferential Flow Paths in Shallow Groundwater Systems as Indicated by Tracer Experiments and Geophysical Surveys, in *Aquifer Characterization* (ed. Bridge and Hyndman) , SEPM special publication No. 80, pp. 79-91.
- Cortis, A., Gallo, C., Scher, H., and Berkowitz, B. (2004) Numerical simulation of non-Fickian transport in geological formations with multiple-scale heterogeneities, *Water Resources Research*, 40, W04209.
- Deutsch, C.V. (2002), *Geostatistical Reservoir Modeling*, New York, Oxford University Press, 376 pp.
- Deutsch, C.V., and Journel, A.G. (1998), *GSLIB – Geostatistical Software Library Users Guide*, New York, Oxford University Press, 384 pp.

- Fleckenstein, J.H., Niswonger, R.G., and Fogg, G.E. (2006), River-aquifer interactions, geologic heterogeneity, and low-flow management, *Ground Water*, 44(4), 837-852.
- Huggenberger, P. (1993), Radar facies: recognition of facies patterns and heterogeneities within Pleistocene Rhine gravels, NE Switzerland, in *Braided Rivers* (ed. C.L. Best and C.S. Bristow), Geological Society Special Publication 75, pp. 163-176.
- Journel, A.G., and Huijbregts, Ch.J. (1978), *Mining geostatistics*: Academic Press. San Diego, California., 600 p.
- Knight, R., Tercier, P., and Jol, H. (1997), The role of ground penetrating radar and geostatistics in reservoir description, *The Leading Edge*, November 1997, 1576-1582.
- Koltermann, C.E., and Gorelick, S.M. (1996), Heterogeneity in sedimentary deposits: a review of structure-imitating, process-imitating, and descriptive approaches, *Water Resources Research*, 32(9), 2617-2658.
- Kowalsky, M.B., Rubin, Y., and Dietrich, P. (2004), The use of ground-penetrating radar for characterizing sediments under transient flow conditions, in *Aquifer Characterization* (ed. Bridge and Hyndman), SEPM special publication No. 80, pp. 107-127.
- Lesmes, D.P., and Friedman, S.P. (2005), Relationships between the electrical and hydrogeological properties of rocks and soils, in *Hydrogeophysics* (ed. Y. Rubin and S.S. Hubbard), pp. 87-128.
- Levy, M., and Berkowitz, B. (2003), Measurement and analysis of non-Fickian dispersion in heterogeneous porous media, *Journal of Contaminant Hydrology*, 64, 203-226.
- Lira, J., and Frulla, L. (1997), An automated region growing algorithm for segmentation of texture regions in SAR images, *International Journal of Remote Sensing*, 19(18), 3595-3606.
- Lunt, I.A., Bridge, J.S., and Tye, R.S. (2004a), Development of a 3-D depositional model of braided-river gravels and sands to improve aquifer characterization, in *Aquifer Characterization* (ed. Bridge and Hyndman), SEPM special publication No. 80, pp. 139-169.
- Lunt, I.A., Bridge, J.S., and Tye, R.S. (2004b), A qualitative, three-dimensional depositional model of gravelly braided rivers, *Sedimentology*, 51, 377-414.
- Mehnert, A., and Jackway, P. (1997), An improved seeded region growing algorithm, *Pattern Recognition Letters*, 18(10), 1065-1071.

- Neal, A. (2004), Ground-penetrating radar and its use in sedimentology: principles, problems, and progress, *Earth Science Reviews*, 66, 261-330.
- Novakovic, D., White, C.D., Corbeanu, R.M., Hammon III, W.S., Bhattacharya, J.P., and McMechan, G.A. (2002), Hydraulic Effects of Shales in Fluvial-Deltaic Deposits: Ground-Penetrating Radar, Outcrop Observations, Geostatistics, and Three-Dimensional Flow Modeling for the Ferron Sandstone, Utah, *Mathematical Geology*, 34(7), 857-893.
- Rea, J. and Knight, R. (1998), Geostatistical analysis of ground-penetrating radar data: A means of describing spatial variation in the subsurface, *Water Resources Research*, 34(3), 329-339.
- Regli, C., Huggenberger, P., and Rauber, M. (2002), Interpretation of drill core and georadar data of coarse gravel deposits, *Journal of Hydrology*, 255, 234-252.
- Revol-Muller, C., Peyrin, F., Carrillon, Y., and Odet, C. (2002), Automated 3D growing algorithm based on an assessment function, *Pattern Recognition Letters*, 23(1-3), 137-150.
- Ritzi, R.W. (2000), Behavior of indicator variograms and transition probabilities in relation to the variance in lengths of hydrofacies, *Water Resources Research*, 36(11), 3375-3381.
- Rubin, Y., Lunt, I.A., and Bridge, J.S. (2006), Spatial variability in river sediments and its link with river channel geometry, *Water Resources Research*, 42, W06D16.
- Sensors & Software (1999), *Technical Manual 25: Pulse-EKKO 100 Run, User's Guide v1.2.*, Sensors and Software, Ontario.
- Vandenberghe, J. and van Overmeeren, R.A. (1999) Ground penetrating radar images of selected fluvial deposits in the Netherlands, *Sedimentary Geology*, 128, 245-270.
- Wan, S., and Higgins, W.E. (2003), Symmetric region growing, *IEEE Transactions on Image Processing*, 12(9), 1007-1015.
- Weissmann, G. S., Carle, S.F., and Fogg, G.E. (1999), Three-Dimensional Hydrofacies Modeling Based on Soil Surveys and Transition Probability Geostatistics, *Water Resources Research*, 35(6), 1761-1770.
- Weissmann, G.S., and Fogg, G.E. (1999), Multi-scale alluvial fan heterogeneity modeled with transition probability geostatistics in a sequence stratigraphic framework, *Journal of Hydrology*, 226(1-2), 48-65.

Xu, W., and Cumming, I. (1999), A region-growing algorithm for InSAR phase unwrapping, *IEEE Transactions on Geoscience and Remote Sensing*, 37(1), pp. 124-134.

Zheng, C., and Gorelick, S.M. (2003) Analysis of solute transport in flow fields influenced by preferential flowpaths at the decimeter scale, *Ground Water*, 41(2), pp. 142-155.

Tables

Table 1. Summary statistics of the five InMod realizations (denoted by “GPR13_”) and the five transition probability realizations (denoted by “tsim_”). The measured volumetric proportions used for simulation were 0.19, 0.55 and 0.26 for the fine, medium and coarse hydrofacies. The arithmetic and geometric K variances were computed against the respective mean K values.

R name	Mean K		K Variance		Volumetric Proportions		
	Arithmetic	Geometric	Arithmetic	Geometric	Fines	Sands	Coarse
GPR13_R1	2.714	3.167	0.919	1.687	0.22	0.485	0.295
GPR13_R2	2.901	3.275	1.233	2.037	0.237	0.501	0.262
GPR13_R3	2.802	3.202	1.073	1.824	0.23	0.473	0.297
GPR13_R4	2.833	3.231	1.13	1.898	0.231	0.491	0.278
GPR13_R5	2.861	3.249	1.188	1.924	0.234	0.496	0.27
tsim_GPR1	2.626	3.133	0.803	1.599	0.21	0.499	0.291
tsim_GPR2	2.648	3.146	0.819	1.642	0.211	0.503	0.286
tsim_GPR3	2.59	3.117	0.743	1.531	0.206	0.503	0.291
tsim_GPR4	2.651	3.15	0.826	1.646	0.212	0.506	0.282
tsim_GPR5	2.694	3.171	0.883	1.699	0.216	0.505	0.279

Figures

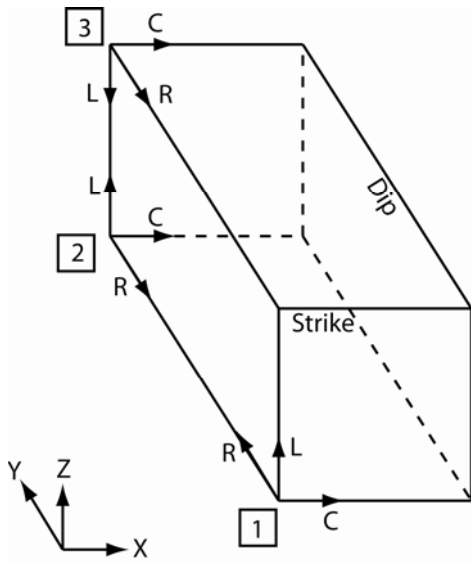


Figure 1. Row (R), Layer (L) and Column (C) coordinate system conventions for 1. TPROGS, 2. Integrated Model, and 3. MODFLOW. A typical cartesian coordinate system is shown in the lower left corner for comparison.

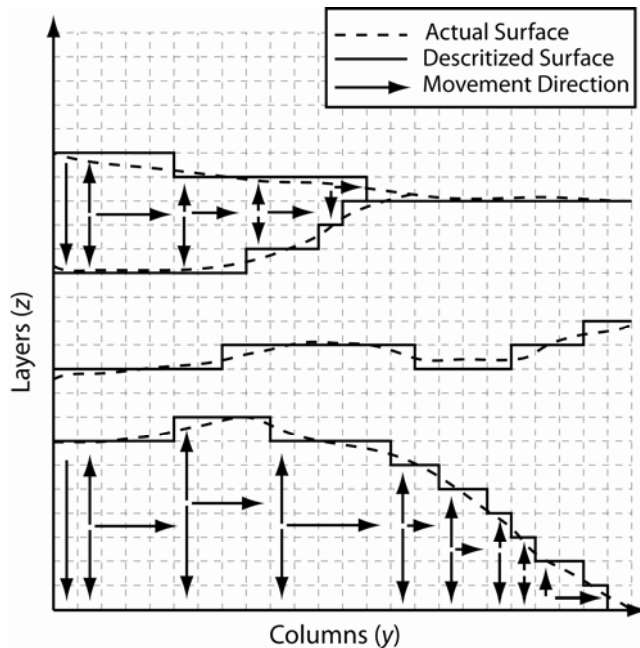


Figure 2. Movement of the self-centering growing algorithm through the discretized bounding surface regions.

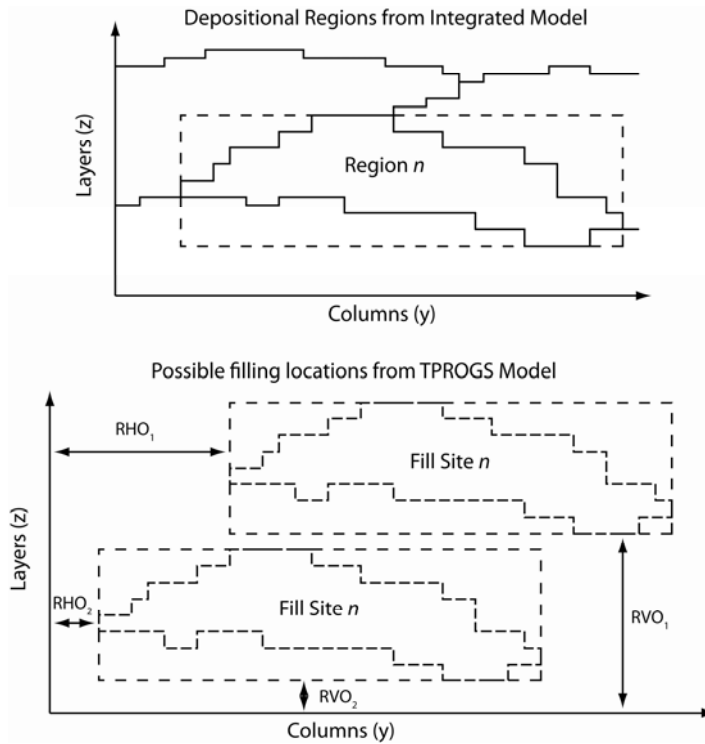


Figure 3. Behavior of the random moving window lookup routine in 2-D. Two possible cases are shown but any number of location shifts are possible for regions without hard conditioned data. In three dimensions, the routine is allowed to shift position along the x axis as well.

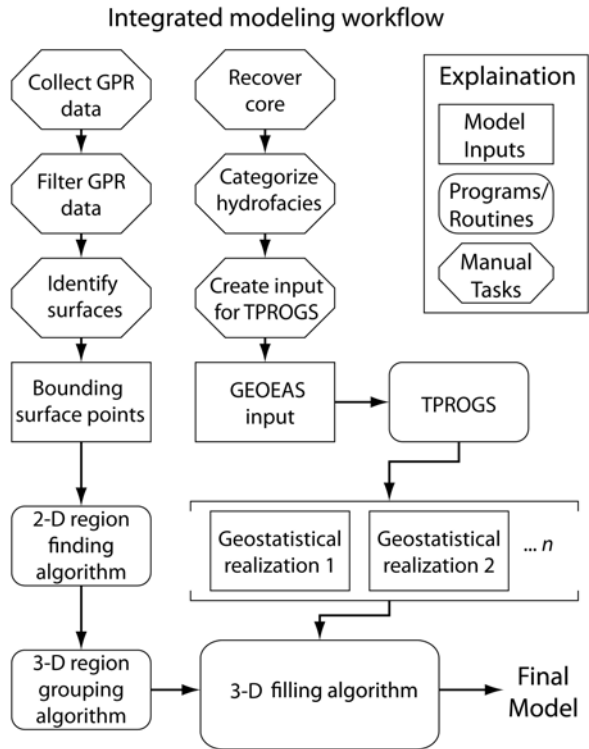


Figure 4. Overview of the integrated modeling process, presented here using GPR and core data for conditioning.

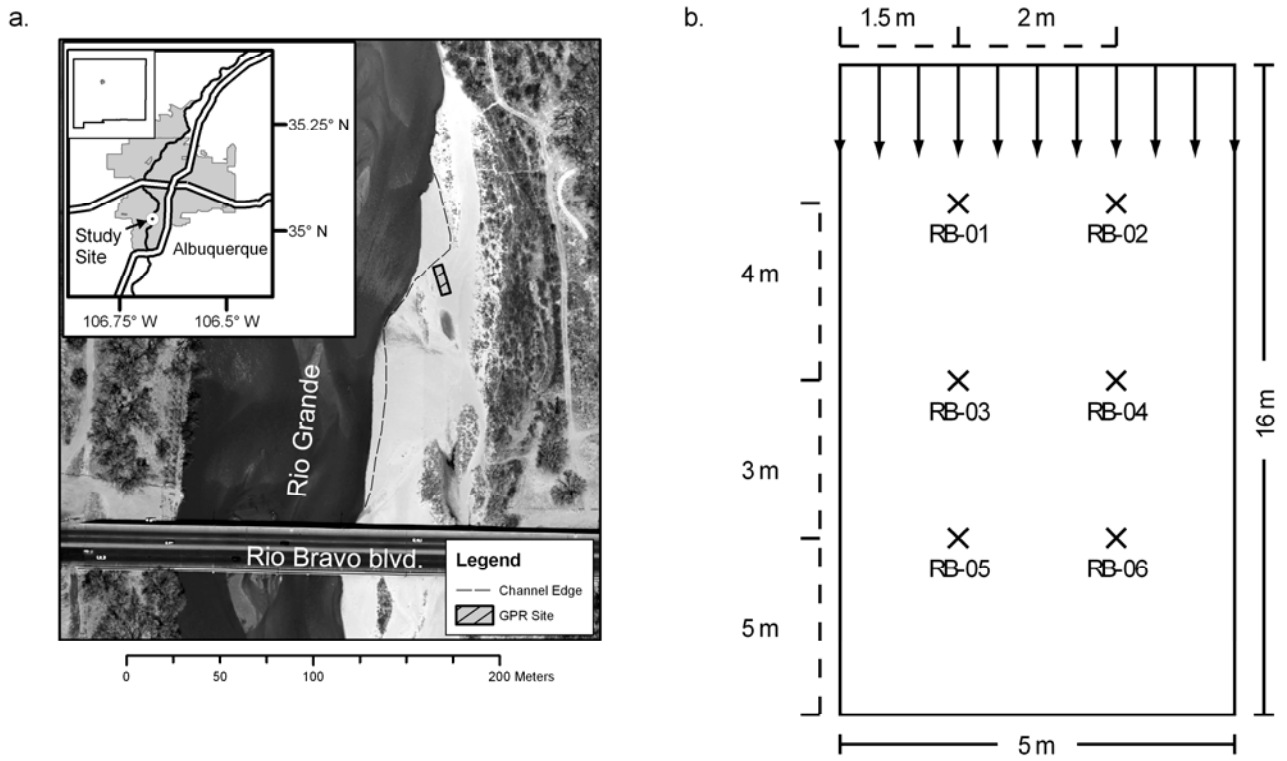


Figure 5. (a) Study site location near the southern end of Albuquerque in central New Mexico. The dashed channel edge line represents the position of the river edge during data collection, (b) Site layout where crosses mark the locations of the core samples and the arrows along the top edge indicate the positive y direction of each GPR line.

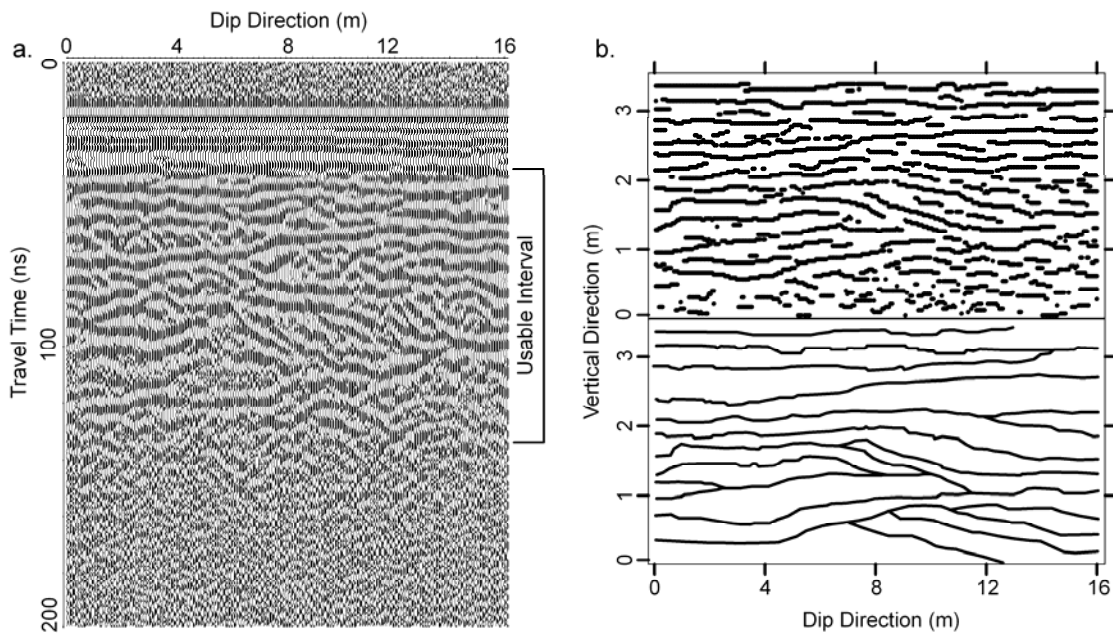


Figure 6. (a) Example of migrated GPR data with the usable portion of the data indicated along the right edge and (b) (upper) Point locations of the peaks of the data from figure 6a and the interpreted bounding surfaces from the same data (lower)

$$TP_x = \begin{bmatrix} l=2.00\text{ m} & 0.775 & 0.225 \\ 0.200 & l=3.00\text{ m} & 0.800 \\ 0.341 & 0.659 & l=1.50\text{ m} \end{bmatrix}$$

$$TP_y = \begin{bmatrix} l=6.80\text{ m} & 0.775 & 0.225 \\ 0.450 & l=10.00\text{ m} & 0.550 \\ 0.057 & 0.943 & l=7.00\text{ m} \end{bmatrix}$$

$$TP_z = \begin{bmatrix} l=0.10\text{ m} & 0.700 & 0.300 \\ 0.736 & l=0.30\text{ m} & 0.264 \\ 0.503 & 0.497 & l=0.25\text{ m} \end{bmatrix}$$

Figure 7. Embedded transition probability matrices used for the construction of the pool of geostatistical realizations in each principle direction denoted by the subscripts x, y, z .

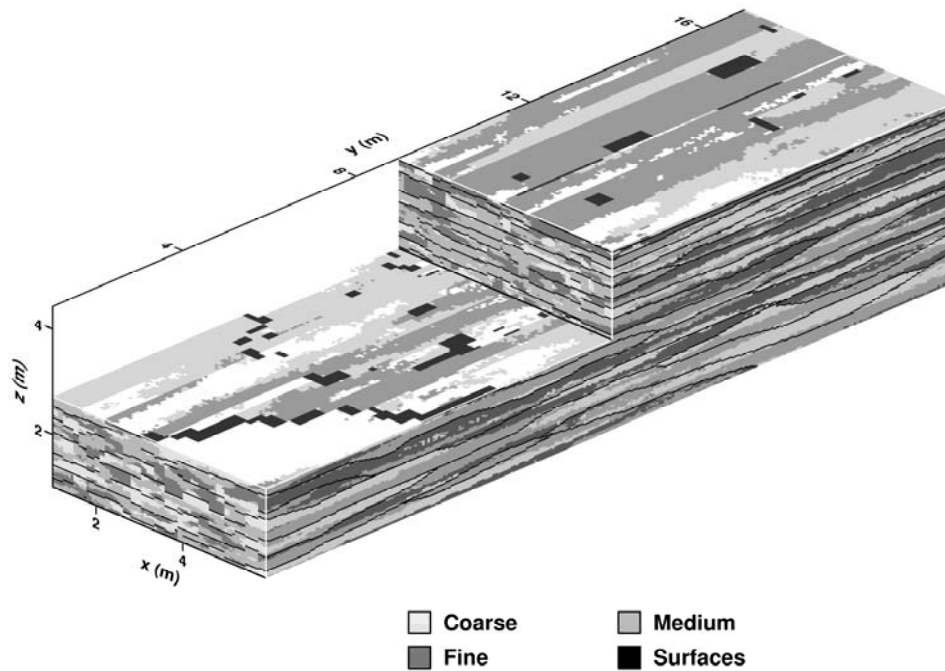


Figure 8. Final model produced by the integrated method (InMod). Bounding surfaces are shown here in black.

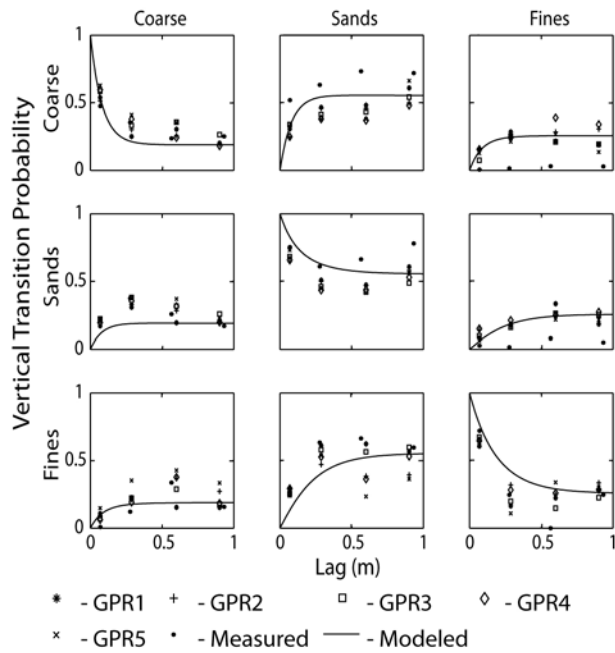


Figure 9. Comparison of the vertical transition probabilities of 5 subsurface realizations generated using the integrated method (InMod) to the measured probabilities of the core data and the Markov chain model used to create the pool of geostatistical models.

Anisotropic transport rates in heterogeneous porous media

Nicholas B. Engdahl and Gary S. Weissmann

1.0 - Introduction

The cornerstone of finite difference groundwater modeling is the assumption that the system being modeled can be approximated at some scale by a homogeneous, representative elementary volume (REV) [Domenico and Schwartz, 1998]. Under many circumstances, this assumption can be reasonable in that, as the size of the REV increases, the variance of the hydraulic conductivity (K) field tends to converge to a stationary value up to some limiting volume [Fitts, 2002]. Provided that the selected REV results in a mean K value that satisfies the conditions of the homogeneous assumption, the resulting flow model can provide a reasonable representation of the hydraulic behavior of the system being modeled [Oreskes *et al.*, 1994].

Despite the relatively good agreement between measured and modeled heads in a well constructed model, many field tracer tests have shown that subsurface transport is not as easily described by the same methods [Eggleston and Rojstaczer, 1998; Benson *et al.*, 2000; Berkowitz *et al.*, 2001]. Two of the most well known tracer tests that have solidified this idea are the Macrodispersion experiment (MADE) conducted at Columbus Air Force Base in Mississippi, and the natural gradient tracer test at the Canadian Forces Base, near Borden, Ontario. The results from the Borden site are described by MacKay *et al.* [1986], Freyberg [1986], and Sudicky, [1986]. Despite the high level of aquifer

characterization at both sites, the measured transport data proved difficult to model using the standard methods of the time. Similar results were observed for the MADE site, which had a significantly higher variance of the natural log K field [Adams and Gelhar, 1992; Boggs *et al.*, 1992]. Eggleston and Rojstaczer [1998] revisited the results of the MADE site and included two large scale geologic regions within the subsurface model. The inclusion of these simple heterogeneities improved the residuals of the travel time analysis relative to the observed values from Adams and Gelhar [1992] but not all the variability was described. Feehley *et al.* [2000] evaluated transport through the MADE site using a variety of aquifer characterization and transport simulation techniques but none could consistently reproduce the entire observed trend. More recently, Zhang and Benson [2008] applied a fractional advection-dispersion equation solution to the MADE site with notable improvements to the fit transport behavior at the site but the applicability of the method to other sites is limited by the detail of available K data. Rather than representing small-scale heterogeneities explicitly, this method provides a way of simulating their bulk effect when aquifer parameters are well known and calibration data exist.

The poor agreement between observed and modeled behavior, from these and other tracer tests, implies that either the subsurface descriptions within many models are flawed or that there are elements below the scale of the REV that are causing anomalous behavior [Cortis *et al.*, 2004]. Most likely it is a combination of both factors. For a complex geologic setting, it can be expected that, even within an REV, there exist unresolved heterogeneities, those which cannot be represented at the effective spatial

resolution of a groundwater model [*Deutsch, 2002; Levy and Berkowitz, 2003; Lunt et al., 2004a; Tartakovsky et al., 2007*]. Though such heterogeneities may not appear to significantly affect the average linear velocity within the Darcy domain, their influence on transport has been largely ignored and assumed equally negligible [*LaBolle and Fogg, 2001*]. The propagation of this assumption over time has produced a great many situations where transport does not match measured data from field tracer tests even in “homogeneous” aquifers [*MacKay et al., 1994; Julian et al., 2001; Berkowitz et al., 2001*]. The disagreement of simulated and field data may be a function of the resolution needed to capture unresolved heterogeneities. This resolution is usually well below that of the available data being used to construct a heterogeneity model. Detailed, high resolution data collection, such as *Lunt et al. [2004b]*, is labor intensive, expensive and often impossible [*Whittaker and Teutsch, 1999; Schulmeister et al., 2004*]. Even with the use of high performance computers, many techniques of aquifer characterization simply cannot represent or recreate the detailed geometric architecture of the sedimentary features which supposedly create deviations from the classically expected transport behavior [*Eggleston and Rojstaczer, 1998; Deutsch, 2002*].

Since mainstream characterization methods are unable to accurately represent the presence of unresolved heterogeneities, higher resolution models need to be developed which can preserve the internal structure of the deposit being modeled so that we can investigate the influence of the heterogeneities and build better up-scaled models in the future that capture more realistic velocity distributions. Though this forces us to decrease

the size of our models, smaller models within the domain of a larger model can help advance our understanding of transport properties within an REV.

One of the commonly cited unresolved heterogeneities is the presence of sedimentary features such as cross-beds [Zheng and Gorelick, 2003; Dai *et al.*, 2004; Proce *et al.*, 2004]. It is intuitively expected that subsurface contaminant transport along a cross-bedded paleoflow direction should be faster than flow perpendicular to bedding. Several cases of such behavior, relating to permeability, are given by Davis [1969]. It is hypothesized that within a real fluvial aquifer, there should be a decrease in transport rates as the flow path is rotated from a direction parallel to deposition to a direction perpendicular to deposition. To resolve the directional behavior, we used geostatistical models, a homogeneous approximation, and a recently developed, integrated geophysical/geostatistical method of shallow aquifer characterization to create virtual representations of a section of aquifer that is the size of a cell block (or REV) within a larger scale model near the selected study site. The heterogeneous models, and the homogenous approximation, were then used to investigate the influence of small scale (several cm) sedimentary features on the directional properties of subsurface transport.

2.0 - Model development

Evaluation of the directional effects of bedding on transport required the creation of several models of the subsurface configuration using the highest possible resolution. Three types of models were selected for comparison: a geostatistically based model created using transition probability geostatistics or TPROGS [Carle and Fogg, 1996;

Carle, 1999], a model created using an integrated geophysical/geostatistical modeling approach proposed by *Engdahl et al.* [chapter 2, this volume] hereafter referred to as InMod, and a homogeneous approximation of the aquifer. The selected study site (Figure 1) lies within the domain of a recently constructed ground water/surface water interaction model along the Rio Grande, in Albuquerque, NM, where U.S. Geological Survey piezometer nests provide information about hydraulic conditions near the site [*Engdahl et al.*, chapter 1, this volume]. This site is located along the edge of the main stem channel and is seasonally flooded, indicating a history of deposition and erosion during at least part of the year. The seasonal flooding and observed sedimentary structures in nearby outcrops make the site a good candidate for preserved sedimentary structures.

2.1 - Transition Probability Geostatistics

Transition probability geostatistics are based on the likelihood of finding one categorical hydrofacies juxtaposed beside another at a given separation distance [*Carle and Fogg*, 1996]. The available data for a given site is translated into distinct hydrofacies and the measured transition probabilities are fit using a Markov chain model in each principle direction. The combined Markov chain model is used to generate plausible realizations of the subsurface configuration which can then be mapped to a finite difference numerical flow modeling code. The number of papers published using this method is rapidly increasing and the authors refer you to *Carle and Fogg* [1996], *Weissmann and Fogg* [1999], *Weissmann et al.* [1999], and *Fleckenstein et al.* [2006] for more detailed explanations.

2.2 - Integrated Geophysical/Geostatistical modeling

Newer, integrated models are able to utilize several sources of traditionally incompatible input data to generate subsurface realizations. The integrated modeling method for shallow aquifer characterization (InMod) combines ground penetrating radar (GPR) and geostatistical data to improve the subsurface approximation by preserving geologically expected features that cannot be reproduced using geostatistics alone. The method is based on the concept that individual periods of sedimentation are separated by an erosional surface and can be described by a stationary set of geostatistics [Ritzi, 2000]. GPR surveys are not always a direct analog to K since the propagation of the radar wave is affected by a great number of factors [Rea and Knight, 1998; Neal, 2004; Annan, 2005]. and the use of GPR within InMod is restricted to the identification of the erosional contacts or bounding surfaces surrounding individual periods of deposition. Using GPR it is possible to create an image map of the location of the bounding surfaces several meters into the subsurface. The spaces between the surfaces are then “filled-in” using geostatistical realizations computed with conditioning from core samples and other field data.

Construction of a model with InMod begins by manually interpreting the GPR image map into a three-dimensional bounding surface indicator database. This process is done visually using the peaks of the GPR signal which represent the greatest local variability in the dielectric properties of the subsurface [Neal, 2004]. These points are the physical representation of a change in grain size, lithology or orientation of the sediments

and are interpreted to be the bounding surfaces [Vandenberghe and van Overmeeren, 1999; Lunt et al., 2004a). The erosional surfaces are treated as indicator variables and depositional units between bounding surfaces are identified automatically by a region growing algorithm. The algorithm initially processes the data as a series of parallel two-dimensional slices in the y-z plane of the model (Figure 2). The depositional regions of each slice are grouped into three dimensions using another algorithm which utilizes basic rules to determine if the adjacent regions should be grouped. Any rules which are based on the geometry of the regions (e.g. center of mass, aspect ratio, region size, etc...) may be programmed into the algorithm and assigned a series of threshold values which form the basis of the matching. The two-dimensional model slices are then combined into three-dimensional volumes and the geostatistical filling routine takes over.

The depositional regions within the model are filled with a heterogeneous distribution of hydrofacies from a pool of several geostatistical realizations using a randomly shifting “window” within the model space. The realizations may be generated by any appropriate means but since a Markov chain model already existed at the site, TPROGS was selected. For regions lacking conditioning data, a geostatistical realization is randomly selected to be used in the final model and hydrofacies assignments are inserted into the final model from a random location within the selected realization, corresponding to the size and shape of the region being filled. This routine allows depositional position to be simulated as a random variable where no data exist to constrain the depositional succession. Regions containing conditioning data are filled from the corresponding location within the geostatistical realizations but the choice of which realization to use is still made randomly, preserving some of the uncertainty within

the model domain while honoring real data. So far, the geostatistics used in InMod have used core samples for conditioning although borehole geophysics and drillers logs may also be acceptable input data sets. Similar to the grouping algorithm, the filling routine of InMod is capable of utilizing rules to select realizations based on selected geostatistical models that are related to distributions identified in other depositional unit types (e.g. different lithologic character)

2.3 – Heterogeneity Modeling

The Markov chain models and the geostatistical realizations used in InMod were constructed using lithologic data from six, 2.4-m long cores extracted from the study site. The measured transition probabilities were supplemented with surface observations of mean hydrofacies lengths to generate the principle direction Markov chain models used in simulation, similar to the procedure of *Weissmann et al.* [1999]. For InMod, thirteen (13) hydrofacies realizations were generated for use in the geostatistical filling routine. Five additional TPROGS realizations were created for flow and transport modeling.

GPR data at the site were collected during the low flow period of the river. The GPR scans were conducted on the lowest accessible sand bar adjacent to the main channel where cross bedding and other sedimentary structures were expected and also to minimize signal interference. Eleven (11) GPR lines, each 16-m in length along depositional dip, were collected at a spacing of 0.5-m using the manufacturers recommended antennae separation of 0.5-m with a step size of 0.1-m (Figure 3). The data were combined and interpolated into three dimensions using the ReflexW analysis and

interpretation package [Sandmeier Software, 2006]. The GPR data were manually interpreted as two-dimensional slices using ArcINFO [ESRI inc., Redlands, CA] and translated into an indicator variable data set.

The bounding surfaces, the pool of 13 geostatistical realizations, and the threshold values for region matching were input into InMod, which was in turn used to generate the final facies distribution realizations for flow and transport modeling. To account for some of the uncertainty associated with geostatistically based models, five TPROGS and five InMod realizations were created (Figures 4 and 5). These realizations allow us to capture at least some of the variability between possible geostatistical realizations. The final model resolution was set to be the maximum resolution allowed by the wavelength of the GPR. The model was discretized into 83 columns, 268 rows and 144 layers. The row and column dimensions were set to be 6-cm while the vertical direction was set to be 3-cm for a total model space of 5-m wide by 16-m long by 3.5-m deep. This produced a model grid of approximately 3.2 million nodes.

The models created with InMod were able to reproduce features known to exist within the nearby fluvial deposits, such as channel scours and cross-bedded regions, and those reported to exist within similar environments by *Allen* [1992], *Ritter et al.* [2002] and *Heinz et al.* [2003].

2.4 - Numerical Flow and Transport Modeling

The hydrofacies within the categorical models created using TPROGS and InMod were assigned K values varying by an order of magnitude. The values were arbitrarily

chosen within the range of published values [*Dominico and Schwartz, 1998*] for similar sedimentary deposits to be 0.1, 1 and 10 m/day for the fine, medium and coarse hydrofacies, respectively, and are within reported ranges of nearby deposits [*Hawley and Hasse, 1992*]. A homogeneous realization was assigned a *K* value equal to the average arithmetic mean of the TPROGS and InMod realizations and one other homogeneous realization was assigned the geometric mean *K* value of the other realizations. The 12 subsurface models were then translated onto a finite-difference grid for groundwater flow simulation.

The direction of flow through the model was controlled by the position and magnitude of the boundary conditions. For all of the virtual aquifer configurations, three hydraulic gradient directions were selected for use in modeling (Figure 6). The north-south direction (NS) was oriented parallel to deposition, the east-west direction (EW) gradient was perpendicular to the NS orientation, and the north-west to south-east direction (NWSE) was oriented at 45 degrees to both of the other flow paths. In all directions, the magnitude of the hydraulic gradient was held constant. For the NS models the model top, bottom, east and west edges were assigned zero-flux boundary conditions, and the north and south model edges were specified head boundaries, driving flow from the north to the south. The EW models had similar conditions except that the prescribed head boundaries were moved to the east and west model edges, forcing flow to be from the west to the east. Finally, the NWSE orientation was assigned zero flux conditions for the model top and bottom but all other model edges were assigned a component of the desired gradient such that the vector sum of all prescribed head boundaries drove flow from the north-west to the south-east within the simulations at 45 degrees between the

other model orientations. All of the constructed models were simulated under steady state groundwater flow conditions using MODFLOW 2000 [Harbaugh *et al.*, 2000].

Transport simulations were conducted by releasing an equal number of particles into each model (Figure 6). Particle tracking was conducted using the random walk particle model for simulating transport in heterogeneous permeable media [RWHET, LaBolle, 2006]. Five hundred (500) particles were released in each model at four locations within a plane perpendicular to the gradient (Figure 6) for a total of 2000 active particles. The number of particles was intentionally kept small to minimize clutter within the model and to allow for more detailed analyses of the paths of individual particles. Boundary conditions for the transport models were assigned to compliment the flow models where all zero-flux boundaries in the groundwater flow models were converted into reflecting boundaries within RWHET. Particle concentrations were monitored in a fixed plane parallel to the release plane of the particles in each direction. Any particles passing through the monitoring plane were removed from the active simulation domain.

3.0 - Results and discussion

Since the simulation of transport in each direction was conducted over a different path length, the results of each simulation required normalization prior to comparison. In each orientation, the breakthrough time for all particles was scaled by the straight line path length from the release plane to the breakthrough plane. This transformed the data to

represent the time in each direction required to travel a uniform, one dimensional distance. This transformed time can be thought of as an inverse, generalized transport rate. Cumulative breakthrough counts were normalized to the total number of particles in the simulations, as were the raw particle concentrations at the breakthrough plane.

The simulated behavior of both homogeneous models was essentially constant and showed no substantial variations in transport rates in the different orientations. We consider this behavior to represent directionally independent transport rates (Figure 7). This behavior is predicted by Fick's law and the classical advection dispersion equation for a purely homogeneous medium. The models generated using TPROGS did show some directional variability but with no consistent trend (Figure 8a). Unlike the other model types, the simulations conducted using InMod clearly showed three separate regimes of transport rates which were directionally dependent (Figure 8b).

Compared to the TPROGS models, the results of the InMod simulations were much less scattered. Initially, the decreased scatter in the InMod results was thought to be caused by the hydrofacies assignment at the release point. Investigation of the model architecture showed that the hydrofacies assignments at the release point within each model were not identical but the hydrofacies assignments were similarly distributed between the TPROGS and InMod simulations. The decrease in scatter is attributed to the existence of fewer connected pathways within the InMod models because of the segmented nature of the filling routine which can produce more sharp juxtapositions than TPROGS alone. Conceptually, this means that the TPROGS models force particles to remain within low K regions for longer periods of time but the smaller low K deposits in the InMod simulations allow particles to simply go around them.

A best fit spline was used to average the results of the five InMod simulations to more clearly illustrate the directional behavior (Figure 9). The most rapid transport rates were observed for the NS orientation (parallel to paleoflow), the slowest rates were observed in the EW orientation (perpendicular to paleoflow) and the NWSE orientation fell intermediate between the other orientations. Late time arrivals, or the tails of the breakthrough curves, exhibited similar directionally dependent behavior with the EW direction (flow perpendicular to bedding) displaying longer tails than the NS direction (flow parallel to bedding) (Figure 10a). All of the directional results generated with the InMod realizations were consistent with the directionally dependent permeability behavior reported by *Davis* [1969].

Without additional field data to constrain the flow rate through our model it is not possible to solve for the exact transport parameters associated with each direction. To provide an estimate of possible transport parameters we used the CTRW toolbox [*Cortis and Berkowitz, 2005; Cortis et al., 2005; <http://www.weizmann.ac.il/ESER/People/Brian/CTRW>*]. Using the inverse modeling portion of the toolbox we estimated Fickian and non-Fickian transport parameters using the classical ADE and asymptotic transition rate models (Table 1) [*Cortis et al., 2004*]. The transport velocities and dispersion coefficients estimated by both methods were very similar but the Fickian approximation of the simulated transport curves could not recreate the late time arrivals, or tails, of the breakthrough curves. The non-Fickian, asymptotic transition rate model tended to overestimate the late time behavior but was able to more closely recreate the tails of the breakthrough curves than the classical ADE model (Figure 10b). Although they are not large deviations, ignoring the non-Fickian behavior and approximating transport through

the study site as a Fickian process may introduce significant error into up-scaled simulations.

Using methods similar to our CTRW fitting, it may be possible to define a lateral transport rate ellipse which could be used in future flow and transport models to improve the accuracy of the results at locations such as the Borden and MADE sites. Using our approach with modified boundary conditions, it is possible to evaluate the transport rate anisotropy in the vertical direction but because vertical transport rates tend to be orders of magnitude smaller than horizontal transport rates [*Dominico and Schwartz, 1998*] they were not evaluated at this time.

The numerical confirmation of the hypothesized behavior suggests that the unresolved heterogeneities within this typical REV sized model domain can have a profound impact on transport rates. The consistency of the InMod results may be a result of the forced, sharp juxtaposition of high and low K hydrofacies within the model at some bounding surfaces. Unlike the Borden and MADE sites, the behavior of the InMod results is nearly Fickian, but no laterally extensive, high K zones were forced into the model due to a lack of information about the location of such features. It is likely that high K layers exist within the study site since laterally extensive gravel deposits can be observed elsewhere along the Rio Grande. It is also expected that the inclusion of a laterally extensive gravel layer somewhere within the model would create a fast pathway for transport and would result in more distinct non-Fickian breakthrough curves.

4.0 – Conclusions

We constructed a series of heterogeneous and homogeneous groundwater flow models which were used to simulate transport. The simulations were conducted along the principle, horizontal model axes and at an oblique orientation between the principle directions. The models were designed to evaluate the directional anisotropy of transport rates through the model. Three types of models were constructed for groundwater flow and transport modeling: a homogeneous approximation of the subsurface, a series of geostatistical models created with TPROGS, and a series of models created using a new integrated geophysical/geostatistical modeling technique (InMod) which is able to preserve sedimentary structures and relations that geostatistics alone cannot. Flow and transport was simulated for 5 of each kind of heterogeneity realizations and two homogeneous approximations. The one dimensional breakthrough time was scaled by the straight line path distance from the release plane to the monitoring plane, resulting in a relative transport rate for comparison. Of the three types of models constructed, only the models built with InMod were able to show the hypothesized behavior where the fastest transport rates occurred along the paleoflow direction and the slowest rates occurred perpendicular to paleoflow. The models constructed using TPROGS and the homogeneous models were unable to consistently reproduce the expected directional anisotropy. The directional behavior of the InMod models is observed for the entire breakthrough curve, including the late time arrival tail. The modeled data was fit using the CTRW toolbox and it was found that the resulting breakthrough curves were approximated best by a non-Fickian breakthrough model. The results of this study numerically support the directionally dependant transport behavior suggested by *Davis* [1969] and provide a basis for the definition of a transport rate ellipse.

Acknowledgements

The authors would like to thank the New Mexico Institute of Mining and Technology, Department of Geophysics for the use of their GPR equipment for this study. We also thank Fred Gebhardt and Dale Rankin of the U.S. Geological Survey for their assistance in the collection of the core samples and Chris Engdahl for his assistance in the collection of the GPR data. Financial support for this work was provided by the University of New Mexico, Office of Graduate Studies, and the New Mexico Water Resources Research Institute.

References

- Adams, E.E., and Gelhar, L.W. (1992), Field study of dispersion in a heterogeneous aquifer, 2. spatial moment analysis, *Water Resources Research*, 28, 3293-3307.
- Allen, J.R.L. (1992), *Principles of Physical Sedimentology*, 272 pp., The Blackburn Press, Caldwell, New Jersey.
- Annan, A.P. (2005), GPR methods for hydrogeological studies, in *Hydrogeophysics* (ed. Y. Rubin and S.S. Hubbard), pp. 185-213.
- Benson, D.A., Wheatcraft, S.W., and Meerschaert, M.M. (2000), The fractional-order governing equation of Levy motion, *Water Resources Research*, 36(6), 1413-1423.
- Berkowitz, B., Kosakowski, G., Margolin, G., and Scher, H. (2001), Application of continuous time random walk theory to tracer test measurements in fractured and heterogeneous porous media, *Ground Water*, 39 (4), 593-604.
- Boggs, J.M., Young, S.C., and Beard, L.M. (1992), Field study of dispersion in a heterogeneous aquifer, 1. overview and site description, *Water Resources Research*, 28(12), 3281-3291.
- Eggleston, J., and Rojstaczer, S. (1998), Identification of large-scale hydraulic conductivity trends and the influence of trends on contaminant transport, *Water Resources Research*, 34 (9), 2155-2168.
- Carle, S.F. (1999), T-PROGS: Transition probability geostatistical software, users manual version 2.1., 84 pp., University of California, Davis, CA..
- Carle, S.F., and Fogg, G.E. (1996), Transition probability-based indicator geostatistics, *Mathematical Geology*, 28(4), 453-476.
- Cortis, A., Gallo, C., Scher, H., and Berkowitz, B. (2004), Numerical simulation of non-Fickian transport in geological formations with multiple-scale heterogeneities, *Water Resources Research*, 40, W04209, doi:10.1029/2003WR002750.
- Cortis, A., and Berkowitz, B. (2005), Computing anomalous contaminant transport in porous media: the CTRW toolbox, *Ground Water*, 43(6), 947-950.
- Cortis, A., Emmanuel, S., and Berkowitz, B. (2005), The CTRW Matlab toolbox V2.6: a practical user's guide, <http://www.weizmann.ac.il/ESER/People/Brian/CTRW>.

- Dai, Z., Ritzi, R.W., and Dominic, D.F. (2004), Estimating parameters for hierarchical permeability correlation models, in *Aquifer Characterization*, edited by J.S. Bridge and D.W. Hyndman, (*SEPM*) *Society for Sedimentary Geology Special Publication No. 80*, pp. 41-54.
- Davis, S.N. (1969), Porosity and permeability of natural materials, in *Flow through porous materials*, edited by R.J.M. DeWiest, Academic Press, New York, pp. 54-89.
- Dentz, M., Cortis, A., Scher, H., and Berkowitz, B. (2004), Time behavior of solute transport in heterogeneous media: transition from anomalous to normal transport, *Advances in Water Resources*, 27, 155-173.
- Deutsch, C.V., (2002), *Reservoir Geostatistics*, 376 pp., Oxford University Press, New York, New York.
- Dominico, P.A., and Schwartz, F.W. (1998), *Physical and Chemical Hydrogeology*, 2nd edition, 506 pp., John Wiley and Sons, New York, New York.
- Eggleston, J, and Rojstaczer, S. (1998), Identification of large scale hydraulic conductivity trends and the influence of trends on contaminant transport, *Water Resources Research*, 34 (9), 2155-2168.
- Feehley, C.E., Zheng, C., and Molz, F.J. (2000), A dual-domain mass transfer approach for modeling solute transport in heterogeneous aquifers: Application to the Macrodispersion Experiment (MADE) site, *Water Resources Research*, 36 (9), 2501-2515.
- Fitts, C.R. (2002), *Groundwater Science*, 450 pp., Academic Press, San Diego, California.
- Fleckenstein, J.H., Niswonger, R.G., and Fogg, G.E. (2006), River-aquifer interactions, geologic heterogeneity, and low-flow management, *Ground Water*, 44(4), 837-852.
- Freyberg, D.L. (1986), A natural gradient experiment on solute transport in a sand aquifer, 2. spatial moments and the advection and dispersion of nonreactive tracers, *Water Resources Research*, 22 (13), 2031-2046.
- Harbaugh, A.W., Banta, E.R., Hill, M.C., and McDonald, M.G. (2000), MODFLOW-2000, the U.S. Geological Survey modular ground-water model – user guide to modularization concepts and the ground-water flow process, *Open-File Report 00-92*, 107 pp., U.S. Geological Survey.

- Hawley, J.W., and Haase, C.S. (compilers) (1992), Hydrogeologic framework of the northern Albuquerque Basin, *Open-File Report 387*, New Mexico Bureau of Mines and Mineral Resources.
- Heinz, J., Kleineidam, K., Teutsch, G., and Aigner, T. (2003), Heterogeneity patterns of quaternary glaciofluvial gravel bodies (SW-Germany): application to hydrogeology, *Sedimentary Geology*, 158, 1-23.
- Julian, H.E., Boggs, J.M., Zheng, C., and Feehley, C.E. (2001), Numerical simulation of a natural gradient tracer experiment for the natural attenuation study: flow and physical transport, *Ground Water*, 39 (4), 534-545.
- LaBolle, E.M., and Fogg, G.E. (2001), Role of molecular diffusion in contaminant migration and recovery in an alluvial aquifer system, *Transport in Porous Media*, 42, 155-179.
- LaBolle, E.M. (2006), RWHet: random walk particle model for simulating transport in heterogeneous permeable media, user's manual and program documentation, Version 3.2, 27 pp.
- Levy, M., and Berkowitz, B. (2003) Measurement and analysis of non-Fickian dispersion in heterogeneous porous media, *Journal of Contaminant Hydrology*, 64, 203-226.
- Lunt, I.A., Bridge, J.S., and Tye, R.S. (2004a), Development of a 3-D depositional model of braided river deposits, in *Aquifer Characterization*, edited by J.S. Bridge and D.W. Hyndman, (*SEPM*) *Society for Sedimentary Geology Special Publication No. 80*, pp. 139-169.
- Lunt, I.A., Bridge, J.S., and Tye, R.S. (2004b), A quantitative, three-dimensional depositional model of gravelly braided rivers, *Sedimentology*, 51, 377-414.
- MacKay, D.M., Freyberg, D.L., Roberts, P.V., and Cherry, J.A. (1986), A natural gradient experiment on solute transport in a sand aquifer, 1. approach and overview of plume movement, *Water Resources Research*, 22 (13), 2017-2029.
- MacKay, D.M., Bianchi-Mosquera, G., Kopania, A.A., Kianjah, H.h and Thornjarnarson, K.W. (1994), A forced-gradient experiment on solute transport in the Borden aquifer, 1. Experimental methods and moment analyses of results, *Water Resources Research*, 30(2), 369-383.
- Neal, A. (2004), Ground-penetrating radar and its use in sedimentology: principles, problems and progress, *Earth Science Reviews*, 66, pp. 261-330.
- Oreskes, N.K., Shrader-Frechette, and Belitz, K. (1994), Verification, validation, and confirmation of numerical models in earth sciences, *Science*, 263, 99-102.

- Proce, C.J., Ritzi, R.W., Dominic, D.F., and Dai, Z. (2004) Modeling multiscale heterogeneity and aquifer interconnectivity, *Ground Water*, 42(5), 658-670.
- Rea, J. and Knight, R. (1998), Geostatistical analysis of ground-penetrating radar data: A means of describing spatial variation in the subsurface, *Water Resources Research*, 34(3), 329-339.
- Ritter, D.F., Kochel, R.C., Miller, J.R. (2002), *Process Geomorphology*, 4th edition, 560 pp., McGraw-Hill, New York.
- Ritzi, R.W. (2000), Behavior of indicator variograms and transition probabilities in relation to the variance in lengths of hydrofacies, *Water Resources Research*, 36(11), 3375-3381.
- Schulmeister, M.K., Butler, J.J., Franseen, E.K., Wysocki, D.A., and Dolittle, J.A. (2004), High-resolution stratigraphic characterization of unconsolidated deposits using direct-push electrical conductivity logging: a floodplain-margin example, in *Aquifer Characterization*, edited by J.S. Bridge and D.W. Hyndman, (*SEPM Society for Sedimentary Geology Special Publication No. 80*), pp. 67-78.
- Sudicky, E.A. (1986), A natural gradient experiment on solute transport in a sand aquifer: spatial variability of hydraulic conductivity and its role in the dispersion processes, *Water Resources Research*, 22 (13), 2069-2082.
- Tartakovsky, D.M., Wohlberg, B., and Guadagnini, A. (2007), Nearest-neighbor classification for facies delineation, *Water Resources Research*, 43, W07201.
- Vandenberghe, J., and van Overmeeren, R.A. (1999) Ground penetrating radar images of selected fluvial deposits in the Netherlands, *Sedimentary Geology*, 128, 245-270.
- Weissmann, G.S., and Fogg, G.E. (1999), Multi-scale alluvial fan heterogeneity modeled with transition probability geostatistics in a sequence stratigraphic framework, *Journal of Hydrology*, 226(1-2), 48-65.
- Weissmann, G.S., Carle, S.F., and Fogg, G.E. (1999), Three-dimensional hydrofacies modeling based on soil surveys and transition probability geostatistics, *Water Resources Research*, 35 (6), 1761-1770.
- Whittaker, J. and Teutsch, G. (1999) Numerical simulations of subsurface characterization methods: application to a natural aquifer analog, *Advances in Water Resources*, 22 (8), 819-829.
- Zhang, Y., and Benson, D.A. (2008), Lagrangian simulation of multidimensional anomalous transport at the MADE site, *Geophysical research Letters*, 35, L07403, doi:10.1029/2008GL033222.

Zheng, C., and Gorelick, S.M. (2003) Analysis of solute transport in flow fields influenced by preferential flowpaths at the decimeter scale, *Ground Water*, 41(2), pp. 142-155.

Tables

Table 2. CTRW toolbox fitted parameters for the best fit transport simulations for Fickian and non-Fickian behavior, where v is the transport velocity (m/d), D is the dispersion coefficient (m^2/d) and β is the dimensionless fractional order parameter of the asymptotic rate model.

Model Orientation	non-Fickian parameters			Fickian parameters	
	v_β	D_β	β	v_1	D_1
NS	3.79E-02	4.09E-03	1.0758	3.99E-02	4.58E-03
NWSE	3.52E-02	4.59E-03	0.96728	3.10E-02	4.22E-03
EW	3.29E-02	2.04E-03	0.86305	2.62E-02	2.33E-03

Figures

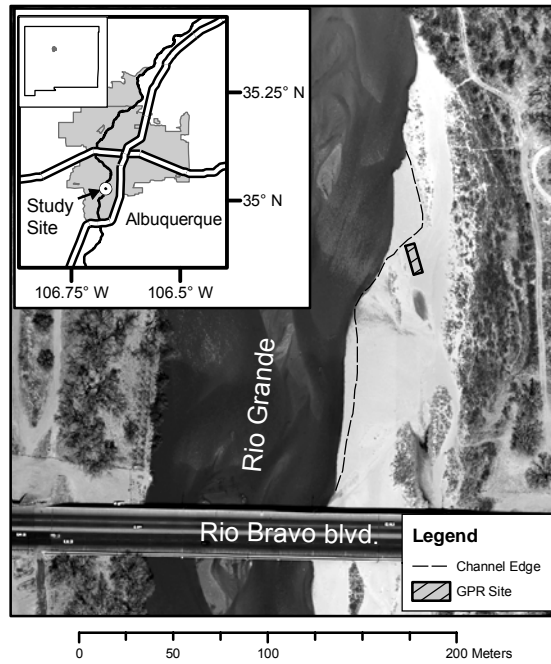


Figure 1. Site location along a channel bar of the main stem of the Rio Grande in southern Albuquerque, NM. Dashed line denotes the channel edge at the time of the GPR survey.

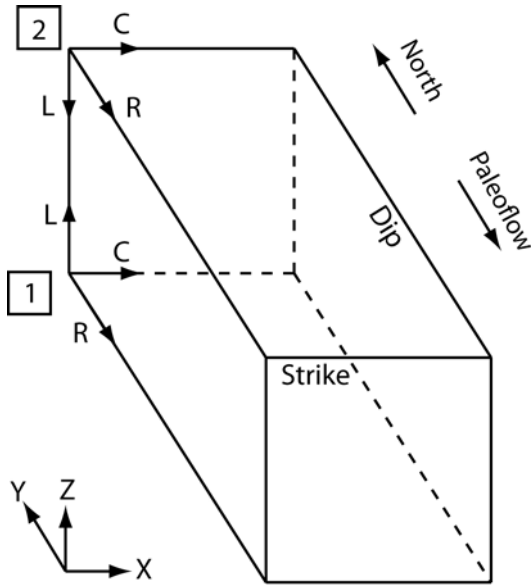


Figure 2. Coordinate system and directional conventions used in the model: 1. InMod origin, 2. MODFLOW 2000 origin. The convention used by TPROGS corresponds to the x-y-z axis show in the lower left. The North and Paleoflow indicators are specific only to this study.

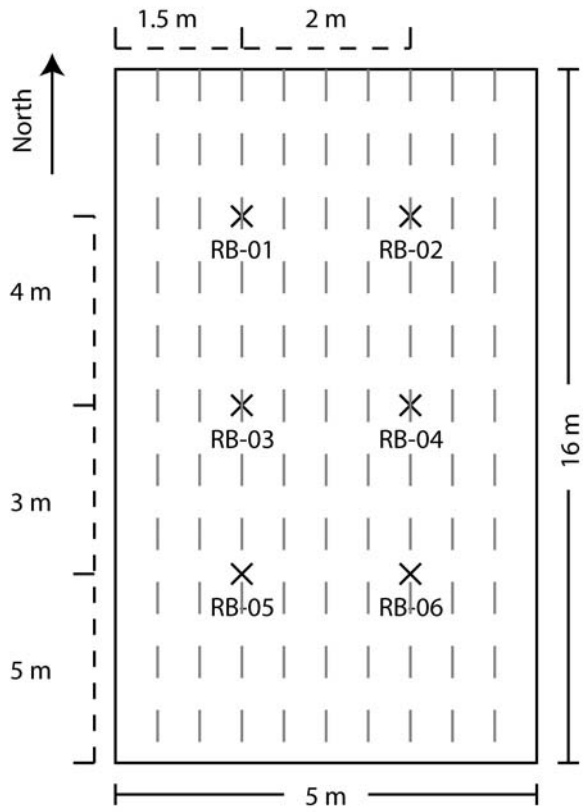


Figure 3. Site data collection layout. Crosses denote locations where core was recovered and the dashed lines indicate the location of the GPR survey lines.

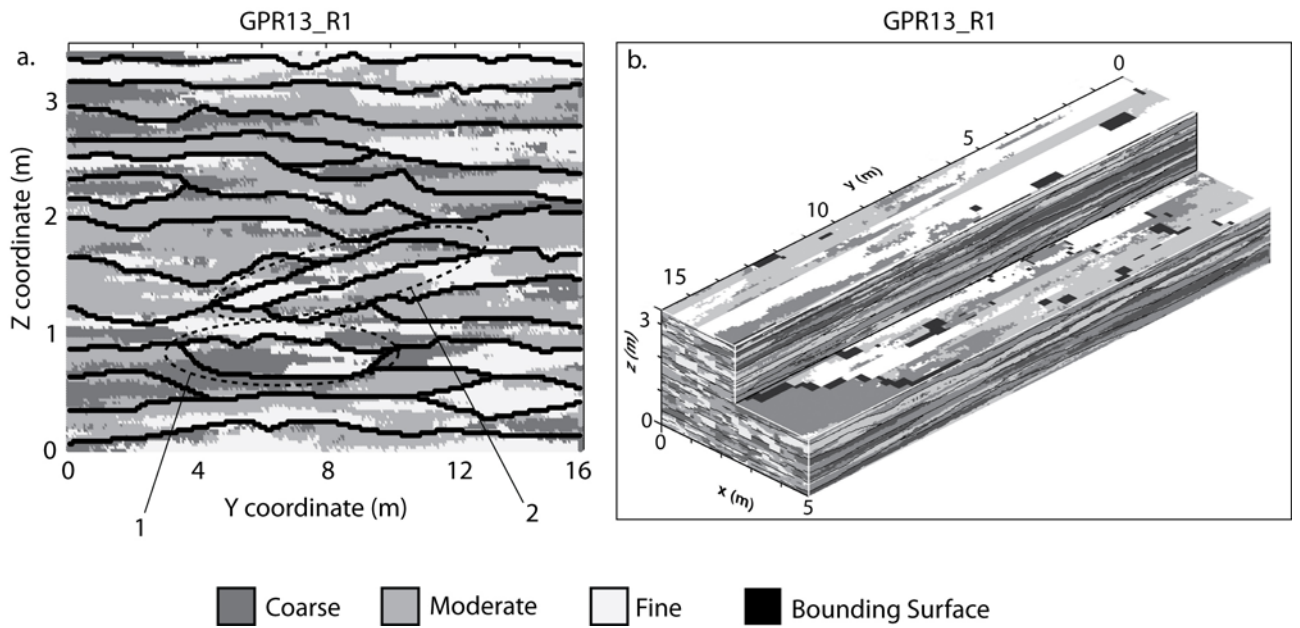


Figure 4. (a) 2-D slice through the center of an InMod realization. Circled region 1 represents a channel scour and region 2 is part of a procession of cross beds. (b) 3-D perspective of the same realization shown in (a) with a section cut away to reveal the interior of the model. In both figures the TPROGS coordinate system is used.

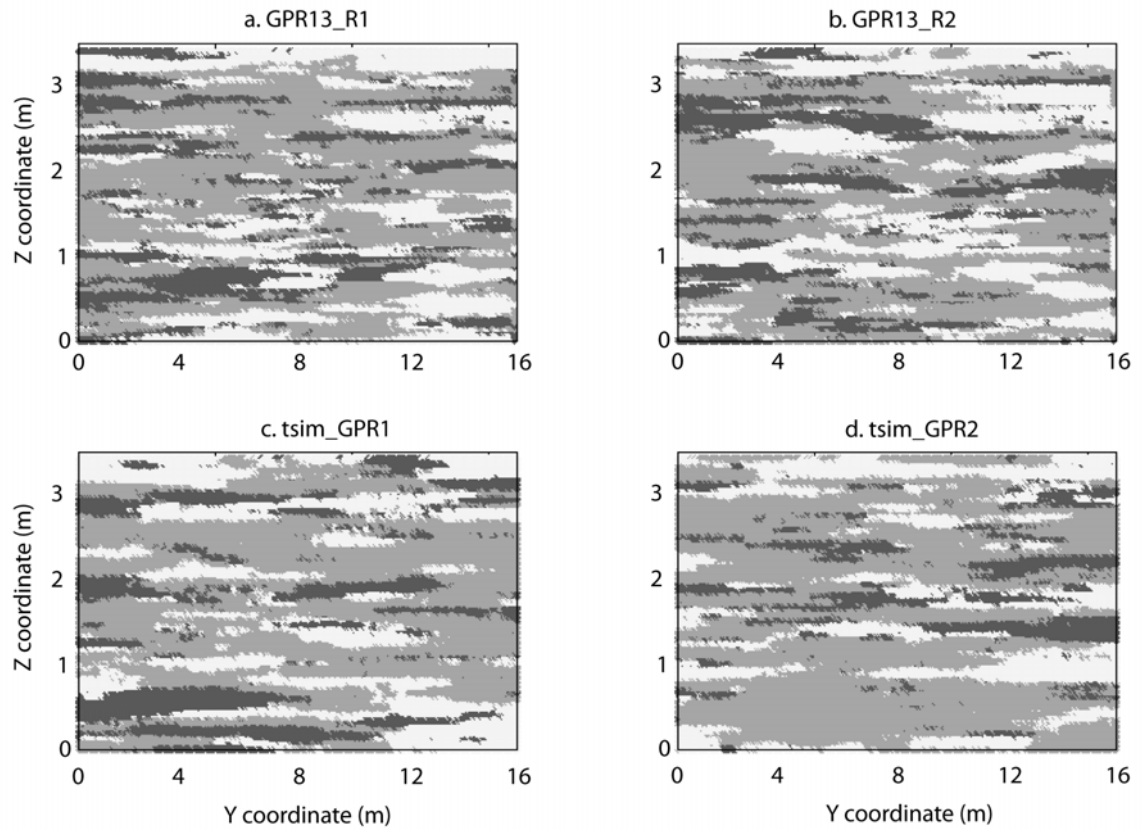


Figure 5. Comparison of selected InMod (a-b) and TPROGS (c-d) heterogeneity models using the TPROGS coordinate convention. Bounding surface locations were omitted for clarity; however, the upper left panel corresponds to the cross section in figure 4 for reference.

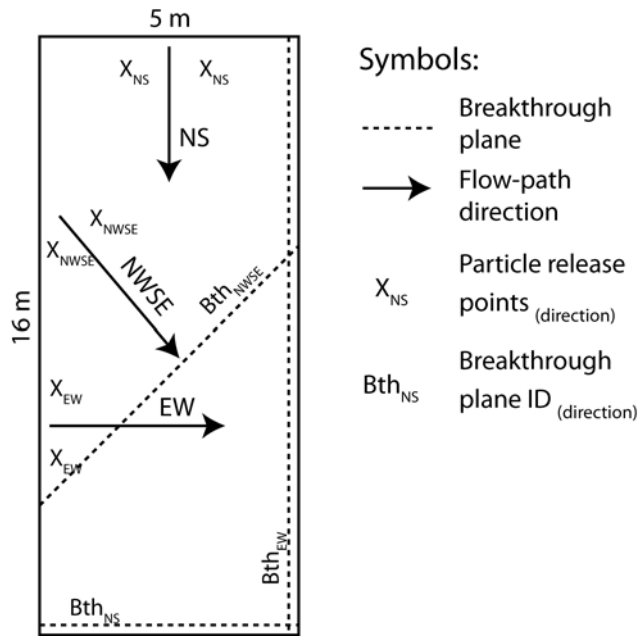


Figure 6. Flow and transport model setup and orientation. The EW particle release points have been shifted south (down) in this image for clarity but were more centrally located for modeling.

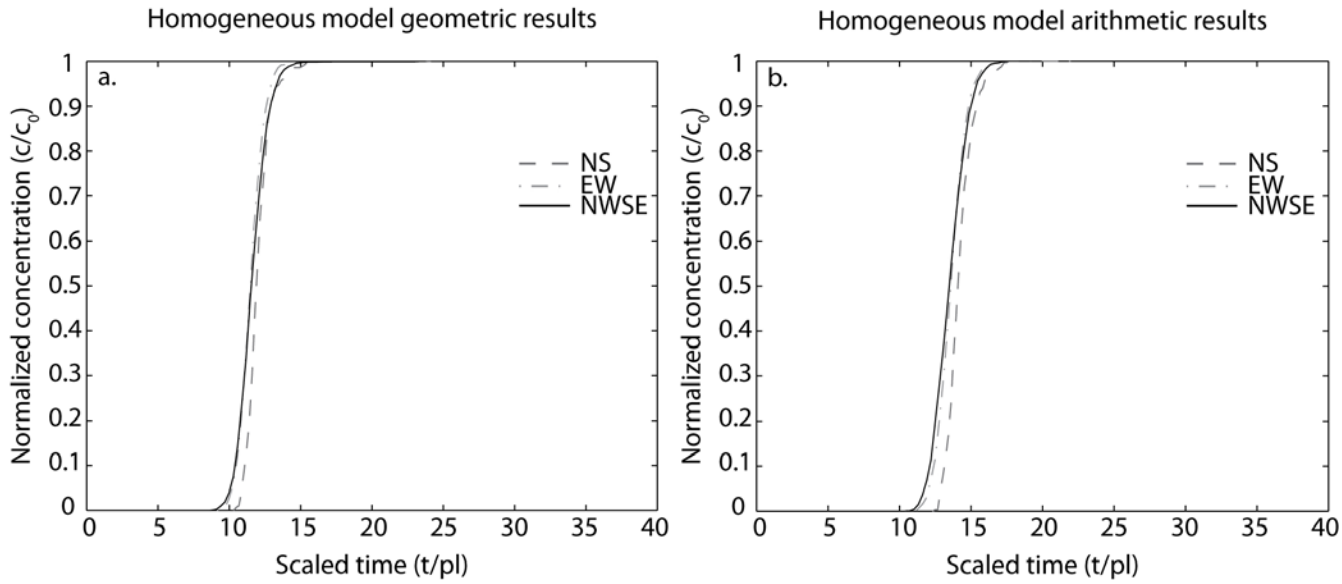


Figure 7. Homogeneous model breakthrough curves for the Geometric (a) and Arithmetic (b) mean hydraulic conductivities.

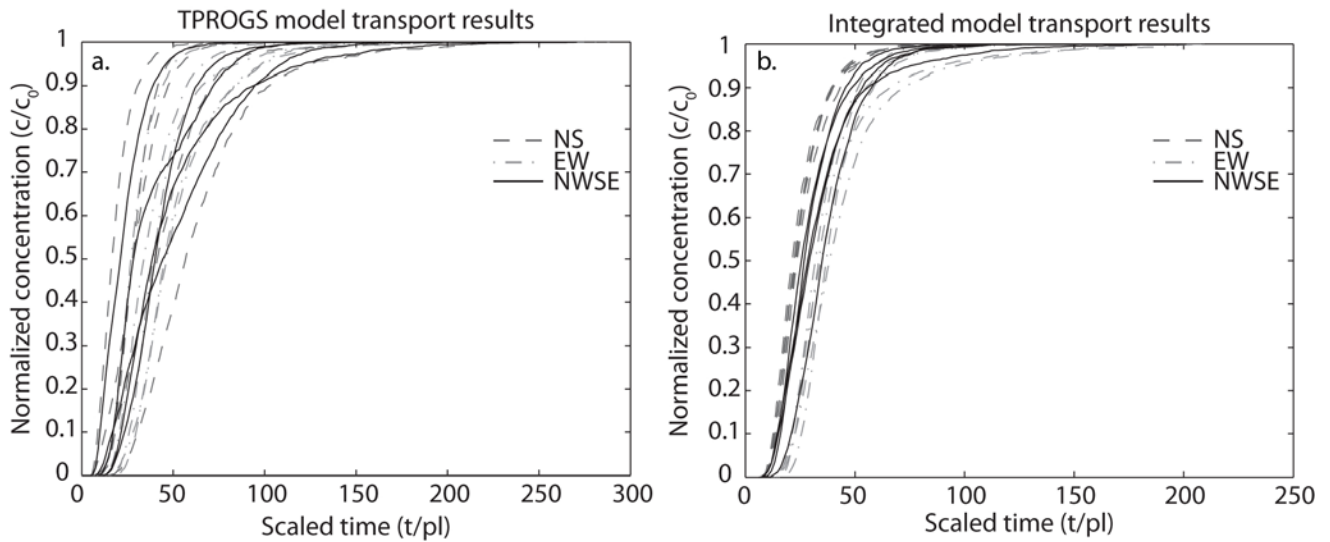


Figure 8. Cumulative breakthrough curves for the five TPROGS (a) and five InMod (b) simulations. Three distinct transport rate regimes can be observed in the InMod results.

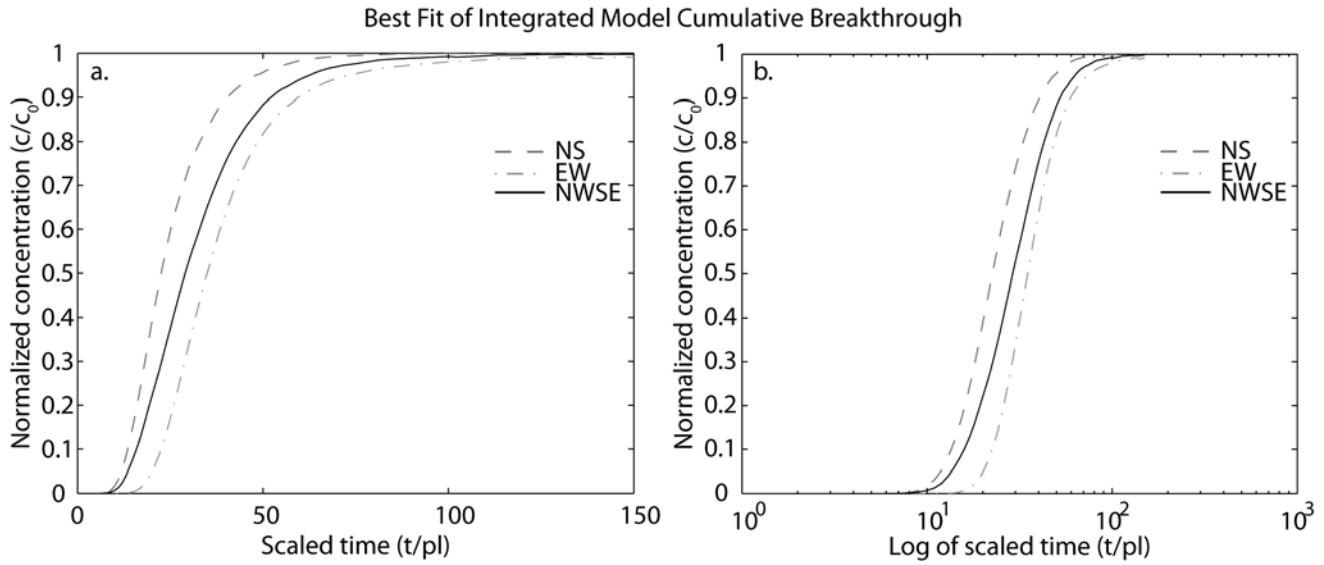


Figure 9. Best fit spline of each of the three model orientations from the InMod results in figure 8b. The fits are shown with linear (a) and logarithmic (b) horizontal axes.

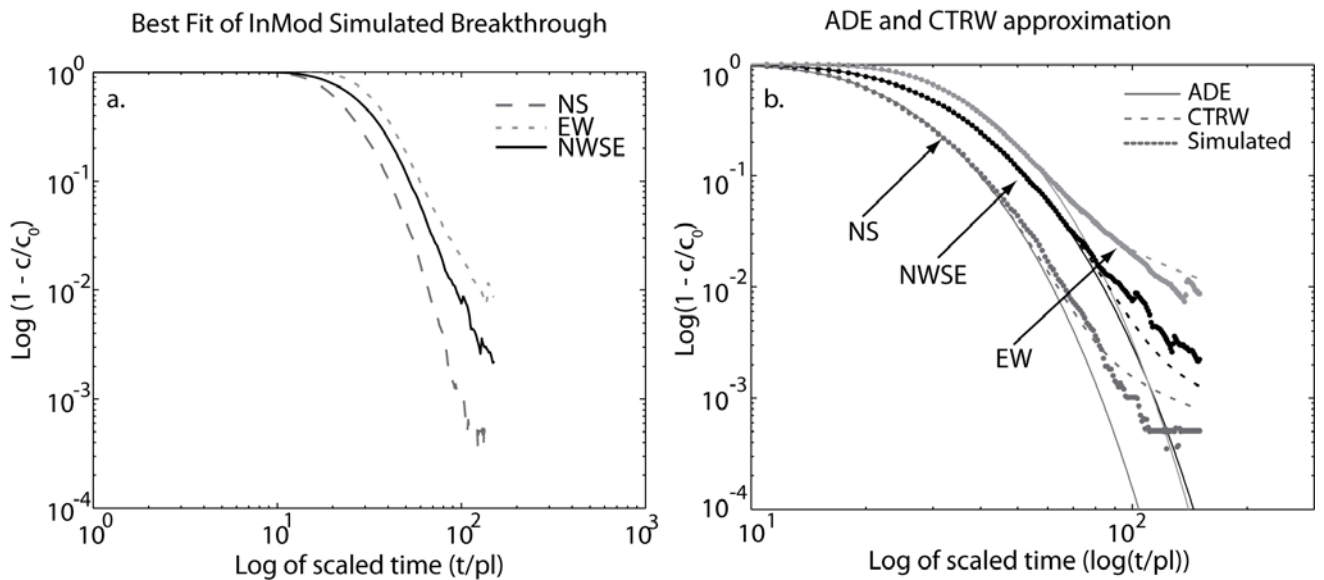


Figure 10. (a) Late time behavior (tails) of the best fit splines of the InMod results and, (b) Comparison of the InMod results to the breakthrough tails fit using the ADE and the asymptotic transition rate model of CTRW. Directionally dependent transport rates are observed throughout the entire breakthrough curve and all profiles deviate from the classical ADE.

Heterogeneity effects on flow and transport within a shallow fluvial aquifer

Nicholas B. Engdahl

Final conclusions

The three chapters of this collection highlight different aspects of the consequences from the assumption of homogeneity. In chapter 1, the assumption of homogeneity produces substantially higher river loss than a heterogeneous model. As the level of heterogeneity is increased, we find that loss decreases. By using previously collected data and quantifying the heterogeneity of the system, we are able to expand our knowledge of the factors that may influence flow through the aquifer at greater resolution than the previously constructed, regional scale models.

The second chapter provides a method for describing subsurface variability at a high resolution. The method (InMod) uses geophysics to delineate major bounding surfaces within the model. The space between bounding surfaces is identified automatically by a simple 3-D region-growing algorithm. The regions are assigned hydrologic property values, using geostatistical realizations, by a lookup routine. The lookup routine may be conditioned to any number of rules based on the geometric properties, such as aspect ratio and center of mass, of the regions identified by the growing algorithm. The models produced with this method are able to reproduce geologically expected features and have higher variance than geostatistics alone was able to produce for the same conditioning data. This method allows us to investigate processes within the a cell of the model in chapter 1.

The final chapter uses the characterization method outlined in chapter 2 to build a high resolution model of flow and transport. We used this model to investigate the directional properties of transport through porous media. It was hypothesized that transport rates should vary with respect to the orientation of bedding. Three types of models were created to evaluate the directional effects of bedding on transport: a homogeneous approximation, heterogeneous models created using geostatistics, and heterogeneous models created with the method developed in chapter 2 (InMod). Flow and transport was simulated in each model in three orientations: parallel to bedding, perpendicular to bedding and an oblique orientation between the first two directions. Of the three methods, only the models created with InMod, which included the sedimentary structures imaged with ground penetrating radar, were able to show consistent regimes of transport rates. The InMod results showed that the fastest transport rates are experienced when flow is parallel to bedding, and the slowest when perpendicular to bedding. The simulated breakthrough curves were fit using non-Fickian and Fickian equations and it was found that the non-Fickian equations better describe the simulated behavior.

These papers challenge hydrogeologists to question when the assumption of homogeneity is necessary and at what scale it should be assumed. Within the same system, we see that different levels of detail are needed to investigate transport as opposed to only flow. As with the flow loss model, a homogeneous assumption in transport results in higher groundwater velocities for a fixed hydraulic gradient. In terms of transport, this means a misrepresentation of the breakthrough curve.

One method for improving ground water models, including the model described in chapter 1 of this volume, would be to create a high resolution model for one cell of

each hydrofacies type and use the transport anisotropy for each hydrofacies in the larger model. A similar method could be applied when transitioning into a regional scale model by which the next smaller scale model enhances the performance of the larger scale. Though the assumption of homogeneity is required in the commonly used finite-difference framework, by quantifying the behavior of flow and transport within the homogeneous "representative" elementary volume we can improve model parameterizations and develop more robust simulations that produce more realistic results.

Appendix A -

**Integrated heterogeneity modeling of geophysical and geostatistical
conditioning data (InMod): general procedures and users manual**

version 1.0

**Nicholas B. Engdahl
Earth and Planetary Science Department
University of New Mexico
Albuquerque, NM 87131**

Table of Contents

Preface.....	111
Release notes.....	111
1.0 - Background.....	112
2.0 - Bounding surfaces and data preparation.....	113
2.1 - Data formats	113
3.0 - Region identification (3dseg)	114
3.1 - Basic functional behavior.....	114
3.2 - Required input files	115
4.0 - Grouping and filling algorithms (con_groups).....	117
4.1 - Basic operation	117
4.2 - Available rules.....	118
4.3 - Known bugs.....	119
4.4 - Geometrically based filling rules.....	119
5.0 - Final Outputs	120
Closing Remarks.....	120

Preface

The collection of programs outlined in this documentation were written for the purposes of expanding the knowledge of groundwater flow and transport systems. The author can only hope that they will be used for such purposes. The program documentation presented here is somewhat generalized since, at the present time, the program has received little refinement beyond the experimental stages. As such, the code is what most users would consider "not very user friendly." As interest arises, the author will refine the code to improve its usefulness and welcomes any questions or comments from persons interested in the application of these routines.

As with many experimental programs, the author can make no claim of responsibility for the accuracy of the programs described herein or the results generated. The programs are supplied as-is with no official support or guarantee of any kind.

Release notes

The versions of the collection of programs contained here are all highly experimental and subject to change without notice. It is highly recommended that, prior to any use of these routines, the practitioner contact the author so that the latest releases or customized versions of the routines may be obtained for the particular application.

1.0 - Background

The integrated heterogeneity modeling of geophysical and geostatistical conditioning data package (InMod) is a collection of programs written to allow the combination of two traditionally incompatible data sources for conditioning subsurface heterogeneity models. The fundamental assumption behind the method is that sedimentary deposits can be described by geostatistics, which can be an appropriate assumption in many cases. Within a sedimentary sequence the degree of stationarity may be different within portions of the deposit or at different scales and methods for describing the variability are needed. The principle used here is similar to the hierarchical approach of *Ritzi* [2000] where bounding surfaces between sedimentary regions are found to mark the change from one probability distribution function (pdf) to another. Here, instead of changing pdf's, we change an aspect of the geostatistics used to describe individual regions. While this may seem to merely be change in terminology, further elaboration will illustrate this is not always the case. This manual is written in the context of a fluvial sedimentary system, since the first application of InMod was applied to such a system. It is important to realize that this method may be applied to nearly any sedimentary system where geophysical and geostatistical data can be collected.

Execution of the programs described herein and the required supplemental programs (a geophysical interpretation suite and a geostatistical modeling package) will result in the generation of a categorical hydrofacies model. All routines and associated programs were written in FORTRAN 95 and are run at the command line prompt. These programs have been successfully compiled and run on Windows XP Professional SP-2 (32-bit OS), two different types of Unix operating systems (different versions of the Sun Unix system) and Windows XP x64 (win32 program running on 64-bit OS). Minor compilation issues have been encountered on the x64 architecture but are in the process of being resolved to create a fully 64 bit, more optimized version of the routines. To execute any of the program routines, place the program executable and all required input files into the same folder and type the name of the routine you wish to run.

2.0 - Bounding surfaces and data preparation

As with any technique that requires several source of input data, we must assume that the reader is familiar with the collection and interpretation of geophysical data. If not, the reader is referred to *Hydrogeophysics* (Rubin, Y. and Hubbard, S.S., eds.) for a crash course in geophysical methods applied to hydrogeology.

The techniques presented here were originally applied to ground penetrating radar (GPR) data but any geophysical method which may be use to create a 2-D or 3-D map of relative dielectric differences in the subsurface may be applied.

2.1 - Data formats

The input data required for the region growing routine is bounding surface locations in 2-D or 3-D. It is crucial that there are no horizontal breaks in the bounding surfaces since the current version of the growing algorithm does not check for such breaks. A routine is available from the author which filters the geophysical data to be only the peaks of the data. These points represent the greatest variability of the local dielectric response and are believed to coincide directly with the bounding surfaces.

A database of bounding surface locations needs to be generated before region growing and matching routine can be applied. This step requires 2-D x,y or 3-D x,y,z coordinate data (as column, row, layer) for all bounding surface locations within the model. Bounding surfaces within the model are treated as indicator variables. All relevant nodes within the model MUST be defined as indicator variables so that all bounding surfaces have a value of 1. The indicator values for the bounding surfaces, from the interpreted geophysical data, are read in to InMod and all other within the prescribed model limits are assumed to have a value of zero. The dimensions of the model are set by the first line of the bounding surface data file and should be in the following order: x,y,z .

Input data for the geostatistical realization used in filling can be generated in any way so long as the output is a single column ascii file, such as that generated by TPROGS. The coordinate convention system for the geostatistics is assumed to be the lower left (the same as TPROGS). Specification of the number of realizations within InMod will be covered later.

3.0 - Region identification (3dseg)

The areas between bounding surfaces are automatically identified by the routine 3dseg. This routine processes the entire model domain as a series of 2-D, long direction (dip) slices (see chapter 2, main volume, for more details on some of the functionality of this routine). The routine "expands" a region, down the model dip direction (increasing in y), until the terminal conditions are met. The terminal conditions may be modified but the current conditions are explained in section 3.1. All modifications to the routine must be made to the source code as the routine is not yet parameter file driven. After modification, the code will need to be recompiled. The final result of this program is a large file containing a database of regions numbers.

3.1 - Basic functional behavior

The initial point which bounding surfaces are searched from is currently set to the lowest model layer, in the first column ($x = 0$) though the last column could be used instead. Given that most sedimentary deposits that make up the worlds aquifers were filled from the bottom up, this seems like a logical starting point for 3dseg. From the initial point, the model advances vertically (increasing in z) until a bounding surface is encountered. From this elevation, the routine calculates the height of the current, bounding surface position above the next lowest surface or the model bottom. The purpose of the height calculation is to determine the midpoint of the region, which is where the routine moves next (decreasing z). From the vertical midpoint, the routine steps one cell along the model dip direction (increasing y) and repeats the vertical search for the next bounding surface. This behavior is notably different from many growing routines or surface tracking routines in that it uses the midpoint of the region instead of following the bounding surface directly. In the case of complex geologic regions formed by an individual period of sedimentation, we believe this routine does a sufficient job of capturing the geometry of the depositional units and the rules for growth based on a midpoint were better understood than for a trace method.

The routine continues the vertical search, center, and step forward routine until one of the following conditions is met: the height of the region goes to zero (convergence of surface limits), the model edge is encountered, or a growth condition is violated. As the first two conditions are self explanatory, only the third terminal condition will be elaborated on. One of the most powerful aspects of this method is the ability to use deterministic rules to constrain the conditions which geometrically define an individual period of deposition. Presently, 3dseg has two conditional statements governing the down-dip growth of regions: a positive change in height threshold and a vertical midpoint shift limit. The vertical midpoint shift condition requires that the midpoint of the current location be within the vertical boundaries of the bounding surfaces of the previous point. This condition, of course, does not apply to the first row (x - z plane) of the model. The second condition may be more easily modified in the source code:

```
! Make sure the next section isn't too big to be the same unit
```

```

If ((cnt .gt. 1) .and. (hh .eq. 3*surfs(cnt-1,6,row))) then

write(*,*) 'Section is TOO tall, removing and ending'
cnt = cnt - 1
write(9,*) 'Failure Condition 0'
MoveOn = .false.
go to 800
EndIf

```

In this excerpt from the 3dseg source, the scaling limit is contained within the If statement as “3*surfs...” indicating that the current vertical slice of the region can be no more than three times the height of the previous point. A condition could easily be added to allow for a minimum threshold as well.

The regional growth routine assigns each region a group number when the growth of the region is terminated. These are assigned sequentially based on the vertical search order. Region numbers are assigned for only one column at a time and are indexed by column and number by the next routine. Once all regions have been processed and assigned their group number, 3dseg generates a large output file containing the x,y,z coordinates of all nodes within the model as well as the region number within that column.

3.2 - Required input files

The growing algorithm routine requires a series of input/output (I/O) filenames. The primary files are:

```

Infile = 'GPR_All_Cols.txt'
Outfile = 'BndTst.txt'
Dbgfile = 'Debug.txt'
Sfile = 'Scratch.txt'

```

It should be noted that some early versions of the source code have a redundant definition of the 'OUTFILE' name from the debugging process and a search should be conducted to verify that the desired file name is specified. The 'INFILE' specifies the name of the file containing the coordinates, x , y , z , a (where a is some arbitrary constant that originally had a purpose), of the bounding surfaces. Note, here the x,y,z coordinates refer to the COLUMN, ROW, and LAYER number, respectively, these are not absolute coordinates. The intent of the a variable was to identify the type of bounding surface within a hierarchy but this has not yet been implemented. The 'OUT' and 'DBG' files are generated by the program and comprise the region number output file to be used in the next routine and the debugging output. The debugging output in this program may not be suppressed at this time, so if you don't want it, delete the file. The 'Sfile' is a scratch file used by the program and is automatically deleted prior to program termination, this file may have any name that does not conflict with other required files.

A note about the bounding surface data input file, the first line of this file determines the size of the model and is identical to a TPROGS ascii header line ($nx ny nz$), however, the y direction convention of InMod is the opposite of TPROGS. This means the row 1 in an InMod model corresponds to the maximum row number in

TPROGS. This confusing concept was created because the growing of the regions in 3dseg mimic the depositional process direction while TPROGS, generally, does not. It is recommended that the perceived direction of deposition be assigned as the long dimension for the creation of InMod realizations.

Development note: The output of this routine can be a potentially huge file (>150Mb). The 64 bit version (x64 architecture, not win32 compatible) will eventually address this issue and store the output of 3dseg as a one byte integer binary grid file to be read into the next routine.

Also in the fully 64 bit version, the explicitly defined variables will be replaced by an include file. All parameters will be set at the beginning of the include file and will not require detailed searching to modify.

4.0 - Grouping and filling algorithms (con_groups)

The output data from 3dseg serves as the input data for the second routine. The two routines were intended to function as one routine but have been retained as separate programs for simpler modification of the grouping rules. The routine 'con_groups' replaces the earlier routine 'groups'. The difference being that 'con_groups' is a conditioned filling routine which is able to honor the geostatistical input data and 'groups' was purely random. The application of the con_groups routine is a two step process. First, the 2-D regions identified by 3dseg are grouped into their 3-D equivalents and second, the 3-D regions are filled with hydrofacies assignments. The final output file mimics a TPROGS ascii output file in format and coordinate system convention. As a minor aside, the final model will be one unit smaller in each direction than the input data to minimize edge effects and search errors associated with close proximity to edges.

4.1 - Basic operation

The con_groups algorithm is far more computationally intensive than 3dseg, primarily because the code has not been streamlined and conducts several seemingly redundant steps which could hypothetically be combined. Any persons wishing to do improve the speed of the routine are certainly welcome to attempt so, the rest of us will wait patiently.

The routine begins processing the output data from 3dseg after reading the file in. As this can take several minutes, a dialog will appear at the command prompt confirming the data has been successfully read in. The grouping routine begins in model column 1 ($x = 0$, y - z plane) with the first region. con_groups then computes several characteristic geometric properties of the region which currently are: the 2-D center of mass (centroid), vertical and lateral limits (y_{min} , y_{max} , z_{min} , z_{max}), area (count of nodes), and the aspect ratio (dz/dy). These are the available parameters for developing rules used in the grouping of adjacent regions. An exception to these parameters was allowed for the case when the centroid lies outside of the region (careful consideration will convince yourself this is possible). In such case the vertical coordinate of the centroid is shifted vertically to be the midpoint of the region at the given position along y , the reason for this will become clear.

After determining the geometric parameters of the current column/region, the routine moves into the next adjacent model slice (column/ y - z plane) at the centroid location of the first column. The geometric parameters of the region in the second column are computed and compared to those of the region in the first column. The parameters are within all prescribed threshold values, the grouping is accepted and the routine will advance to the third model column for comparison to the second and so forth. The lateral growth of the regions is continued until a growth threshold is violated or the edge of the model is encountered. As with the growing algorithm, when a region is terminated it is assigned a group number and the next ungrouped location is used for an initial region until all space within the model has been filled.

Once all regions have been grouped into 3-D volumes, the routine beings to fill in the volumes with hydrofacies values from the geostatistical realizations. The number of available realizations must be set manually within the con_groups program near line 750:

```

root= 'tsim_GPR'    ! base filename
ext = '.asc'       ! base filename extension
Sims = 13          ! number of TSIM realizations available

```

Presently, the realizations are limited to the TPROGS ascii file convention and binary grid files are not accepted. The filling routine assumes that all realizations have the same root, extension and have the distinguishing number immediately following the extension. Also, the routine requires sequential numbering of realizations from 1 to the maximum number (e.g. tsim_GPR.asc1, tsim_GPR.asc2,...tsim_GPR.asc13 for the above code).

The operation of the filling routine begins by computing a 3-D rectangular bounding box of the region to be filled. This box simply uses the 3-D limits of each region as the sides of the box. The program utilizes two modes for geostatistical filling: conditioned and unconditioned. In unconditioned filling, the routine first randomly selects a realization from the available pool to use in filling. The unconditioned mode uses a series of random offsets to determine where within the geostatistical realization the appropriate hydrofacies assignments should be taken from. The routine randomly selects x , y , z offset values with the only requirement being that the offset does not shift the bounding box outside of the model boundaries. When operating in the conditioned filling mode the routine functions quite differently. Using the geostatistical convention of TPROGS, hard conditioned data within the models are represented as the negative value of the corresponding hydrofacies. These correspond to locations within the geostatistical models where actual data exist (usually core samples or geophysical logs). The routine `con_groups` automatically determines if the region possess conditioning data by searching for negative numbers within the geostatistical model. If any negative hydrofacies categories reside within the region, conditioned filling is executed. The known conditioning data are enforced by abandoning the random offset used in unconditioned filling and the actual position within the selected geostatistical realization is used instead. However, it should be noted that even in conditioned filling the realization from which the hydrofacies are assigned is still selected randomly so successive executions of the filling routine will result in different hydrofacies configurations. Conceptually, this routine ensures that regions with conditioning data are true to the field data but the hydrofacies configuration surrounding those data are allowed a degree of uncertainty. Similarly, if no data is available for conditioning, we make no assumption about the location of the region within the pool of possible configurations.

4.2 - Available rules

The geometric matching rules are defined as a series of threshold ratios. Within the source code the matching section begins at label 525, near line 302. Inspection of the code will indicate how the rules function but generally it is the satisfaction of a logical type variable 'match'. The threshold values for the example rule, the size and aspect ratio conditions are given in the following:

```

If ((real(cnt) .lt. (1.5*real(bnds(i-1,j,k,6)))) .and.
+(real(cnt) .gt. (0.5*real(bnds(i-1,j,k,6)))) .and.

```

```

+((AR) .lt. (1.6*real(aspect(i-1,j,k)))) .and.
+((AR) .gt. (0.4*real(aspect(i-1,j,k)))) then

```

The threshold for size (cnt) is set as +/- 50% and the threshold for aspect ratio is +/- 60%. Additional rules may be added inline and the storage location of all geometric parameters stored in 'bnds' are indicated on line 225 and the aspect ratio values are stored as the index data in the array 'aspect'.

4.3 - Known bugs

For reasons beyond the understanding of the author, occasionally the filling routine will become stuck in a seemingly infinite loop. This behavior will be obvious because one of the following will occur: the output to the terminal will stop updating, or the output will repeat the same section on a more frequent basis than the initial processing period. In either event, the user must manually interrupt the program execution by pressing ctrl+c on the keyboard (for Windows OS) and the routine must be restarted. Input files will be unaffected by this and any output generated up to this point, including the debugging file, will be saved. Outputs will be overwritten when the program is executed again. It is suspected that this seemingly infinite loop is a case where the random number generator is being called too frequently between seed initializations or that duplicate numbers are being generated. Regardless, since the problem is infrequent no further efforts were put into resolving the issue at this time. As an interesting point, this bug has not been observed while running on a 64 bit computer.

4.4 - Geometrically based filling rules

One potentially powerful capability of this method that has not yet been implemented, but deserves mention, is to use the previously computed geometric parameters to determine a class of geostatistical realizations to use. In many depositional environments, fluvial for this case, different flow regimes will generally produce very different deposits. This results in variation the final geometric parameters of these regions. For example, it can be expected that low energy floodplain deposits will be more uniform in hydraulic character and be thinner than within channel aggradational deposits. It may be reasonable in such a case to define these regions using a rule involving the aspect ratio of the deposit. If these regions can be confidently delineated on the basis of any geometric parameter, or combination of parameters, and a series of separate geostatistical models can be generated to describe the field deposits, they may be filled separately. As with the other rules this would be threshold based so, for example, regions having an aspect ratio less than 0.5 would be filled from pool "A" of geostatistical realizations and all other aspect ratios would be filled from pool "B" of realizations. This was not implemented in the initial application of the InMod suite because the core used in TPROGS modeling was not recovered in a great enough percentage for correlations of this nature to be conducted. It may also be possible to incorporate other features like the orientation of the deposit to more accurately capture cross bed sets though this has not been investigated.

5.0 - Final Outputs

The final output of the InMod package is a single column ascii file with a three integer heading row. As with most matrix conventions, the first line contains the x , y , and z dimensions of the rectangular grid but the order is of the TPROGS lower left corner convention. The matrix cycles first in x (increasing from left to right), then y (increasing up), and finally z (also increasing in the upward direction). For comparison, MODFLOW requires the upper left convention where the matrix cycles in x (increasing from left to right), then y (increasing towards the bottom), and finally z (increasing downward). For conversion of the InMod output file to the MODFLOW convention, the author has several programs to convert into various formats or the user may write their own. For example images of the realizations, 2-D cross sections and additional details on the use of the final modes please refer to chapters 2 and 3 of this volume.

Closing Remarks

The author hopes that this program will be useful in future hydrologic investigations needing to combine geophysical and geostatistical data in sedimentary aquifers and welcomes any question, comments, or suggestions related to this work.

Appendix B -

Input data for TPROGS geostatistical package

**Nicholas B. Engdahl
Earth and Planetary Science Department
University of New Mexico
Albuquerque, NM 87131**

Table of Contents

Explanation of the data	123
1.0 - MCMOD parameter files.....	124
1.1 - Based on the measured geostatistics/data.....	124
1.2 - Based on the embedded transition probabilities.....	125
2.0 - TSIM Parameter File	126
3.0 - GEOEAS Input file.....	127
4.0 - Supplemental stratigraphic columns.....	141
Rio Bravo, East side, southern transect	142
Rio Bravo, East side, northern transect.....	143
Rio Bravo, West side, southern transect.....	144
Rio Bravo, West side, northern transect	145

Explanation of the data

The data file contained within this appendix is composed of three sections: the MCMOD and TSIM parameter files and the GEOEAS input data. Those not familiar with the use and operation of the TPROGS package are referred to *Carle and Fogg* [1996] and *Carle* [1999] (citations found in chapter 1 of this volume). As an aside, the simulations were conducted using a modified version of the original TSIM.f program. Only minor changes were made to create a one byte integer, binary grid output for use in RWHET and well as reduction of the size of the integer size in the ascii versions. Also, the include file was increased to allow for the processing of a model of increased size.

Soft conditioning was implemented in the GEOEAS file. For those unfamiliar with this practice this is a way of allowing a probability of occurrence of a hydrofacies type instead of specifying an individual hydrofacies. Further details of this practice can be found in chapter 1 of this volume.

1.0 - MCMOD parameter files

1.1 - *Based on the measured geostatistics/data*

```
3
0.189 0.554 0.257
3
../mcmmod/mcmmod.dbg
../GPRLith/MCMOD/GPR_tp_xyz.bgr
../GPRLith/MCMOD/GPR_det.bgr
0.05 0.05 0.05
0.06 0.06 0.024
../GPRLith/MCMOD/GPR_tpx_m1.eas
500 0.01
2
../GPRLith/GAMEAS/GPR_tpx.eas
1
../GPRLith/MCMOD/GPR_tpy_m1.eas
500 0.032
2
../GPRLith/GAMEAS/GPR_tpy.eas
1
../GPRLith/MCMOD/GPR_tpz_m1.eas
500 0.007
2
../GPRLith/GAMEAS/GPR_tpz.eas
1
```

1.2 - Based on the embedded transition probabilities

```
3
0.253 0.465 0.282
2
../mcmmod/mcmmod.dbg
../GPRLith/MCMOD/lith_tp_xyz.bgr
../GPRLith/MCMOD/lith_det.bgr
0.03 0.03 0.03
0.06 0.06 0.024
../GPRLith/MCMOD/lith_tpx_mle.eas
500 0.002
3
0.2390 0.8920 0.1080
0.6970 0.3316 0.3030
0.1500 0.8500 0.5237
../GPRLith/MCMOD/lith_tpy_mle.eas
500 0.002
3
4 0.8920 0.1080
0.6970 6 0.3030
0.1500 0.8500 5
../GPRLith/MCMOD/lith_tpz_mle.eas
500 0.002
3
0.3 0.5730 0.4270
0.6380 0.5 0.3620
0.60 0.5700 0.3
```

2.0 - TSIM Parameter File

```
3
0.189 0.554 0.257
../TSIM/tsim_GPR.asc
2
2
../tsim/tsim.dbg
4175
1
0 84 0.06
0 268 0.06
0 144 0.024
1 1
1
0.001
../MCMOD/GPR_tp_xyz.bgr
../MCMOD/GPR_det.bgr
../RGRB_final.eas
0. 0.
0. 0.
junk.bgr
junk.bgr
0 9.98341748397e-005 1
0.01
```

3.0 - GEOEAS Input file

Core description from GPR site - FINAL VERSION 09.28.2008

6

x = model strike direction (m)

y = model dip direction (m)

z = relative elevation (m)

1 = Coarse Sands

2 = Medium Sands

3 = Fine Sands

1.5	12	3.50	0	0	1
1.5	12	3.49	0	0	1
1.5	12	3.48	0	0	1
1.5	12	3.47	0	0	1
1.5	12	3.46	0	0	1
1.5	12	3.45	0	0	1
1.5	12	3.44	0	0	1
1.5	12	3.43	0	0	1
1.5	12	3.42	0	0	1
1.5	12	3.41	0	0.3	0.7
1.5	12	3.40	0	0.3	0.7
1.5	12	3.39	0	0.3	0.7
1.5	12	3.38	0	0.3	0.7
1.5	12	3.37	0	0.3	0.7
1.5	12	3.36	0	0.3	0.7
1.5	12	3.35	0	0.3	0.7
1.5	12	3.34	0	0.3	0.7
1.5	12	3.33	0	0.3	0.7
1.5	12	3.32	0	0.3	0.7
1.5	12	3.31	0	0.7	0.3
1.5	12	3.30	0	0.7	0.3
1.5	12	3.29	0	0.7	0.3
1.5	12	3.28	0	0.7	0.3
1.5	12	3.27	0	0.7	0.3
1.5	12	3.26	0	0.7	0.3
1.5	12	3.25	0	0.7	0.3
1.5	12	3.24	0	0.7	0.3
1.5	12	3.23	0	1	0
1.5	12	3.22	0	1	0
1.5	12	3.21	0	1	0
1.5	12	3.20	0	1	0
1.5	12	3.19	0	1	0
1.5	12	3.18	0	1	0
1.5	12	3.17	0	1	0
1.5	12	3.16	0	1	0
1.5	12	3.15	0	1	0
1.5	12	3.14	0	1	0
1.5	12	3.13	0	1	0
1.5	12	3.12	0	1	0
1.5	12	3.11	0	1	0
1.5	12	3.10	0	1	0
1.5	12	3.09	0	1	0
1.5	12	3.08	0	1	0
1.5	12	3.07	0.1	0.9	0
1.5	12	3.06	0.2	0.8	0

1.5	12	3.05	0.3	0.7	0
1.5	12	3.04	0.4	0.6	0
1.5	12	3.03	0.5	0.5	0
1.5	12	3.02	0.6	0.4	0
1.5	12	3.01	0.7	0.3	0
1.5	12	3.00	0.8	0.2	0
1.5	12	2.99	0.9	0.1	0
1.5	12	2.98	1	0	0
1.5	12	2.97	1	0	0
1.5	12	2.96	1	0	0
1.5	12	2.95	1	0	0
1.5	12	2.94	1	0	0
1.5	12	2.93	1	0	0
1.5	12	2.92	1	0	0
1.5	12	2.91	1	0	0
1.5	12	2.90	1	0	0
1.5	12	2.28	0	0.9	0.1
1.5	12	2.27	0	0.9	0.1
1.5	12	2.26	0	0.9	0.1
1.5	12	2.25	0	0.9	0.1
1.5	12	2.24	0	0.9	0.1
1.5	12	2.23	0	0.9	0.1
1.5	12	2.22	0	0.9	0.1
1.5	12	2.21	0	0.9	0.1
1.5	12	2.20	0	0.9	0.1
1.5	12	2.19	0	0.9	0.1
1.5	12	2.18	0	0.9	0.1
1.5	12	2.17	0	1	0
1.5	12	2.16	0	1	0
1.5	12	2.15	0	1	0
1.5	12	2.14	0	1	0
1.5	12	2.13	0	1	0
1.5	12	2.12	0	1	0
1.5	12	2.11	0	1	0
1.5	12	2.10	0	1	0
1.5	12	2.09	0	1	0
1.5	12	2.08	0	1	0
1.5	12	2.07	0	1	0
1.5	12	2.06	0.2	0.8	0
1.5	12	2.05	0.4	0.6	0
1.5	12	2.04	0.6	0.4	0
1.5	12	2.03	0.8	0.2	0
1.5	12	2.02	1	0	0
1.5	12	2.01	1	0	0
1.5	12	2.00	1	0	0
1.5	12	1.99	1	0	0
1.5	12	1.98	1	0	0
1.5	12	1.97	1	0	0
1.5	12	1.96	1	0	0
1.5	12	1.95	0.8	0.2	0
1.5	12	1.94	0.6	0.4	0
1.5	12	1.93	0.4	0.6	0
1.5	12	1.92	0.2	0.8	0
1.5	12	1.91	0	1	0
1.5	12	1.90	0	1	0
1.5	12	1.89	0	1	0
1.5	12	1.88	0	1	0

1.5	12	1.87	0	1	0
1.5	12	1.86	0	1	0
1.5	12	1.85	0.3	0.7	0
1.5	12	1.84	0.3	0.7	0
1.5	12	1.83	0.3	0.7	0
1.5	12	1.82	0.3	0.7	0
1.5	12	1.81	0.3	0.7	0
1.5	12	1.80	0.3	0.7	0
1.5	12	1.79	0.3	0.7	0
1.5	12	1.78	0.3	0.7	0
1.5	12	1.77	0.3	0.7	0
1.5	12	1.76	1	0	0
1.5	12	1.75	1	0	0
1.5	12	1.74	1	0	0
1.5	12	1.73	1	0	0
1.5	12	1.72	1	0	0
1.5	12	1.71	1	0	0
1.5	12	1.70	1	0	0
1.5	12	1.69	0.9	0.1	0
1.5	12	1.68	0.7	0.3	0
1.5	12	1.67	0.5	0.5	0
1.5	12	1.66	0.5	0.5	0
1.5	12	1.65	0.7	0.3	0
1.5	12	1.64	0.9	0.1	0
1.5	12	1.63	0	1	0
1.5	12	1.62	0	1	0
1.5	12	1.61	0	1	0
1.5	12	1.60	0	1	0
1.5	12	1.59	0	1	0
1.5	12	1.58	0	1	0
1.5	12	1.57	0	1	0
1.5	12	1.56	0	1	0
1.5	12	1.55	0	1	0
1.5	12	1.54	0	1	0
1.5	12	1.53	0.2	0.8	0
1.5	12	1.52	0.2	0.8	0
1.5	12	1.51	0.2	0.8	0
1.5	12	1.50	0.2	0.8	0
1.5	12	1.49	0.2	0.8	0
1.5	12	1.48	0.2	0.8	0
1.5	12	1.47	0.2	0.8	0
1.5	12	1.46	0.2	0.8	0
1.5	12	1.45	0.2	0.8	0
1.5	12	1.44	0.2	0.8	0
1.5	12	1.43	0.2	0.8	0
3.5	12	3.50	0	0	1
3.5	12	3.49	0	0	1
3.5	12	3.48	0	0	1
3.5	12	3.47	0	0	1
3.5	12	3.46	0	0	1
3.5	12	3.45	0	0	1
3.5	12	3.44	0	0	1
3.5	12	3.43	0	0	1
3.5	12	3.42	0	0	1
3.5	12	3.41	0	0	1
3.5	12	3.40	0	0	1
3.5	12	3.39	0	0	1

3.5	12	3.38	0	0	1
3.5	12	3.37	0	0	1
3.5	12	3.36	0	0	1
3.5	12	3.35	0	0	1
3.5	12	3.34	0	0	1
3.5	12	3.33	0	0	1
3.5	12	3.32	0	0	1
3.5	12	3.31	0	0	1
3.5	12	3.30	0	0	1
3.5	12	3.29	0	0	1
3.5	12	3.28	0	0	1
3.5	12	3.27	0	0	1
3.5	12	3.26	0	0	1
3.5	12	3.25	0	0	1
3.5	12	3.24	0	0	1
3.5	12	3.23	0	0	1
3.5	12	3.22	0	0	1
3.5	12	3.21	0	0	1
3.5	12	3.20	0	0	1
3.5	12	3.19	0	0.1	0.9
3.5	12	3.18	0	0.2	0.8
3.5	12	3.17	0	0.3	0.7
3.5	12	3.16	0	0.3	0.7
3.5	12	3.15	0	0.4	0.6
3.5	12	3.14	0	0.5	0.5
3.5	12	3.13	0	0.5	0.5
3.5	12	3.12	0	0.6	0.4
3.5	12	3.11	0	0.6	0.4
3.5	12	3.10	0	0.7	0.3
3.5	12	3.09	0	0.8	0.2
3.5	12	3.08	0	0.9	0.1
3.5	12	3.07	0	1	0
3.5	12	3.06	0	1	0
3.5	12	3.05	0	1	0
3.5	12	3.04	0	1	0
3.5	12	3.03	0	1	0
3.5	12	3.02	0	1	0
3.5	12	3.01	0	1	0
3.5	12	3.00	0	1	0
3.5	12	2.99	0	1	0
3.5	12	2.28	1	0	0
3.5	12	2.27	1	0	0
3.5	12	2.26	1	0	0
3.5	12	2.25	1	0	0
3.5	12	2.24	1	0	0
3.5	12	2.23	0	1	0
3.5	12	2.22	0	1	0
3.5	12	2.21	0	1	0
3.5	12	2.20	0	1	0
3.5	12	2.19	0	1	0
3.5	12	2.18	0	1	0
3.5	12	2.17	0	1	0
3.5	12	2.16	0	1	0
3.5	12	2.15	0	1	0
3.5	12	2.14	0	1	0
3.5	12	2.13	0	1	0
3.5	12	2.12	0	1	0

3.5	12	2.11	0	1	0
3.5	12	2.10	0	1	0
3.5	12	2.09	0	1	0
3.5	12	2.08	0	1	0
3.5	12	2.07	0	1	0
3.5	12	2.06	0	1	0
3.5	12	2.05	0.1	0.9	0
3.5	12	2.04	0.2	0.8	0
3.5	12	2.03	0.3	0.7	0
3.5	12	2.02	0.4	0.6	0
3.5	12	2.01	0.5	0.5	0
3.5	12	2.00	0.6	0.4	0
3.5	12	1.99	0.7	0.3	0
3.5	12	1.98	0.8	0.2	0
3.5	12	1.97	1	0	0
3.5	12	1.96	1	0	0
3.5	12	1.95	1	0	0
3.5	12	1.94	1	0	0
3.5	12	1.93	1	0	0
3.5	12	1.92	1	0	0
3.5	12	1.91	1	0	0
3.5	12	1.90	1	0	0
3.5	12	1.89	1	0	0
3.5	12	1.88	1	0	0
3.5	12	1.87	0.5	0.5	0
3.5	12	1.86	0.5	0.5	0
3.5	12	1.85	0.5	0.5	0
3.5	12	1.84	0.5	0.5	0
3.5	12	1.83	0.5	0.5	0
3.5	12	1.82	0.5	0.5	0
3.5	12	1.81	0.5	0.5	0
3.5	12	1.80	0.5	0.5	0
3.5	12	1.79	0.5	0.5	0
3.5	12	1.78	0.5	0.5	0
3.5	12	1.77	0.5	0.5	0
3.5	12	1.76	0.5	0.5	0
3.5	12	1.75	0.5	0.5	0
3.5	12	1.74	0.5	0.5	0
3.5	12	1.73	0.5	0.5	0
3.5	12	1.72	0.7	0.3	0
3.5	12	1.71	0.7	0.3	0
3.5	12	1.70	0.7	0.3	0
3.5	12	1.69	0.7	0.3	0
3.5	12	1.68	0.7	0.3	0
3.5	12	1.67	0.7	0.3	0
3.5	12	1.66	0.7	0.3	0
3.5	12	1.65	0.7	0.3	0
3.5	12	1.64	0.7	0.3	0
3.5	12	1.63	0.7	0.3	0
3.5	12	1.62	0.7	0.3	0
3.5	12	1.61	0.7	0.3	0
3.5	12	1.60	0.7	0.3	0
3.5	12	1.59	0.7	0.3	0
3.5	12	1.58	0.7	0.3	0
3.5	12	1.57	0.7	0.3	0
3.5	12	1.56	0.7	0.3	0
3.5	12	1.55	0.7	0.3	0

3.5	12	1.54	0	1	0
3.5	12	1.53	0	1	0
3.5	12	1.52	0	1	0
3.5	12	1.51	0	1	0
3.5	12	1.50	0	1	0
3.5	12	1.49	0	1	0
3.5	12	1.48	0	1	0
3.5	12	1.47	0	1	0
3.5	12	1.46	0	1	0
3.5	12	1.45	0	1	0
3.5	12	1.44	0	1	0
1.5	8	3.50	0	0	1
1.5	8	3.49	0	0	1
1.5	8	3.48	0	0	1
1.5	8	3.47	0	0	1
1.5	8	3.46	0	0	1
1.5	8	3.45	0	0	1
1.5	8	3.44	0	0	1
1.5	8	3.43	0	0	1
1.5	8	3.42	0	0	1
1.5	8	3.41	0	1	0
1.5	8	3.40	0	1	0
1.5	8	3.39	0	1	0
1.5	8	3.38	0	1	0
1.5	8	3.37	0	0	1
1.5	8	3.36	0	0	1
1.5	8	3.35	0	0	1
1.5	8	3.34	0	0	1
1.5	8	3.33	0	0	1
1.5	8	3.32	0	0	1
1.5	8	3.31	0	0	1
1.5	8	3.30	0	0	1
1.5	8	3.29	0	0	1
1.5	8	3.28	0	0	1
1.5	8	3.27	0	0	1
1.5	8	3.26	0	0	1
1.5	8	3.25	0	0	1
1.5	8	3.24	0	0.3	0.7
1.5	8	3.23	0	0.5	0.5
1.5	8	3.22	0	0.7	0.3
1.5	8	3.21	0	1	0
1.5	8	3.20	0	1	0
1.5	8	3.19	0	1	0
1.5	8	3.18	0	1	0
1.5	8	3.17	0	1	0
1.5	8	3.16	0	1	0
1.5	8	3.15	0	1	0
1.5	8	3.14	0	1	0
1.5	8	3.13	0	1	0
1.5	8	3.12	0	1	0
1.5	8	3.11	0.1	0.9	0
1.5	8	3.10	0.1	0.9	0
1.5	8	3.09	0.1	0.9	0
1.5	8	3.08	0.1	0.9	0
1.5	8	3.07	0.1	0.9	0
1.5	8	3.06	0.2	0.8	0
1.5	8	3.05	0.2	0.8	0

1.5	8	3.04	0.2	0.8	0
1.5	8	3.03	0.2	0.8	0
1.5	8	3.02	0.2	0.8	0
1.5	8	3.01	0.2	0.8	0
1.5	8	3.00	0.2	0.8	0
1.5	8	2.99	0.3	0.7	0
1.5	8	2.98	0.3	0.7	0
1.5	8	2.97	0.3	0.7	0
1.5	8	2.96	0.3	0.7	0
1.5	8	2.95	0.3	0.7	0
1.5	8	2.28	0	1	0
1.5	8	2.27	0	1	0
1.5	8	2.26	0	1	0
1.5	8	2.25	0.2	0.8	0
1.5	8	2.24	0.2	0.8	0
1.5	8	2.23	0.2	0.8	0
1.5	8	2.22	0.2	0.8	0
1.5	8	2.21	0.2	0.8	0
1.5	8	2.20	0	1	0
1.5	8	2.19	0	1	0
1.5	8	2.18	0	1	0
1.5	8	2.17	0	1	0
1.5	8	2.16	0	1	0
1.5	8	2.15	0	1	0
1.5	8	2.14	0	1	0
1.5	8	2.13	0	1	0
1.5	8	2.12	0	1	0
1.5	8	2.11	0	1	0
1.5	8	2.10	0	1	0
1.5	8	2.09	0	1	0
1.5	8	2.08	0	1	0
1.5	8	2.07	0	1	0
1.5	8	2.06	0	1	0
1.5	8	2.05	0	1	0
1.5	8	2.04	0	1	0
1.5	8	2.03	0	1	0
1.5	8	2.02	0	1	0
1.5	8	2.01	0	1	0
1.5	8	2.00	0	1	0
1.5	8	1.99	0	1	0
1.5	8	1.98	0	1	0
1.5	8	1.97	0.1	0.9	0
1.5	8	1.96	0.1	0.9	0
1.5	8	1.95	0.1	0.9	0
1.5	8	1.94	0.1	0.9	0
1.5	8	1.93	0.1	0.9	0
1.5	8	1.92	0.1	0.9	0
1.5	8	1.91	0.1	0.9	0
1.5	8	1.90	0.1	0.9	0
1.5	8	1.89	0.1	0.9	0
1.5	8	1.88	0.1	0.9	0
1.5	8	1.87	0.1	0.9	0
1.5	8	1.86	0.2	0.8	0
1.5	8	1.85	0.2	0.8	0
1.5	8	1.84	0.2	0.8	0
1.5	8	1.83	0.3	0.7	0
1.5	8	1.82	0.3	0.7	0

1.5	8	1.81	0.3	0.7	0
1.5	8	1.80	1	0	0
1.5	8	1.79	1	0	0
1.5	8	1.78	1	0	0
1.5	8	1.77	1	0	0
1.5	8	1.76	1	0	0
1.5	8	1.75	1	0	0
1.5	8	1.74	1	0	0
1.5	8	1.73	0	1	0
1.5	8	1.72	0	1	0
1.5	8	1.71	0	1	0
1.5	8	1.70	0	1	0
1.5	8	1.69	0	1	0
1.5	8	1.68	0	1	0
1.5	8	1.67	0	1	0
1.5	8	1.66	0	0.7	0.3
1.5	8	1.65	0	0.7	0.3
1.5	8	1.64	0	0.7	0.3
1.5	8	1.63	0	0.7	0.3
1.5	8	1.62	0	0.7	0.3
1.5	8	1.61	0	0.7	0.3
1.5	8	1.60	0	0.7	0.3
1.5	8	1.59	0	0.7	0.3
1.5	8	1.58	0	0.7	0.3
1.5	8	1.57	0	0.7	0.3
1.5	8	1.56	0	0.7	0.3
1.5	8	1.55	0	0.7	0.3
1.5	8	1.54	0	0.7	0.3
3.5	8	3.50	0	0	1
3.5	8	3.49	0	0	1
3.5	8	3.48	0	0	1
3.5	8	3.47	0	0	1
3.5	8	3.46	0	0	1
3.5	8	3.45	0	0	1
3.5	8	3.44	0	0	1
3.5	8	3.43	0	0	1
3.5	8	3.42	0	0	1
3.5	8	3.41	0	0	1
3.5	8	3.40	0	0	1
3.5	8	3.39	0	0	1
3.5	8	3.38	0	0	1
3.5	8	3.37	0	0	1
3.5	8	3.36	0	0	1
3.5	8	3.35	0	0	1
3.5	8	3.34	0	0	1
3.5	8	3.33	0	0	1
3.5	8	3.32	0	0	1
3.5	8	3.31	0	0	1
3.5	8	3.30	0	0	1
3.5	8	3.29	0	0	1
3.5	8	3.28	0	0	1
3.5	8	3.27	0	0	1
3.5	8	3.26	0	0	1
3.5	8	3.25	0	0	1
3.5	8	3.24	0	0	1
3.5	8	3.23	0	0	1
3.5	8	3.22	0	0	1

3.5	8	3.21	0	0	1
3.5	8	3.20	0	0.5	0.5
3.5	8	3.19	0	0.5	0.5
3.5	8	3.18	0	0.5	0.5
3.5	8	3.17	0	0.5	0.5
3.5	8	3.16	0	0.5	0.5
3.5	8	3.15	0	0.5	0.5
3.5	8	3.14	0	0.5	0.5
3.5	8	3.13	0	0.5	0.5
3.5	8	2.28	0	1	0
3.5	8	2.27	0	1	0
3.5	8	2.26	0	1	0
3.5	8	2.25	0	1	0
3.5	8	2.24	0	1	0
3.5	8	2.23	0	1	0
3.5	8	2.22	0	1	0
3.5	8	2.21	0.3	0.7	0
3.5	8	2.20	0.3	0.7	0
3.5	8	2.19	0.3	0.7	0
3.5	8	2.18	0	1	0
3.5	8	2.17	0	1	0
3.5	8	2.16	0	1	0
3.5	8	2.15	0	1	0
3.5	8	2.14	0	1	0
3.5	8	2.13	0	1	0
3.5	8	2.12	0	1	0
3.5	8	2.11	0	1	0
3.5	8	2.10	0	1	0
3.5	8	2.09	0	1	0
3.5	8	2.08	0	1	0
3.5	8	2.07	0	1	0
3.5	8	2.06	0	1	0
3.5	8	2.05	0.1	0.9	0
3.5	8	2.04	0.2	0.8	0
3.5	8	2.03	0.2	0.8	0
3.5	8	2.02	0.3	0.7	0
3.5	8	2.01	0.3	0.7	0
3.5	8	2.00	0.4	0.6	0
3.5	8	1.99	0.4	0.6	0
3.5	8	1.98	0.4	0.6	0
3.5	8	1.97	0.4	0.6	0
3.5	8	1.96	0.4	0.6	0
3.5	8	1.95	0.3	0.7	0
3.5	8	1.94	0.2	0.8	0
3.5	8	1.93	0.2	0.8	0
3.5	8	1.92	0.1	0.9	0
3.5	8	1.91	0	1	0
3.5	8	1.90	0	1	0
3.5	8	1.89	0	1	0
3.5	8	1.88	0	1	0
3.5	8	1.87	0	1	0
3.5	8	1.86	0	1	0
3.5	8	1.85	0	1	0
3.5	8	1.84	0	1	0
3.5	8	1.83	0	1	0
3.5	8	1.82	0	1	0
3.5	8	1.81	0.2	0.8	0

3.5	8	1.80	0.2	0.8	0
3.5	8	1.79	0.2	0.8	0
3.5	8	1.78	0.2	0.8	0
3.5	8	1.77	0.2	0.8	0
3.5	8	1.76	0.2	0.8	0
3.5	8	1.75	0.2	0.8	0
3.5	8	1.74	0.2	0.8	0
3.5	8	1.73	0.2	0.8	0
3.5	8	1.72	0.2	0.8	0
3.5	8	1.71	0.2	0.8	0
3.5	8	1.70	0.2	0.8	0
3.5	8	1.69	0.2	0.8	0
1.5	5	3.50	0	0	1
1.5	5	3.49	0	0	1
1.5	5	3.48	0	0	1
1.5	5	3.47	0	0	1
1.5	5	3.46	0	0	1
1.5	5	3.45	0	0	1
1.5	5	3.44	0	0	1
1.5	5	3.43	0	0	1
1.5	5	3.42	0	0	1
1.5	5	3.41	0	0	1
1.5	5	3.40	0	0	1
1.5	5	3.39	0	0	1
1.5	5	3.38	0	0	1
1.5	5	3.37	0	0	1
1.5	5	3.36	0	0	1
1.5	5	3.35	0	0	1
1.5	5	3.34	0	0	1
1.5	5	3.33	0	0	1
1.5	5	3.32	0	0	1
1.5	5	3.31	0	0	1
1.5	5	3.30	0	0	1
1.5	5	3.29	0	0	1
1.5	5	3.28	0	0	1
1.5	5	3.27	0	0	1
1.5	5	3.26	0	0	1
1.5	5	3.25	0	0	1
1.5	5	3.24	0	0	1
1.5	5	3.23	0	0	1
1.5	5	3.22	0	0	1
1.5	5	3.21	0	0	1
1.5	5	3.20	0	0	1
1.5	5	3.19	0	0	1
1.5	5	3.18	0	0	1
1.5	5	3.17	0	0.7	0.3
1.5	5	3.16	0	0.7	0.3
1.5	5	3.15	0	0.7	0.3
1.5	5	3.14	0	0.7	0.3
1.5	5	3.13	0	0.7	0.3
1.5	5	3.12	0	0.7	0.3
1.5	5	2.28	0	0	1
1.5	5	2.27	0	0	1
1.5	5	2.26	0	0	1
1.5	5	2.25	0	0	1
1.5	5	2.24	0	0	1
1.5	5	2.23	0	0	1

1.5	5	2.22	0	0	1
1.5	5	2.21	0	0	1
1.5	5	2.20	0	0	1
1.5	5	2.19	0	1	0
1.5	5	2.18	0	1	0
1.5	5	2.17	0	1	0
1.5	5	2.16	0	1	0
1.5	5	2.15	0	1	0
1.5	5	2.14	0	1	0
1.5	5	2.13	0	1	0
1.5	5	2.12	0	1	0
1.5	5	2.11	0	1	0
1.5	5	2.10	0	1	0
1.5	5	2.09	0	1	0
1.5	5	2.08	0	1	0
1.5	5	2.07	0	1	0
1.5	5	2.06	0	1	0
1.5	5	2.05	0	1	0
1.5	5	2.04	0	1	0
1.5	5	2.03	0	1	0
1.5	5	2.02	0	1	0
1.5	5	2.01	0	1	0
1.5	5	2.00	0	1	0
1.5	5	1.99	0	1	0
1.5	5	1.98	0	1	0
1.5	5	1.97	0	1	0
1.5	5	1.96	0	1	0
1.5	5	1.95	0	1	0
1.5	5	1.94	0.1	0.9	0
1.5	5	1.93	0.2	0.8	0
1.5	5	1.92	0.3	0.7	0
1.5	5	1.91	0.4	0.6	0
1.5	5	1.90	0.5	0.5	0
1.5	5	1.89	0.6	0.4	0
1.5	5	1.88	0.7	0.3	0
1.5	5	1.87	0.8	0.2	0
1.5	5	1.86	0.9	0.1	0
1.5	5	1.85	1	0	0
1.5	5	1.84	1	0	0
1.5	5	1.83	1	0	0
1.5	5	1.82	1	0	0
1.5	5	1.81	1	0	0
1.5	5	1.80	1	0	0
1.5	5	1.79	1	0	0
1.5	5	1.78	1	0	0
1.5	5	1.77	1	0	0
1.5	5	1.76	1	0	0
1.5	5	1.75	1	0	0
1.5	5	1.74	1	0	0
1.5	5	1.73	1	0	0
1.5	5	1.72	0.7	0.3	0
1.5	5	1.71	0.5	0.5	0
1.5	5	1.70	0.3	0.7	0
1.5	5	1.69	0	1	0
1.5	5	1.68	0	1	0
1.5	5	1.67	0	1	0
1.5	5	1.66	0	1	0

1.5	5	1.65	0	1	0
1.5	5	1.64	0	1	0
3.5	5	3.50	0	0	1
3.5	5	3.49	0	0	1
3.5	5	3.48	0	0	1
3.5	5	3.47	0	0	1
3.5	5	3.46	0	0	1
3.5	5	3.45	0	0	1
3.5	5	3.44	0	0	1
3.5	5	3.43	0	0	1
3.5	5	3.42	0	0	1
3.5	5	3.41	0	0	1
3.5	5	3.40	0	0	1
3.5	5	3.39	0	0	1
3.5	5	3.38	0	0	1
3.5	5	3.37	0	0	1
3.5	5	3.36	0	0	1
3.5	5	3.35	0	0	1
3.5	5	3.34	0	0	1
3.5	5	3.33	0	0	1
3.5	5	3.32	0	0	1
3.5	5	3.31	0	0	1
3.5	5	3.30	0	0	1
3.5	5	3.29	0	0	1
3.5	5	3.28	0	0	1
3.5	5	3.27	0	0	1
3.5	5	3.26	0	0	1
3.5	5	3.25	0	0	1
3.5	5	3.24	0	0	1
3.5	5	3.23	0	0	1
3.5	5	3.22	0	0	1
3.5	5	3.21	0	0.2	0.8
3.5	5	3.20	0	0.3	0.7
3.5	5	3.19	0	0.5	0.5
3.5	5	3.18	0	0.6	0.4
3.5	5	3.17	0	0.7	0.3
3.5	5	3.16	0	0.8	0.2
3.5	5	3.15	0.2	0.8	0
3.5	5	3.14	0.2	0.8	0
3.5	5	3.13	0.2	0.8	0
3.5	5	3.12	0.2	0.8	0
3.5	5	3.11	0.2	0.8	0
3.5	5	3.10	0.2	0.8	0
3.5	5	3.09	0.2	0.8	0
3.5	5	3.08	0.2	0.8	0
3.5	5	3.07	0.2	0.8	0
3.5	5	3.06	0.2	0.8	0
3.5	5	3.05	0.2	0.8	0
3.5	5	3.04	0.2	0.8	0
3.5	5	3.03	0.2	0.8	0
3.5	5	3.02	0.2	0.8	0
3.5	5	3.01	0.2	0.8	0
3.5	5	3.00	0.2	0.8	0
3.5	5	2.99	0.2	0.8	0
3.5	5	2.98	0	1	0
3.5	5	2.97	0	1	0
3.5	5	2.96	0	1	0

3.5	5	2.95	0	1	0
3.5	5	2.94	0	1	0
3.5	5	2.93	0	1	0
3.5	5	2.92	0	1	0
3.5	5	2.91	0	1	0
3.5	5	2.90	0	1	0
3.5	5	2.89	0	1	0
3.5	5	2.88	0	1	0
3.5	5	2.87	0	1	0
3.5	5	2.86	0	1	0
3.5	5	2.85	0	1	0
3.5	5	2.84	0	1	0
3.5	5	2.83	0	1	0
3.5	5	2.82	0	1	0
3.5	5	2.28	0	0	1
3.5	5	2.27	0	0	1
3.5	5	2.26	0	0	1
3.5	5	2.25	0	0	1
3.5	5	2.24	0	0.5	0.5
3.5	5	2.23	0	1	0
3.5	5	2.22	0.3	0.7	0
3.5	5	2.21	0.3	0.7	0
3.5	5	2.20	0.3	0.7	0
3.5	5	2.19	0.3	0.7	0
3.5	5	2.18	0.3	0.7	0
3.5	5	2.17	0.3	0.7	0
3.5	5	2.16	0.3	0.7	0
3.5	5	2.15	0	1	0
3.5	5	2.14	0	1	0
3.5	5	2.13	0	1	0
3.5	5	2.12	0	1	0
3.5	5	2.11	0	1	0
3.5	5	2.10	0	1	0
3.5	5	2.09	0	1	0
3.5	5	2.08	0	1	0
3.5	5	2.07	0	1	0
3.5	5	2.06	0	1	0
3.5	5	2.05	0.4	0.6	0
3.5	5	2.04	0.4	0.6	0
3.5	5	2.03	0.4	0.6	0
3.5	5	2.02	0.4	0.6	0
3.5	5	2.01	0.4	0.6	0
3.5	5	2.00	1	0	0
3.5	5	1.99	1	0	0
3.5	5	1.98	1	0	0
3.5	5	1.97	1	0	0
3.5	5	1.96	1	0	0
3.5	5	1.95	1	0	0
3.5	5	1.94	1	0	0
3.5	5	1.93	0.2	0.8	0
3.5	5	1.92	0.2	0.8	0
3.5	5	1.91	0.2	0.8	0
3.5	5	1.90	0.2	0.8	0
3.5	5	1.89	0.2	0.8	0
3.5	5	1.88	0.2	0.8	0
3.5	5	1.87	0.2	0.8	0
3.5	5	1.86	0.2	0.8	0

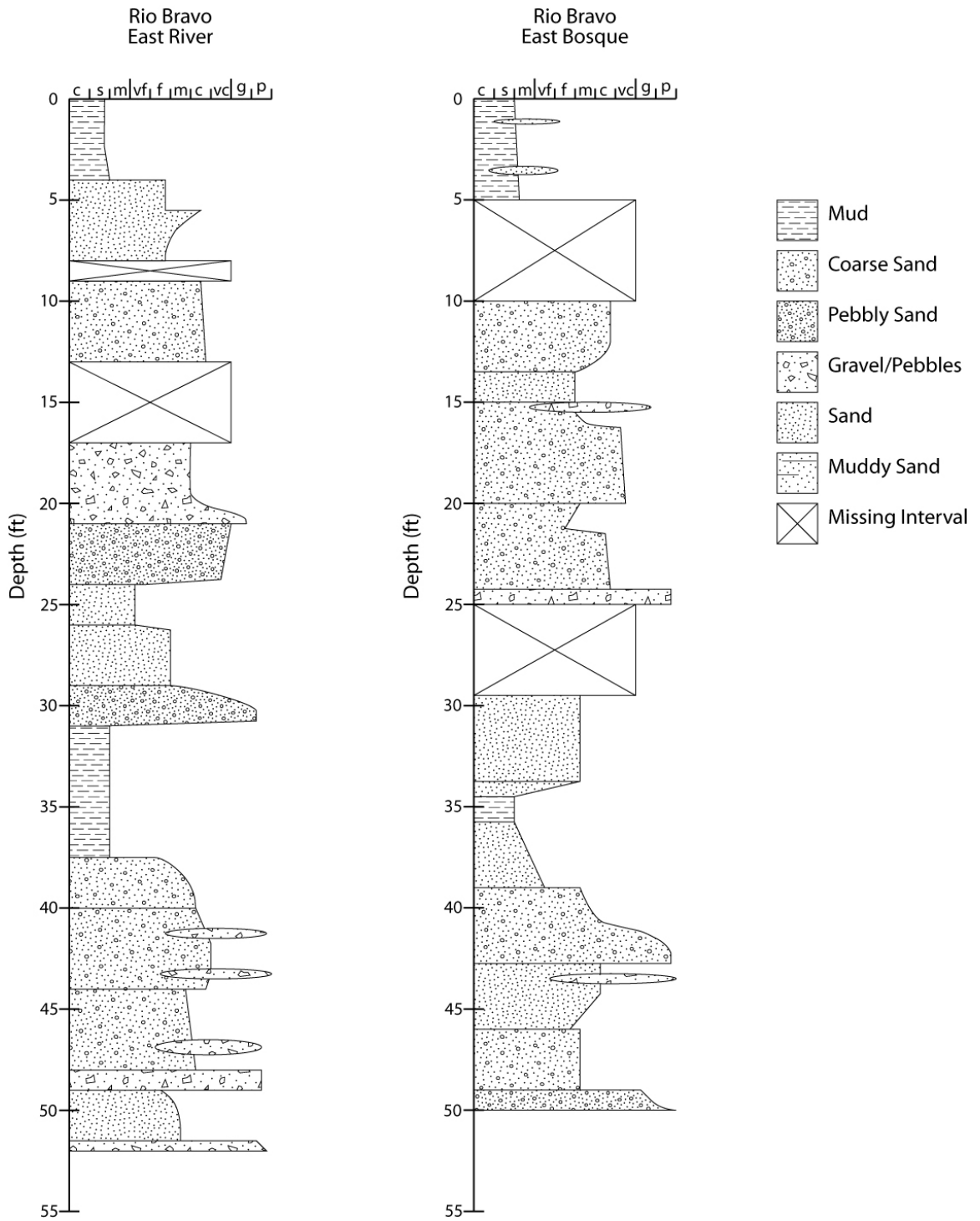
3.5	5	1.85	0.2	0.8	0
3.5	5	1.84	0.2	0.8	0
3.5	5	1.83	0.2	0.8	0
3.5	5	1.82	0.3	0.7	0
3.5	5	1.81	0.3	0.7	0
3.5	5	1.80	0.3	0.7	0
3.5	5	1.79	0.3	0.7	0
3.5	5	1.78	0.3	0.7	0
3.5	5	1.77	0.3	0.7	0
3.5	5	1.76	0.4	0.6	0
3.5	5	1.75	0.4	0.6	0
3.5	5	1.74	0.4	0.6	0
3.5	5	1.73	0.4	0.6	0
3.5	5	1.72	0.4	0.6	0
3.5	5	1.71	0.4	0.6	0
3.5	5	1.70	0.4	0.6	0
3.5	5	1.69	0.4	0.6	0
3.5	5	1.68	0.4	0.6	0
3.5	5	1.67	0.4	0.6	0
3.5	5	1.66	0.4	0.6	0
3.5	5	1.65	0.4	0.6	0
3.5	5	1.64	0.4	0.6	0
3.5	5	1.63	0.4	0.6	0
3.5	5	1.62	0.4	0.6	0

4.0 - Supplemental stratigraphic columns

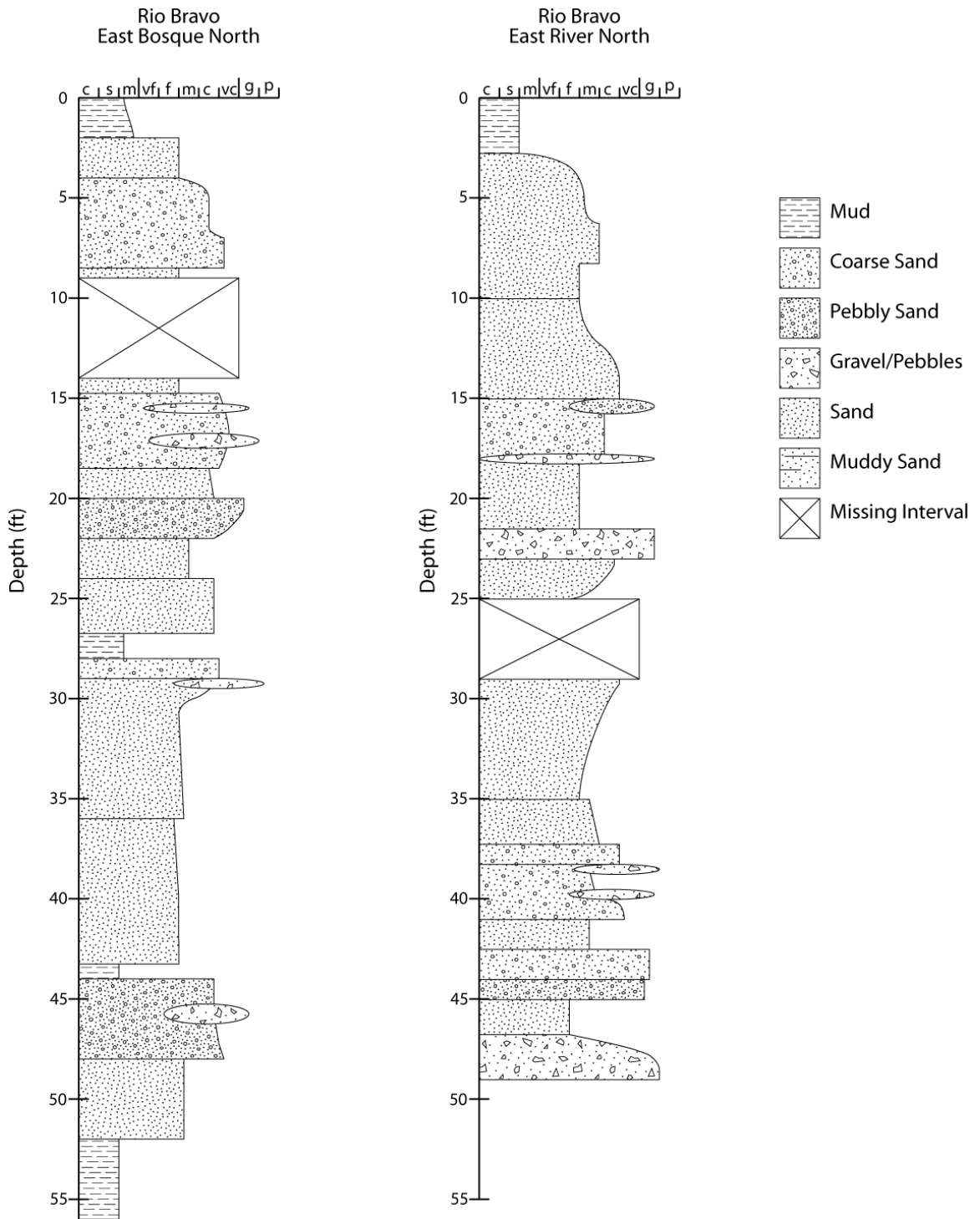
The stratigraphic columns contained within this section are those not pictured in chapter 1 of this volume (*Heterogeneity effects on river loss...*) but also include the previously shown columns. These columns have not been edited or modified significantly from their original versions and may contain errors. They are provided as a general reference tool only.

The descriptive names of the stratigraphic columns correspond to those used in the flow loss study. Generally, "river" locations are located adjacent or very near the bankfull river channel and "bosque" locations are within the riparian corridor but within the levees that run along the Rio Grande. As can be seen in the site map from chapter 1, there is greater spacing between cored locations on the east side of the river than the west side.

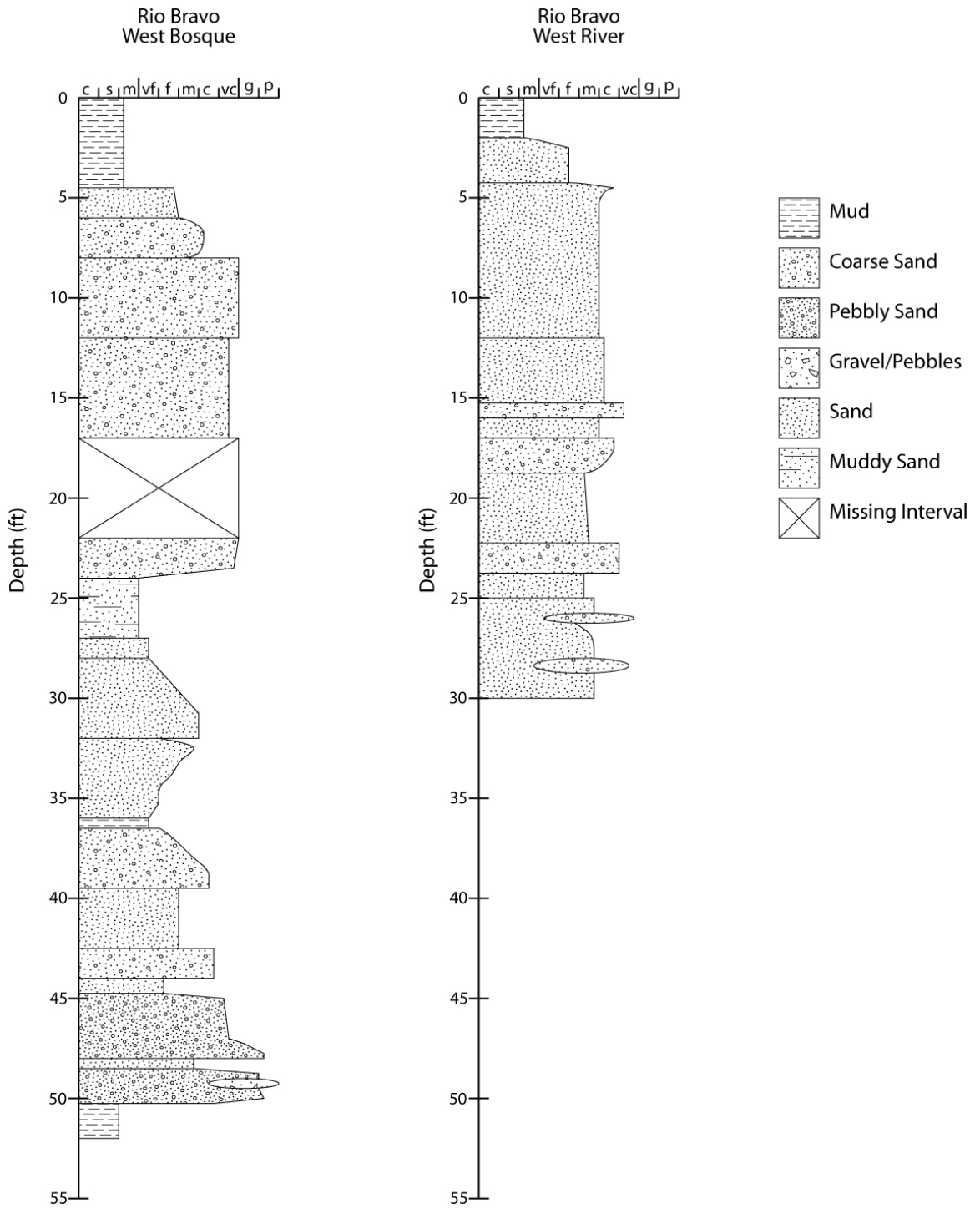
Rio Bravo, East side, southern transect



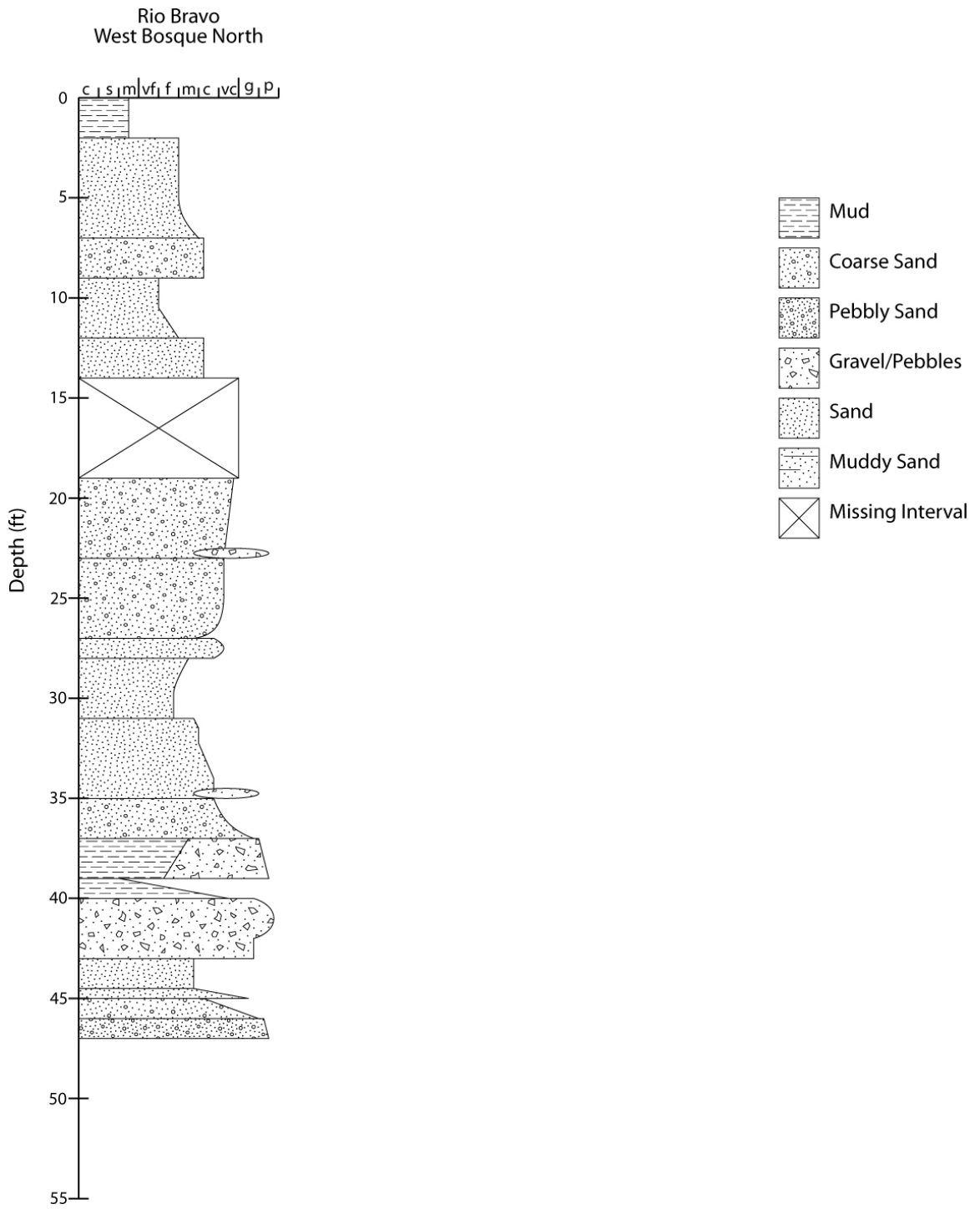
Rio Bravo, East side, northern transect



Rio Bravo, West side, southern transect



Rio Bravo, West side, northern transect



Appendix C -

**Ground Penetrating Radar Lines and data collection information from
the Integrated Modeling site**

**Nicholas B. Engdahl
Earth and Planetary Science Department
University of New Mexico
Albuquerque, NM 87131**

Table of contents

Detailed Site Layout	148
Site Layout Photographs	149
GPR Line 1	151
GPR Line 2	152
GPR Line 3	153
GPR Line 4	154
GPR Line 5	155
GPR Line 6	156
GPR Line 7	157
GPR Line 8	158
GPR Line 9	159
GPR Line 10	160
GPR Line 11	161

Detailed Site Layout

The ground penetrating radar (GPR) data used in the integrated modeling and transport studies of this collection were collected in February of 2008. As described in the text, this coincided with the annual low flow period of the river and allowed collection of the data as close to the water table as possible. This location was optimal to allow for the maximum transfer of energy below the water table to image within the saturated zone. To ensure that the data was collected on a regular grid, stake were laid out along all four edges of the survey site and connected using string. Each line was collected individually along a non-conductive tape measure laid out next to the string to create uniform step sizes during data collection. All data were collected using a Pulse-Ekko 100 system and analyzed with the ReflexW analysis and interpretation package (citations in main text).

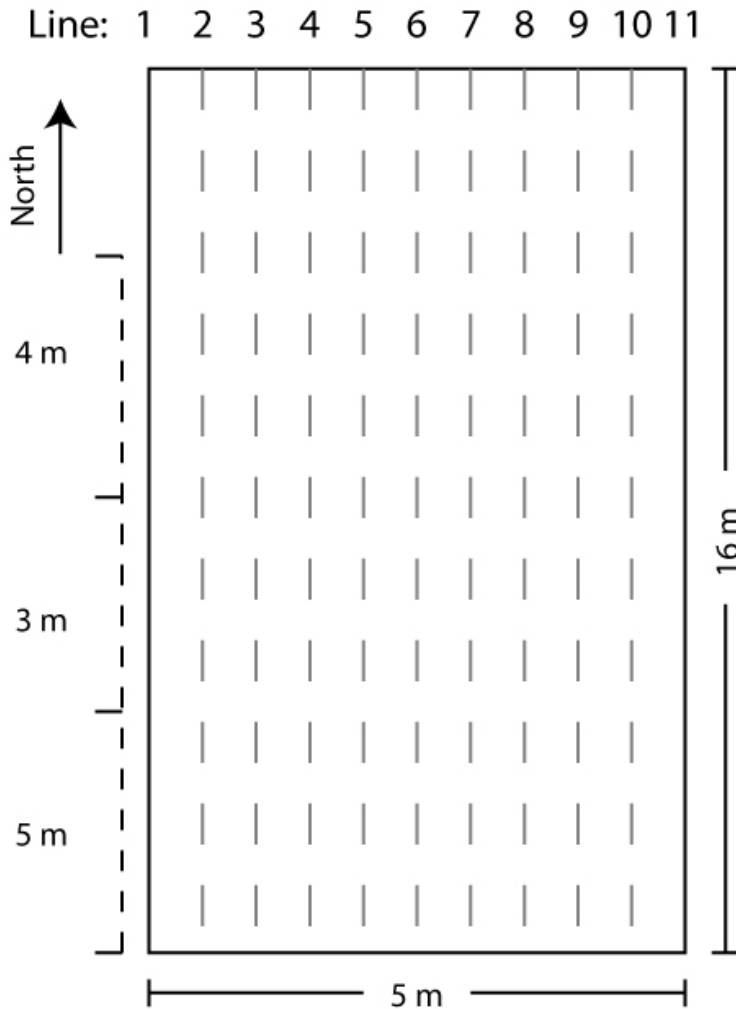


Figure 1 - Layout of GPR data collection grid for integrated modeling.

Site Layout Photographs



Figure 2 - Site layout during GPR data collection. The black stakes represent 2m separation along the long edge and 0.5m separation along the short edge.

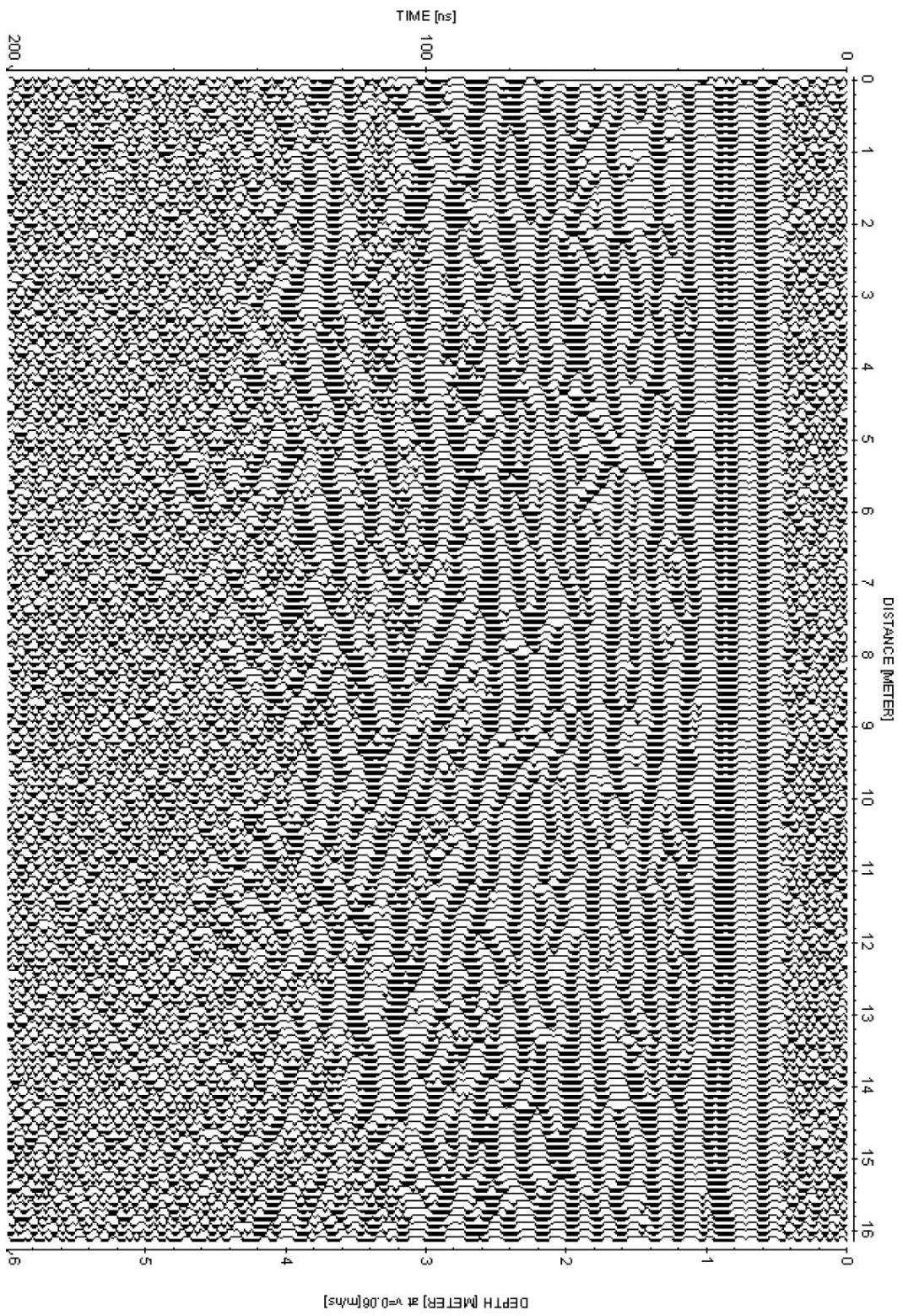


Figure 3 – View of the integrated modeling study site from the southwest of the model looking towards true north. GPR data collection remained stationary during data collection and can be seen on the right edge of the photograph.



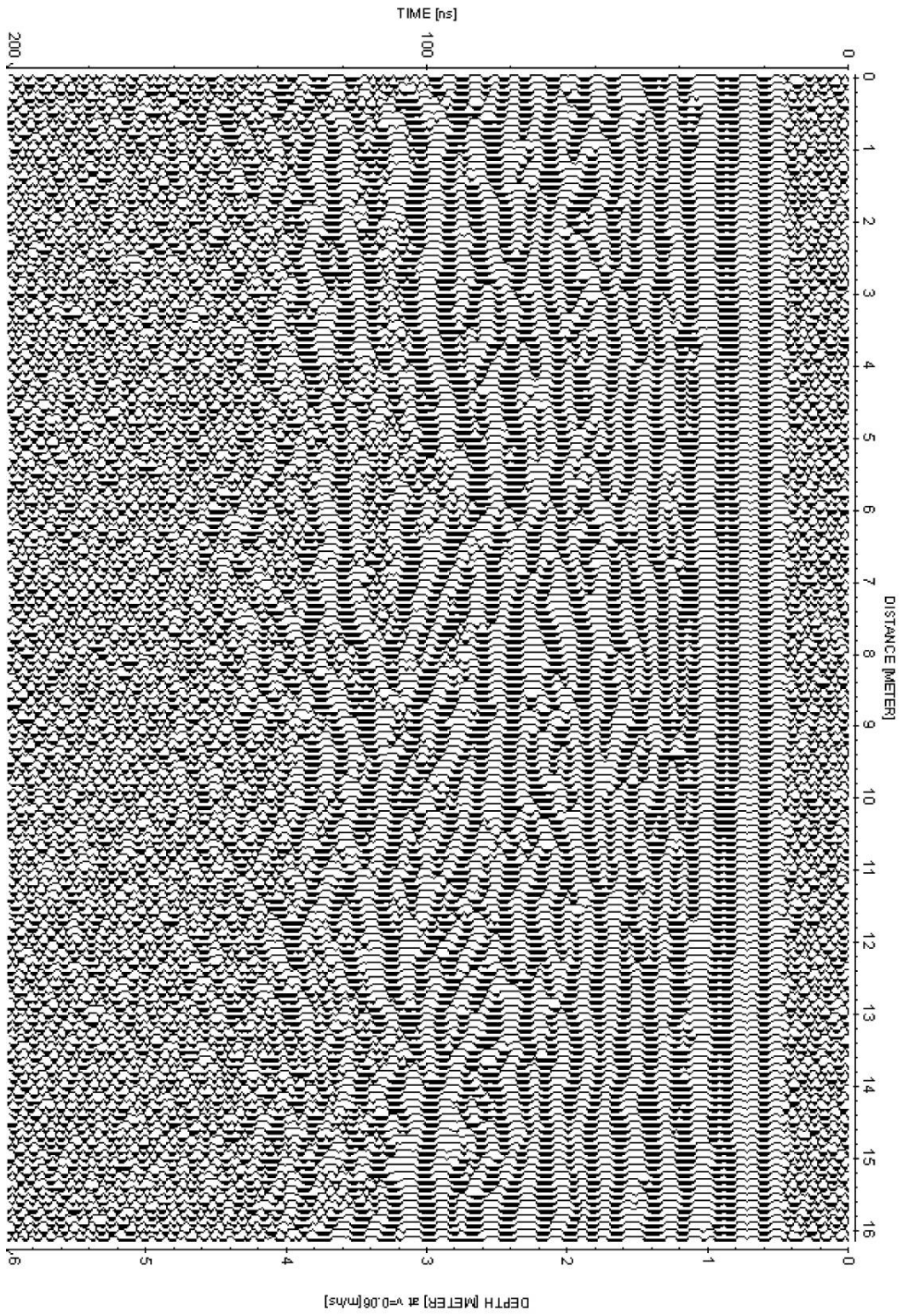
Figure 10 - Northern most edge of the GPR survey site, directly along the Rio Grande. Survey markers, string, the non-conductive tape measure and GPR equipment are visible on the left side of the photograph. Hand probing into the study site after data collection confirmed that depth to water was only several centimeters throughout the study site.

GPR Line 1



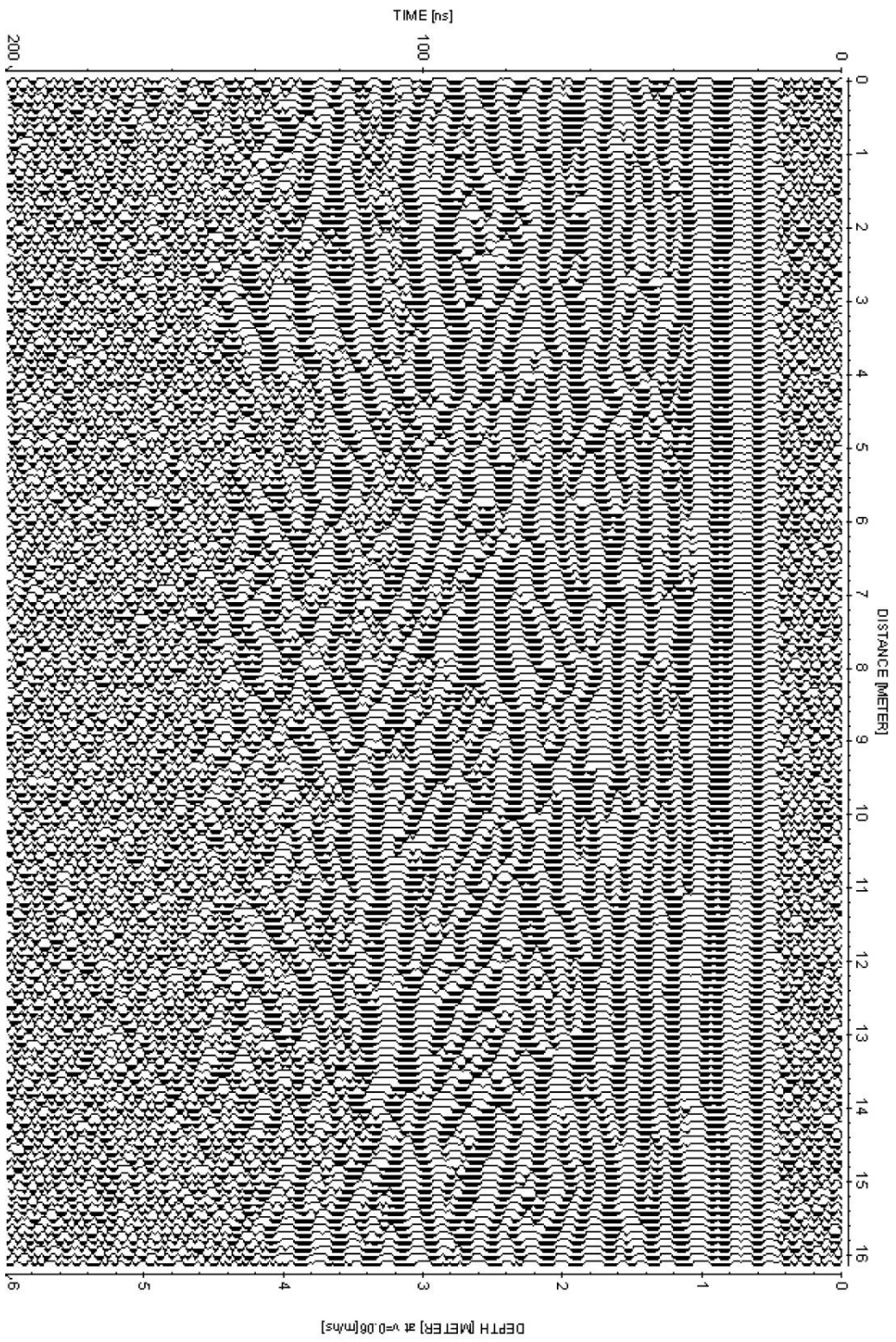
Rio Bravo transport simulation site GPR Line at x = 0.00m

GPR Line 2

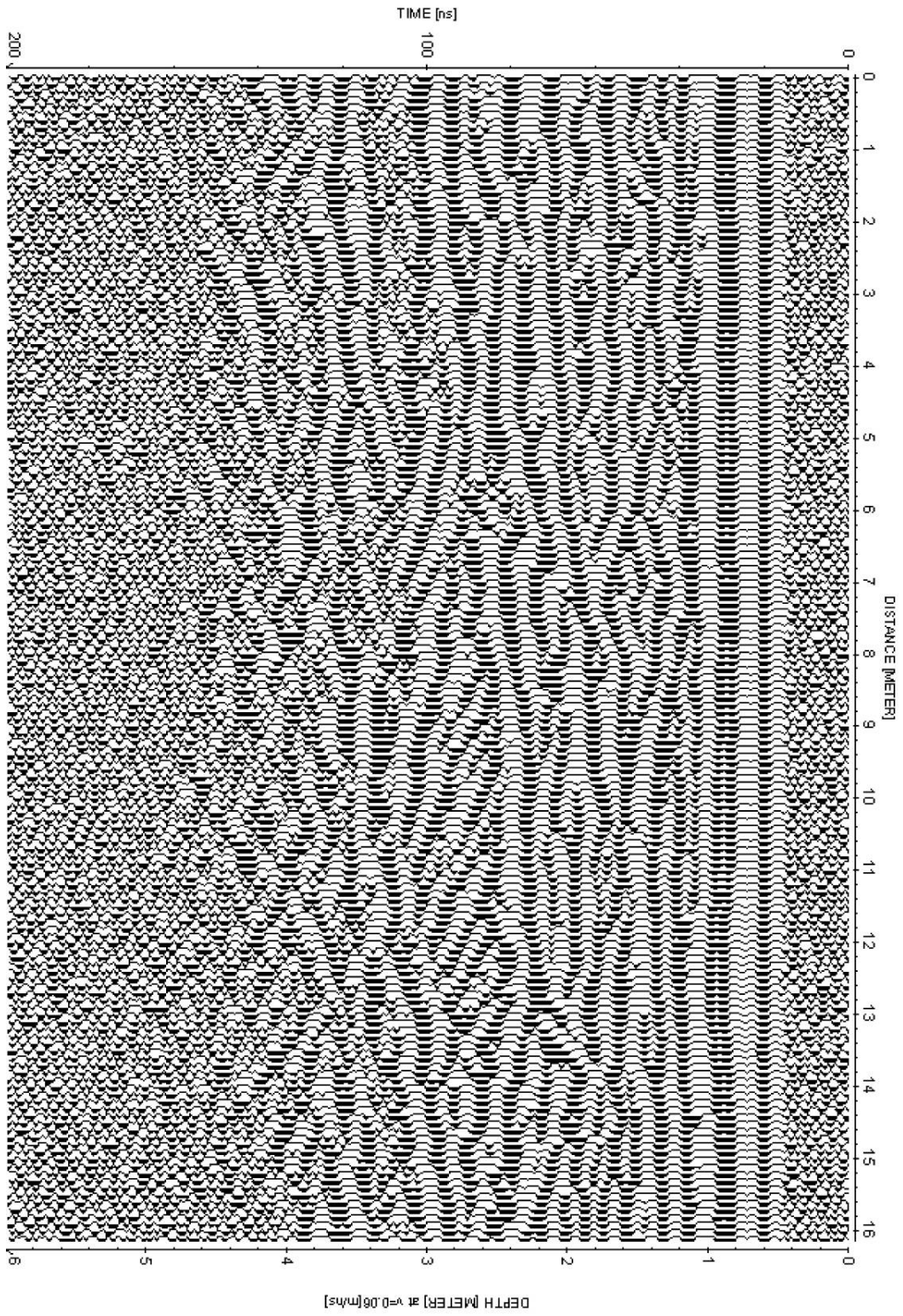


Rio Bravo transport simulation site GPR Line at x = 0.50m

Rio Bravo transport simulation site GPR Line at x = 1.00m

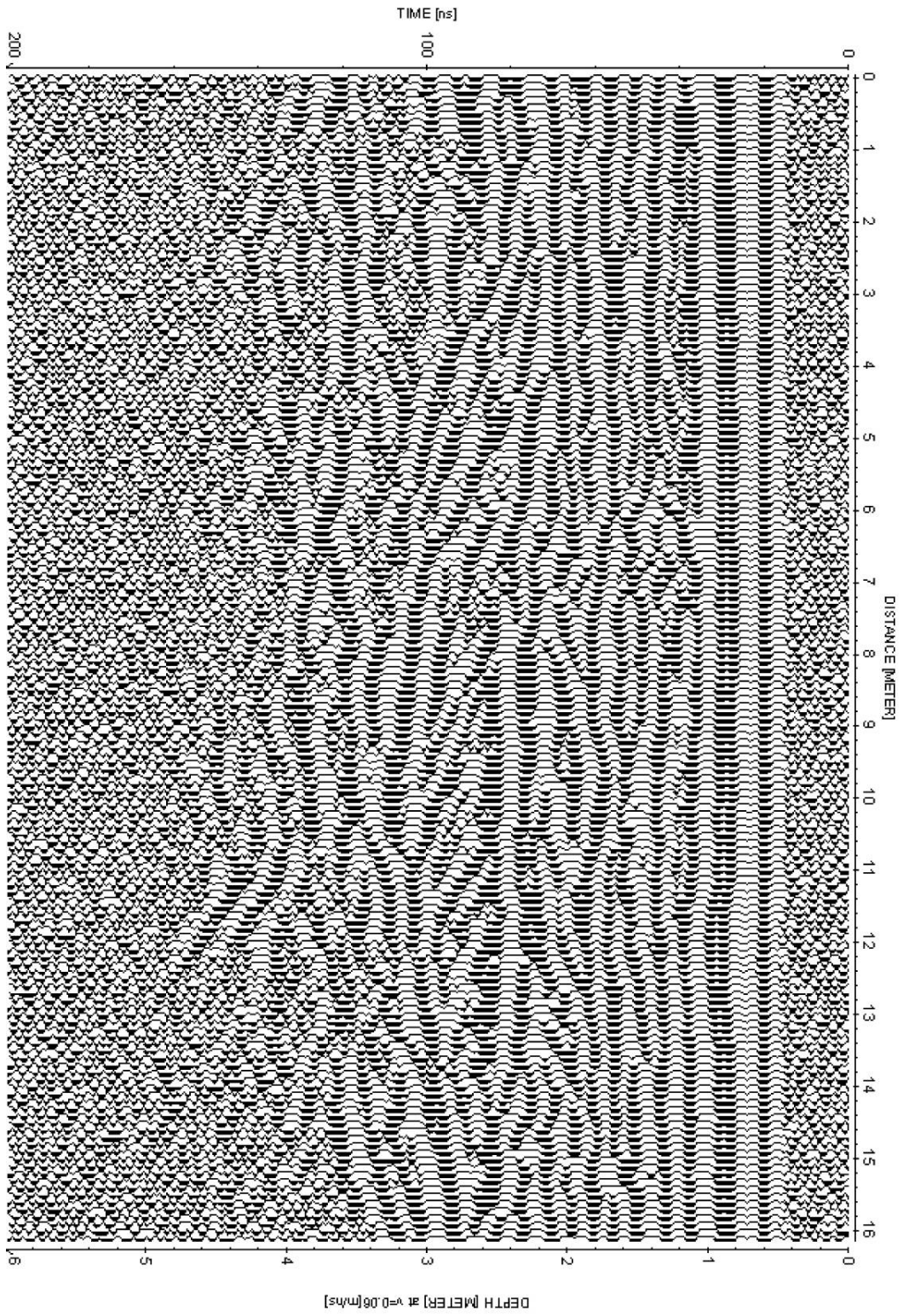


GPR Line 4



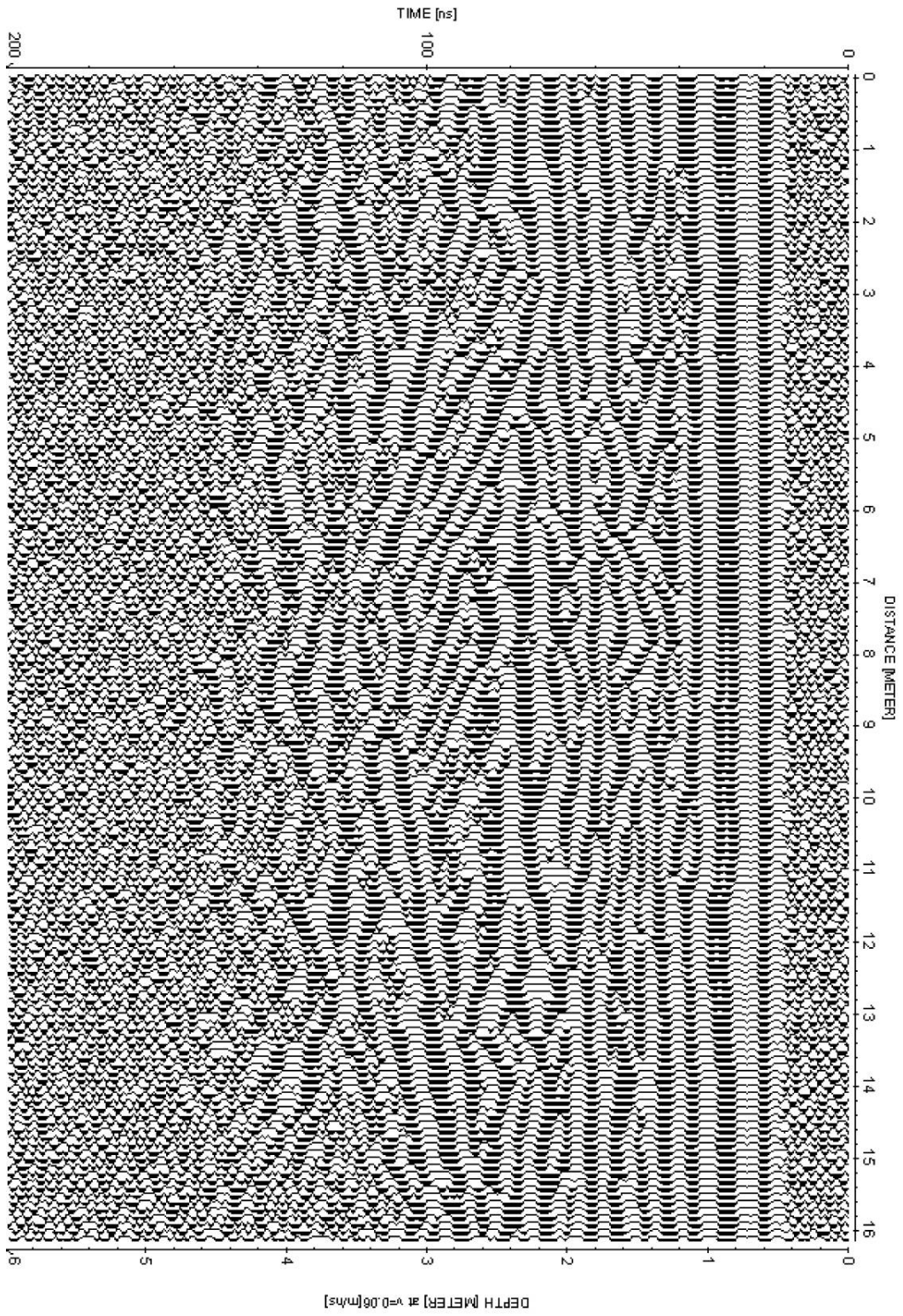
Rio Bravo transport simulation site GPR Line at x = 1.50m

GPR Line 5



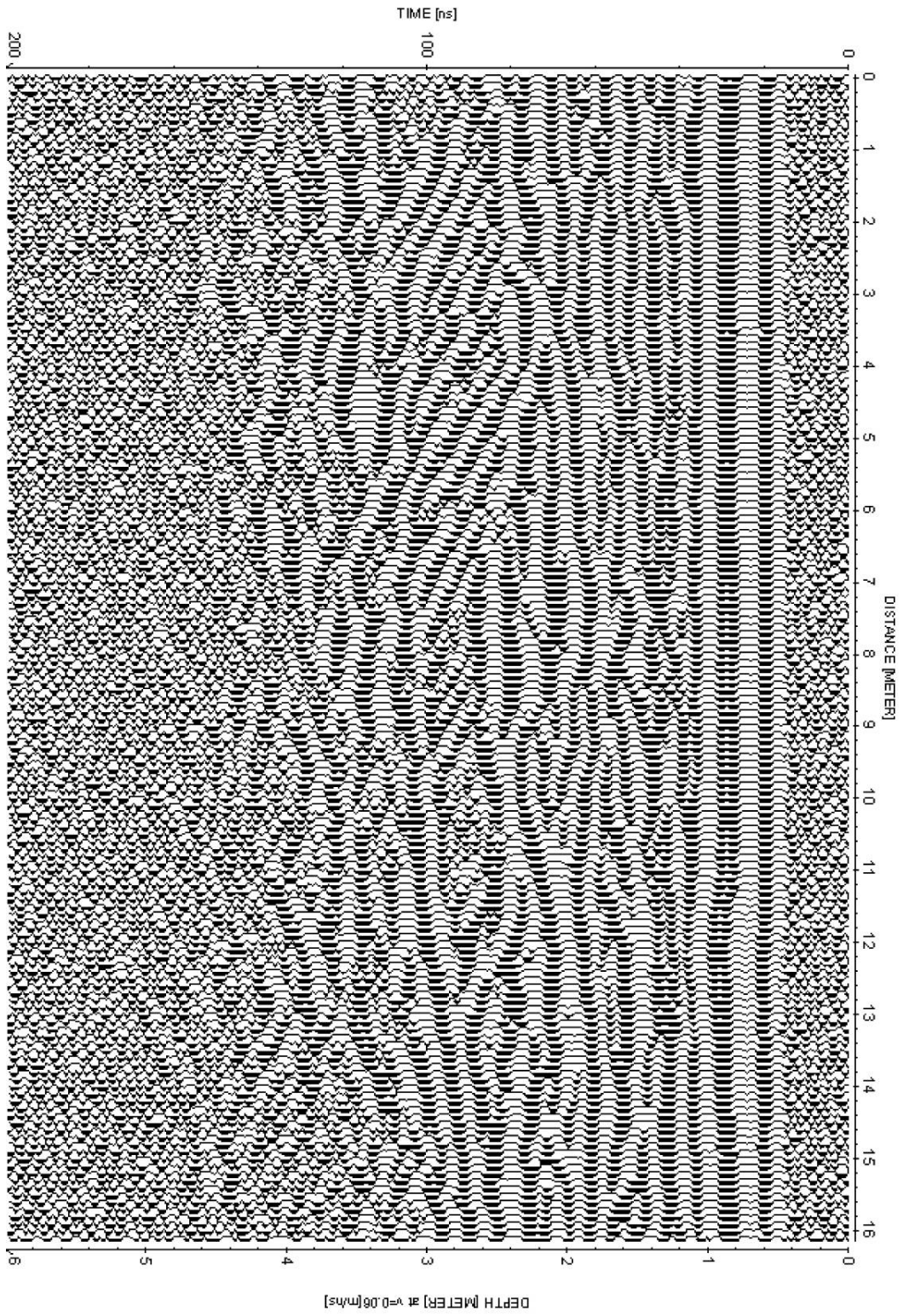
Rio Bravo transport simulation site GPR Line at x = 2.00m

GPR Line 6



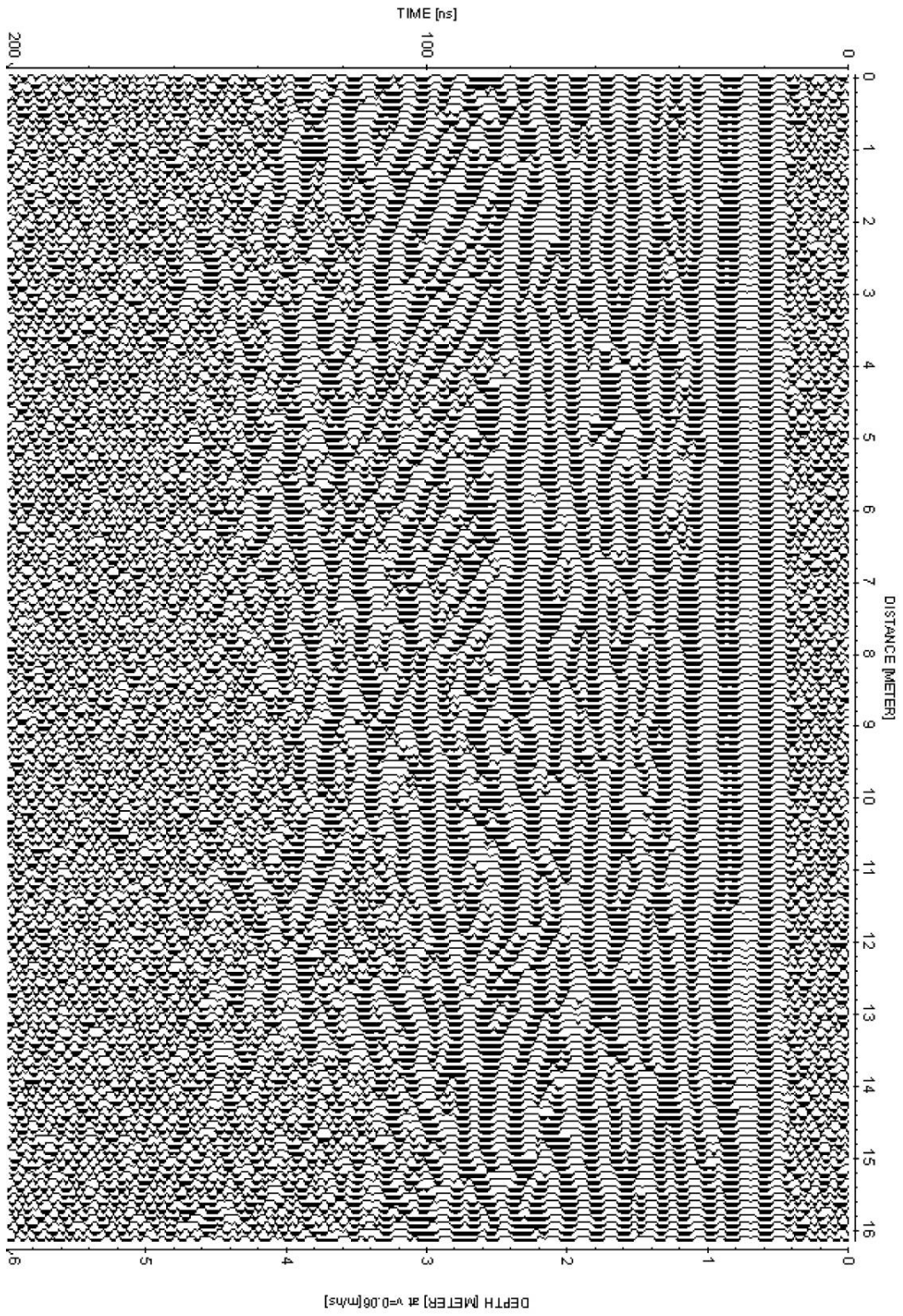
Rio Bravo transport simulation site GPR Line at x = 2.50m

GPR Line 7



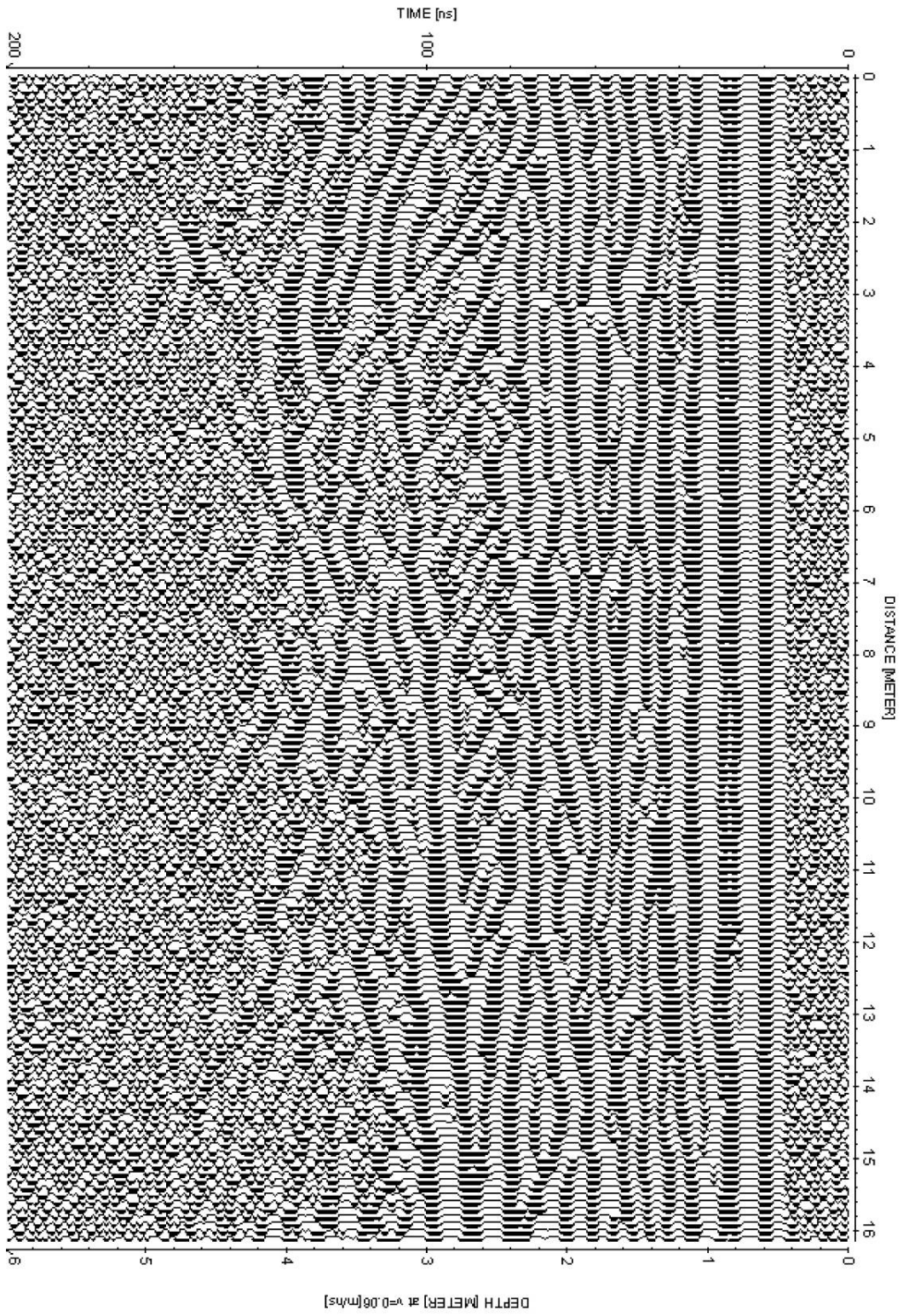
Rio Bravo transport simulation site GPR Line at x = 3.00m

GPR Line 8



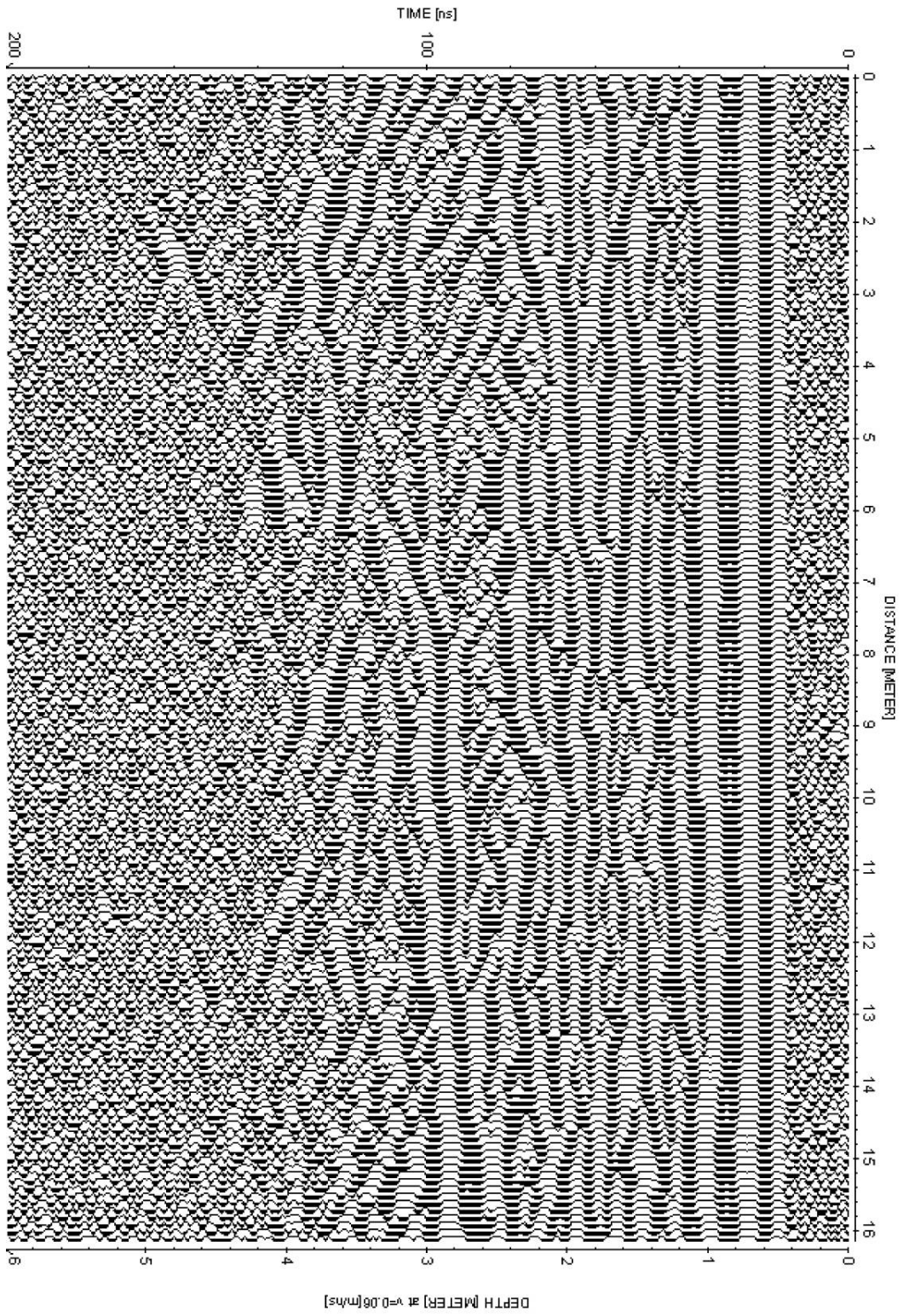
Rio Bravo transport simulation site GPR Line at x = 3.50m

GPR Line 9



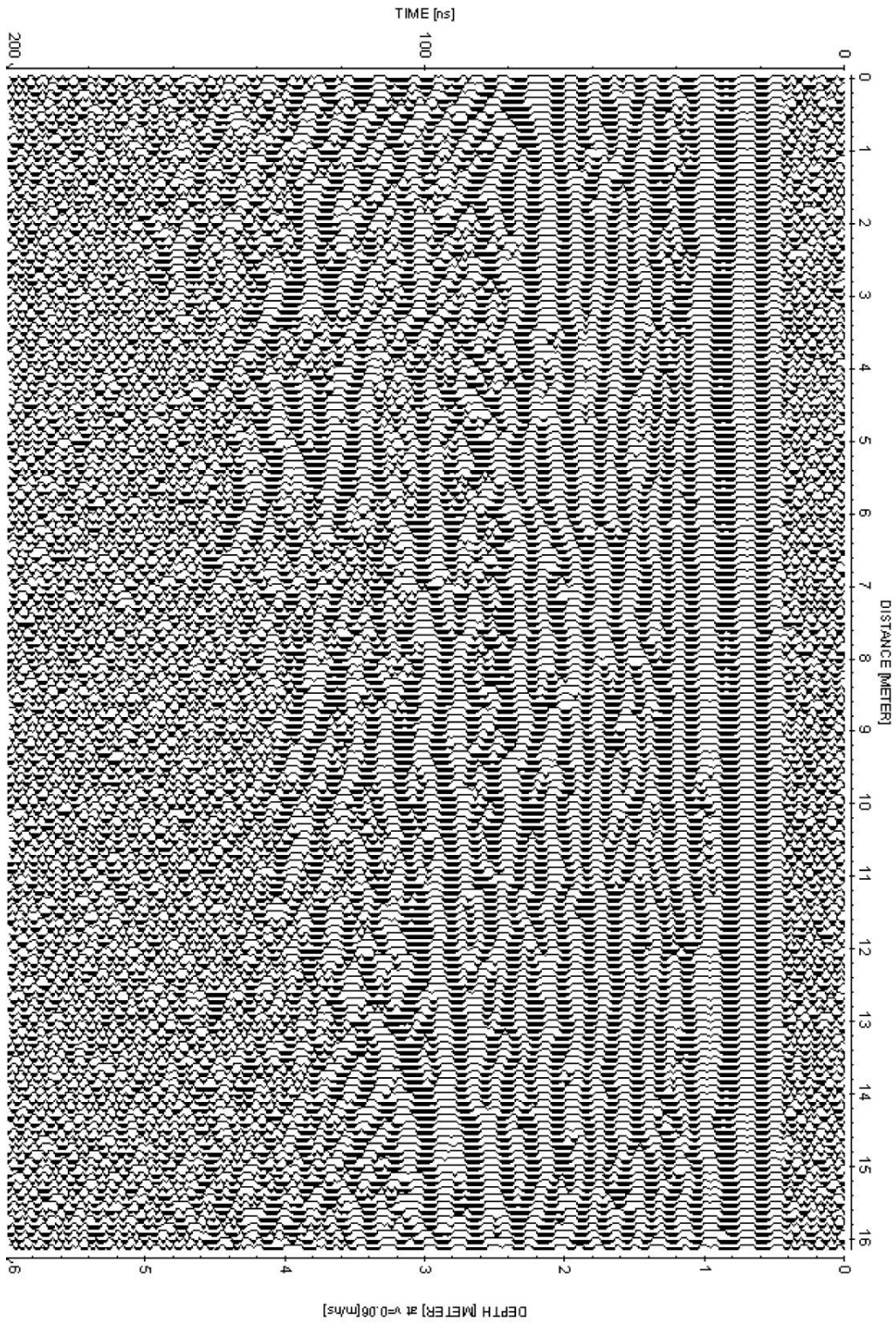
Rio Bravo transport simulation site GPR Line at x = 4.00m

GPR Line 10



Rio Bravo transport simulation site GPR Line at x = 4.50m

GPR Line 11



Rio Bravo transport simulation site GPR Line at x = 5.00m

Appendix D -

Source code for the integrated modeling routines

**Nicholas B. Engdahl
Earth and Planetary Science Department
University of New Mexico
Albuquerque, NM 87131**

Table of Contents

Description of enclosed material	164
Fortran code for InMod routines.....	165
3dseg.....	165
Con_groups.....	173

Description of enclosed material

This appendix is intended to be a supplement for reference purposes only. The actual source code for the Integrated Modeling (InMod) routines contained herein is available from the author. The version of the code presented here is strictly the initial beta version of the code and has not been optimized, streamlined or even fully edited and may contain relics of early versions, inline comments from the author (designated by either a c or ! in the first column) and possibly redundant assignments. The author assumes no responsibility and makes no claim as to the accuracy of the models and potential users are proceeding, solely, at their own risk.

Two routines are presented here: 3dSeg and Con_groups. 3dseg is the region growing and identification module of InMod which is executed first on the filtered GPR peaks data. Con_groups is the region matching and filling routine which requires a pool of geostatistical realizations and the output file from the 3dseg routine. The source code is presented in a reduced font size to decrease the length of this appendix.

The routines have been successfully compiled and run on a Unix system. Presently, only the 32 bit versions of the routines are functional but have been run in compatibility mode on the x64 Windows architecture. Fully 64 bit, optimized (and potentially parallel) versions are under development.

Fortran code for InMod routines

3dseg

```
      Program Seg3d
      implicit none
!
! #####
! #                                     #
! # THE AUTHOR GIVES NO ASSURANCES OF ACCURACY FOR THE RESULTS OF THIS
PROGRAM #
! #                                     #
! #####
!
! Seg3d is a routine that uses regularly gridded input data containing the
! locations of bounding surfaces within a 3-D model space from GPR data.
! It was designed for the purposes of non-fickian transport modeling and the
! improvement of subsurface categorization methods.
!
! Matching is done by aspect ratio / centroid location comparison. A region is
! scanned and logged along the dip and vertical directions and compared to the
! region matching up in the next higher row number.
!
! Version 1.0.0 - 09.08.2008: Initial release
!
! Please direct any comments or questions to:
! Nicholas B. Engdahl
! Hydrogeology Group
! Earth and Planetary Sciences
! University of New Mexico
! or contact the above via:
! Dr. Gary Weissmann
! Earth and Planetary Sciences
! University of New Mexico
!
!
      integer nx,ny,nz,i,j,k,IO,x,y,z,a,b,c,nxyz,p,q,r,n,fac,hh,shf
      integer tx,ty,tz,centZ,centY,D,U,e,f,cnt,row,ks,Rtot,Ost,hmx
      integer lx,ly,runs,xi,yi,zi,h,Smin,Smax,m,rmax,zmax,ymax
      integer xii,yii,zii,LL,TsN,Sims,xshf,yshf,zshf,ckX,ckY,ckZ
      integer region,reg,count,lz,hy,hz
      real, allocatable :: ARs(:)
      real AR,R1,R2,R3,ZOff,XOff,YOff
      integer,allocatable :: bnds(,;,;)
      integer,allocatable :: surfs(,;,;)
      integer,allocatable :: cnts(:)
      character (len=20) rnum
      character (len=40) Infile,Outfile,Sfile,DbgFile,OUTname,TSIM
      character (len=40) root,ext
      logical Intermit, MoveOn, terminal, header
```

```

header = .true.
terminal = .false.
Intermit = .false.

MoveOn = .true.
Infile = 'GPR_All_Cols.txt'
Outfile = 'Seg3d.txt'
Dbgfile = 'Debug.txt'
Sfile = 'Scratch.txt'
root= 'tsim_lith_full'      ! root of TSIM path
ext = '.asc'                ! base filename extension
Sims = 1                    ! number of TSIM realizations available

Open(Unit=9,File=Dbgfile,status='replace',action='write')
Write(9,*) '--- Debug file for 3dseg processing routine ---'
Write(9,*) "
Write(9,*) 'Using the following parameters for Infile,Outfile,
+Dbgfile and Scratch: '
Write(9,*) Infile,Outfile
Write(9,*) Dbgfile,Sfile
Write(9,*) '-----'
Open(Unit=1,File=Infile,status='old',action='read')
IO = 0
Read(1,*) nx,ny,nz
nxyz = nx * ny * nz
allocate (bnds(nx,ny,nz,4))

Do While (IO .eq. 0)
  Read(1,*,IOSTAT=IO) x,y,z
  bnds(x,y,z,1) = 1
! ## bnds(:, :, 1) is the bounding surface flag
!   bnds(:, :, 2) is the modified flag
!   bnds(:, :, 3) is the facies value
!   lims(:, :, 1, :) are the minimums
!   lims(:, :, 2, :) are the maximums
!   lims(:, :, 3, :) are the lengths
!   lims(:, :, 4, :) are the groupings
  enddo
  Close(1)
  Write(9,*) 'Input file data read in, scanning and filling
+edge gaps...'

! ## There should be 3630 points within the Para bounding region over
!   the limits of: <{1:11},{1:11},{1:inf}>
! -----
! ----- Scan edges and fill in gaps of 1 unit -----
! ----- End of edge filling -----
  Do k = 1,nz
! This peice can be modified to greater edge searching but it only looks
! for up to +/- 2 difference for now, just add more conditions at the top/bottom
    If (k .eq. 1) then
      Smin = 0
      Smax = 2
    ElseIf (k .eq. 2) then
      Smin = -1
      Smax = 2

```

```

ElseIf((k .ge. 3) .and. (k .le. (ny-2))) then
  Smin = -2
  Smax = 2
ElseIf(k .eq. ny-2) then
  Smin = -2
  Smax = 1
ElseIf(k .eq. ny) then
  Smin = -2
  Smax = 0
Else
  write(*,*) "
  write(*,*) 'Fatal error in gap filling, routine terminated'
  write(9,*) 'Premature termination in gap filling.'
  STOP
EndIf
! Left Edge
  If (bnds(i,2,k,1) .eq. 1) then
    Do n = Smin,Smax
      If (bnds(i,1,k+n,1) .eq. 1) then
        go to 501
      EndIf
    EndDo
    bnds(i,1,k,1) = 1
  Else
501   EndIf
! Right Edge
  If (bnds(i,(ny - 1),k,1) .eq. 1) then
    Do n = Smin,Smax
      If (bnds(i,ny,k+n,1) .eq. 1) then
        go to 502
      EndIf
    EndDo
    bnds(i,ny,k,1) = 1
  Else
502   EndIf
  EndDo
  Write(*,*) 'Gaps checked. Generating surface/edge distance
+matrix...'
  Write(*,*) "
  Write(9,*) 'Gaps checked. Generating surface/edge distance
+matrix...'
  Write(9,*) "

  rmax = 50   ! maximum number of bounding surfaces for total model
  region = 1
! *****
! #####
  Do row = 1, nx
  Do runs = 1,rmax  !! ### Should loop one row only ### !!
  If (allocated(surfs)) then
  deallocate(surfs)
  write(*,*) 'Should be deallocated...'
  STOP
  EndIf
  allocate (surfs((ny*nz),9,nx))

```



```

Call StartPoint(bnds,i,j,k,nx,ny,nz,row)
write(9,*) '---- Confirming Start Parameters ----'
write(9,*) i,j,k !,nx,ny,nz
write(9,*) bnds(i,j,k,1:3)
write(9,*) '----- End start parameters -----'
i = row
If ((bnds(i,j,k,1) .eq. 1)) then
write(9,*) 'This is an excepted start location.'
write(9,*) ' at location: ',i,j,k
EndIf
If (j == ny) then
write(*,*) 'Reached terminal point'
write(9,*) 'Reached terminal point'
terminal = .true.
go to 2000
EndIf

write(*,*) 'Starting at: ',i,j,k

cnt = 1

! for surfs(:,**,:); 1 = x(i); 2 = y(i); 3 = top z; 4 = MP; 5 = bottom z;
! 6 = heigth; 7 = centY; 8 = centZ; 9 = AR
n = 1
! for lims; 1 = min; 2 = max; 3 = lengths ----> for (i,j,k,**,:)
! 1 = x (i); 2 = y (j); 3 = z (k); ---> for (i,j,k,.,**)

write(9,*) '(1) Currently in row: ',row

! Loops within bounding region
Do while (MoveOn)

u = 0
Do while ((bnds(i,j,k+u,1) .ne. 1) .and. (k+u .lt. nz))
u = u + 1
EndDo
! (k+u) is now either at the top of the model or on a bounding surf

D = 1
Do while (((k+u-D) .gt. 1) .and.
+(bnds(i,j,(k+u-D),1).ne. 1))
D = D + 1
EndDo

surfs(cnt,1,row) = i
surfs(cnt,2,row) = j
surfs(cnt,3,row) = k + u

If (((k+u) .eq. nz) .and. (bnds(i,j,(k+u),1) .ne. 1)) then
surfs(cnt,4,row) = k + u
ElseIf (((k+u) .eq. nz) .and. (bnds(i,j,(k+u),1) .eq. 1)) then
surfs(cnt,4,row) = ANINT((real(((k+u)-D) + (k+u)))/2)
ElseIf (k .le. ANINT(real(nz)/2)) then
surfs(cnt,4,row) = ANINT((real(((k+u)-D) + (k+u)))/2)

```

```

write(9,*) '2:',i,j,k,ANINT((real(((k+u)-D) + (k+u)))/2)
Else
surfs(cnt,4,row) = ANINT((real(((k+u) - D) + (k+u)) - 0.1)/2)
EndIf
write(9,*) 'cnt,row vals: ',cnt,row,k+u-D,k,u,D
surfs(cnt,5,row) = k + u - D ! + D
surfs(cnt,6,row) = D ! - Ost
hh = D ! - + Ost
! Make sure the next section isn't too big to be the same unit

If ((cnt .gt. 1) .and. (hh .eq. 3*surfs(cnt-1,6,row))) then

write(*,*) 'Section is TOO tall, removing and ending'
cnt = cnt - 1
write(9,*) 'Failure Condition 0'
MoveOn = .false.
go to 800
EndIf
! Verify that midpoint has not moved beyond bounds of last point
If ((cnt .gt. 1) .and. ((surfs(cnt,4,row) .gt. surfs(cnt-1,3,row))
+.or. (surfs(cnt,4,row) .lt. surfs(cnt-1,5,row)))) then
write(*,*) 'Excess midpoint shift, removing and ending'
cnt = cnt - 1

write(9,*) 'Failure Condition 0a'
MoveOn = .false.
go to 800
EndIf

write(9,30) i,j,k+u,surfs(cnt,4,row),surfs(cnt,5,row),region,hh

If (hh .gt. 1) then
k = surfs(cnt,4,row)
cnt = cnt + 1
j = j + 1

ElseIf (hh .le. 1) then
c elseif (hh .eq. 1) then
! Is this along the top and NOT a bounding surface?
If (((k + u) .eq. nz) .and. (bnds(i,j,(k+u),1) .ne. 1)) then
If (bnds(i,j+1,nz,1) .ne. 1) then
cnt = cnt + 1
j = j + 1
k = nz
else
c write(*,*) 'Failure Condition 1'
write(9,*) 'Failure Condition 1'
MoveOn = .false.
EndIf

c write(9,*) 'At model top edge'

! Check to see if this is a bottom hugging section
ElseIf ((k + u - D) .le. 1) then ! This loop handles the bottom (#1#)
If (bnds(i,j+1,(k+u-D),1) .ne. 1) then
cnt = cnt + 1

```

```

j = j + 1
k = 1
elseif (bnds(i,j+1,(k+u-D),1) .eq. 1) then
cnt = cnt + 1
j = j + 1
surfs(cnt,1,row) = i
surfs(cnt,2,row) = j
surfs(cnt,3,row) = 1
surfs(cnt,4,row) = 1
surfs(cnt,5,row) = 1
surfs(cnt,6,row) = 0
hh = 0
write(9,30) i,j,k+u,surfs(cnt,4,row),surfs(cnt,5,row),region,hh
write(9,*) 'Failure Condition 2'
MoveOn = .false.
EndIf
else
write(*,*) 'Exception'
write(9,*) 'Failure Condition 3'
MoveOn = .false.

EndIf          ! End of model bottom loop (#1#)

else
write(9,*) 'Failure Condition 4'
MoveOn = .false.
EndIf

If (bnds(i,j,k,2) .eq. 1) then
write(9,*) 'Failure Condition 5',i,j,k

MoveOn = .false.
EndIf

800 If (j + 1 .gt. ny) then
write(9,*) 'Failure Condition 6'
cnt = cnt + 1
MoveOn = .false.
EndIf

EndDo  ! End of single loop

Do m = 1,cnt
Do n = surfs(m,5,row),surfs(m,3,row)
bnds(row,surfs(m,2,row),n,2) = 1
bnds(row,surfs(m,2,row),n,4) = region

EndDo
EndDo

region = region + 1
cnt = 1
MoveOn = .true.
If (allocated(surfs)) then
deallocate(surfs)
EndIf

```

```

EndDo
STOP

30   FORMAT(7I4)

2000  If (terminal) then
      If (allocated(surfs)) then
        deallocate(surfs)
      EndIf
      write(*,*) '** Terminating current row.'

      EndIf

      MoveOn = .true.
      Write(*,*) 'On row: ',row
      Write(9,*) 'On row: ',row
      region = 1
      EndDo ! Loops to multiple rows

! Check maximum heights

      write(*,*) 'Made it...'

      write(OUTFILE,*) 'BndTst.txt'

      open(unit=8,file=adjustl(trim(OUTFILE)),status='replace'
+ ,action='write')
      If (header) then
        write(8,*) nx,(ny-1),(nz-1)
      EndIf
      Do i = 1,nx
        Do j = 1,ny
          Do k = 1,nz
            If (bnds(i,j,k,4) .ne. 0) then
              write(8,*) i,j,k,bnds(i,j,k,4)
            endif
          EndDo
        EndDo
      EndDo
      close(8)
      write(*,*) 'Finished processing model space'
      write(*,*) 'Regions written to: ',adjustl(trim(OUTFILE))
      write(9,*) 'Finished processing model space'
      write(9,*) 'Regions written to: ',adjustl(trim(OUTFILE))

      STOP

```

! final check

```
write(*,*) '** Explicit stop statement encountered.'  
STOP
```

```
End Program
```

```
! #####  
! #####
```

```
Subroutine StartPoint(bnds,i,j,k,nx,ny,nz,row)
```

```
integer,intent(IN) :: nx,ny,nz,row
```

```
integer,intent(OUT) :: i,j,k
```

```
integer,dimension(nx,ny,nz,4) :: bnds
```

```
integer xi,yi,zi
```

```
xi = i
```

```
yi = j
```

```
zi = k
```

```
i = row
```

```
Do j = 1,ny
```

```
Do k = 1,nz
```

```
    If (bnds(i,j,k,2) .ne. 1) then
```

```
        go to 501
```

```
    EndIf
```

```
    EndDo
```

```
502 EndDo
```

```
501 xi = i; yi = j; zi = k
```

```
End Subroutine
```

Con_groups

```
program groups
use dfport
implicit none

!      3-D Grouping algorithm of the GPRegs package (3dseg and con_groups/groups)
!
!      Version 1.0
!
!      Nicholas B. Engdahl
!      Hydrogeology
!      Earth and Planetary Sciences
!      University of New Mexico
!      08-26-2008: Initial version created from groups.f
!
!      This version of the grouping algorithm forces regions with ANY conditioned
!      TPROGS data (val < 0) to be from the corresponding region. All other regions
!      are still treated randomly.
!

integer nx,ny,nz,nn,reg,i,j,k,IO,m,n,o,a,xi,yi,zi
integer mincnt,treg,p,icnt,fcon,cntr,b,SR,idim
integer cnt,row,centZ,centY,region,regs,runs,grp
integer ureg,dreg,ucnt,dcnt,TPROGS
real AR
character(len=40) :: INFILE,OUTFILE,mum,dandt
logical IsFile,match,intermit,allfull,T0,T1,T2,T3
integer,allocatable :: bnds(:, :, :),regrow(:, :)
integer(1),allocatable :: rows(:,),facies(:, :, :)
real,allocatable :: aspect(:, :, :)

c      intermit = .true.
      intermit = .false.

      mincnt = 12
      Call FDATE(dandt)
      write(9,*) 'Routine initilaized at ',adjustl(trim(dandt))
      Call Random_Seed()

c      open(unit=4,file='MtlbIN.txt',action='write',status='replace')
      open(unit=9,file='GrpDbg.txt',action='write',status='replace')
      write(INFILE,*) 'BndTst.txt'
      IO = 1
      inquire(file=INFILE,exist=IsFile)
      If (IsFile) then
      write(*,*) 'Input data file found: ',adjustl(trim(INFILE))
      write(9,*) 'Input data file: ',adjustl(trim(INFILE))
      else
      write(*,*) 'Infile not found. Check file names.'
      write(9,*) 'Infile not found. Check file names.'
      write(*,*) 'Program terminated'
      write(9,*) 'Program terminated'
```

```

STOP
EndIf
open(unit=2,file=INFILE,status='old',action='read')
read(2,*) nx,ny,nz,nn
Close(2)
write(*,*) 'Testing: ',nx,ny,nz,nn
If (nn .gt. 0) then
write(*,*) 'No header row detected. Enter dimensions of model'
write(*,*) 'in the following form: nx ny nz'
! This line is currently screwed up.....

nx = 83
ny = 267
nz = 144

allocate(bnds(nx,ny,nz,6))
allocate(aspect(nx,ny,nz))
allocate(Facies(nx,ny,nz))
open(unit=2,file=INFILE,status='old',action='read')
! This line is currently screwed up too.....
c read(2,*)
do n = 1,nx*ny*nz
c Do while (IO == 1)
read(2,*,IOSTAT=IO) i,j,k,reg
bnds(i,j,k,4) = reg
c EndDo
c If (IO .ne. 1) then
c write(*,*) 'Error condition'
c STOP
c EndIf
c EndDo
write(*,*) 'Input data read in'

else
write(*,*) 'Reading array dimensions from input data file.'
open(unit=2,file=INFILE,status='old',action='read')
read(2,*) nx,ny,nz
allocate(bnds(nx,ny,nz,6))
allocate(aspect(nx,ny,nz))
open(unit=2,file=INFILE,status='old',action='read')

do n = 1,nx*ny*nz
do while (IO == 1)
read(2,*,IOSTAT=IO) i,j,k,reg
bnds(i,j,k,4) = reg
EndDo
If (IO .ne. 1) then
write(*,*) 'Error condition'
STOP
EndIf
EndDo
write(*,*) 'Input data read in'

EndIf
! Need to compute individual AR's, and dims
row = 1

```

```

region = 1

allocate (rows(nx))
write(9,*) 'Generating region count for all rows...'
do m = 1,nx
do n = 1,ny
do o = 1,nz
If (bnds(m,n,o,4) .gt. rows(m)) then
rows(m) = bnds(m,n,o,4)
EndIf
EndDo
EndDo
EndDo
c write(*,*) rows
write(*,*) '.....'

write(9,*) "
write(9,*) 'Calling region procesing routine...'

do i = 1,nx
row = i
do regs = 1,rows(i)
region = regs
Call CentroidAR(bnds,nx,ny,nz,cnt,row,
+centZ,centY,AR,region)
c write(9,(A,5I5,F8.4)) 'Centroid parameters(Y,Z,row,cnt,AR): ',
c +centY,centZ,row,region,cnt,AR
do j = 1,ny
do k = 1,nz
If (bnds(i,j,k,4) .eq. region) then
bnds(i,j,k,1) = centY
bnds(i,j,k,2) = centZ
!!!! NEED TO CREATE A REAL NUMBER ARRAY FOR AR!!!
aspect(i,j,k) = AR
bnds(i,j,k,6) = cnt
If (i .eq. 1) then

EndIf
EndIf
EndDo
EndDo
EndDo
EndDo
c go to 300
! This section check for regions smaller than mincnt and regroupes them
! with the largest adjacent, upstream (to the left) region

do i = 1,nx
do j = 1,ny
do k = 1,nz

If (bnds(i,j,k,6) .lt. mincnt) then
region = bnds(i,j,k,4)
cnt = bnds(i,j,k,6)

```



```

do m = 1,nx
do n = 1,ny
do o = 1,nz
If ((bnds(m,n,o,4) .eq. region).and.(bnds(m,n,o+1,4) .ne. region)
+)then
ucnt = bnds(m,n,o+1,6)
ureg = bnds(m,n,o+1,4)
go to 301
else
endif
enddo
enddo
enddo

301 do m = 1,nx
do n = 1,ny
do o = 1,nz
If ((bnds(m,n,o,4) .eq. region).and.(bnds(m,n,o-1,4) .ne. region)
+)then
dcnt = bnds(m,n,o-1,6)
dreg = bnds(m,n,o-1,4)
go to 302
else
endif
enddo
enddo
enddo
go to 300
302 If (dcnt .ge. ucnt) then
treg = dreg
icnt = dcnt
else
treg = ureg
icnt = ucnt
EndIf

do m = 1,nx
do n = 1,ny
do o = 1,nz
If (bnds(m,n,o,4) .eq. treg) then
bnds(m,n,o,6) = bnds(m,n,o,6) + cnt
EndIf
If (bnds(m,n,o,4) .eq. region) then
bnds(m,n,o,4) = treg
bnds(m,n,o,6) = bnds(m,n,o,6) + icnt
EndIf
enddo
enddo
enddo

EndIf
enddo
enddo
enddo

```

```

300   write(9,*) "
      write(9,*) 'Regions processed successfully...probably...'
      write(9,*) "

! bnds(:,,:**) 1 = centY; 2 = centZ; 3 = Group; 4 = region; 5 = proc. flag; 6 = cnt

! -----
! - At this point the characteristic parameters have been computed and -
! - assigned. The next portion of the program matches based on the   -
! - following selection rules:
!     1. Centroid location with tolerances (Y,Z)
!     2. Aspect ratio of each region
!     3. Cell counts within regions
!     4. Minimum cell count for region
!
! -----

! Regions below the minimum cell count will be grouped in with the
! largest surrounding region

      write(*,*) 'Beginning 3-D grouping...'
      write(9,*) 'Beginning 3-D grouping...'

      Call FDATE(dandt)
      write(9,*) 'Processing started at ',adjustl(trim(dandt))

c     region = 1
c     row = 1
      grp = 1
      allfull = .false.
530   Do      while (allfull .ne. .true.)      ! runs = 1,22
      Call StartPoint(bnds,i,j,k,nx,ny,nz,allfull)
      write(9,'(A,I3)') 'Initial Condition check: ',bnds(i,j,k,5)
      If ((xi .eq. i) .and. (yi .eq. j) .and. (zi .eq. k)) then
c     write(*,*) 'Error, premature repeat in start: ',i,j,k
c     write(*,'(A,4I4)') 'Cent: ',bnds(i,j,k,1),bnds(i,j,k,2),
c     +bnds(i+1,j,k,1),bnds(i+1,j,k,2)
c     write(*,*) 'AR,AR + 1 = ',aspect(i,j,k),aspect(i+1,j,k)
c     write(*,*) 'Cnts = ',bnds(i,j,k,6),bnds(i+1,j,k,6),i,j,k,i+1
      write(9,*) 'Error, premature repeat in start: ',i,j,k
      write(9,'(A,4I4)') 'Cent: ',bnds(i,j,k,1),bnds(i,j,k,2),
      +bnds(i+1,j,k,1),bnds(i+1,j,k,2)
      write(9,*) 'AR,AR + 1 = ',aspect(i,j,k),aspect(i+1,j,k)
      write(9,*) 'Cnts = ',bnds(i,j,k,6),bnds(i+1,j,k,6),i,j,k,i+1
c     cntr = 0
c     do m = 1,nx
c     do n = 1,ny
c     do o = 1,nz
c     If (bnds(i,j,k,5) .ne. 1) then
c     cntr = cntr + 1
c     EndIf
c     enddo
c     enddo
c     enddo
c     write(*,*) '-- Remaining unfilled cell count: ',cntr

```

```

c      write(*,*) '-- Of total cell count: ',nx*ny*nz
c      write(*,*) bnds(i,j,1:40,5)
      go to 706
      STOP
      else
      xi = i
      yi = j
      zi = k
      EndIf
      If (allfull) then
      go to 530
      EndIf
c      If (k .lt. nz) then
c      k = k + 1
c      EndIf
c      write(*,(A,414)) 'Starting at: ',i,j,k,bnds(i,j,k,4)
c      write(9,(A,414)) 'Starting at: ',i,j,k,bnds(i,j,k,4)
c      write(9,*) 'Allocating region-row array'
      allocate(regrow(2*nx,2))
      region = bnds(i,j,k,4)
      a = 1
      centY = 0
      centZ = 0
      AR = 0
      match = .true.

525   Do While (match)
      centY = bnds(i,j,k,1)
      centZ = bnds(i,j,k,2)
      AR = aspect(i,j,k)
      cnt = bnds(i,j,k,6)
! First test is dimensional alignment, If that works, check next condition

```

```

      If (i + 1 .gt. nx) then
      T0 = .false.
      match = .false.
c      write(*,*) 'Failure condition detected (0:3): ',T1,T2,T3
c      write(9,*) 'Failure condition detected (0:3): ',T1,T2,T3

      else
      regrow(a,1) = i
      regrow(a,2) = region

      a = a + 1
      i = i + 1
      j = centY
      k = centZ
      row = row + 1
      region = bnds(i,j,k,4)
      If ((real(cnt) .lt. (1.5*real(bnds(i-1,j,k,6)))) .and.
+(real(cnt) .gt. (0.5*real(bnds(i-1,j,k,6)))) .and.
+((AR) .lt. (1.6*real(aspect(i-1,j,k)))) .and.

```

```

+((AR) .gt. (0.4*real(aspect(i-1,j,k)))) then
c   EndIf
c   write(9,*) 'Advancing to: ',i,j,k
      match = .true.
c   go to 525
c   write(9,*) 'Wow, this might work'
      else

      T0 = .false.
      match = .false.
c   write(*,*) 'Failure condition detected (0:3): ',T1,T2,T3
c   write(9,*) 'Failure condition detected (0:3): ',T1,T2,T3
c   else
c   write(*,*) 'What the hell is wrong'
      EndIf
      EndIf
c   else
c   match = .false.
c   write(9,*) 'Or then again...maybe not...2...secondary fail'
c   fcon = 2
c   EndIf
c   Else
c   match = .false.
c   write(9,*) 'Or then again...maybe not...3...primary fail'
c   fcon = 3
c   EndIf
c   else

c   EndIf
      EndDo

      a = a

!!!!!!!!!!!!!!!!!!!!!!!!!!!!!!!!!!!!!!!!!!!!!!!!!!!!!!
527   If ((Intermit)) then
c     If ((grp .eq. 1) .or. (grp .eq. 2) .or. (grp .eq. 3)) then
      write(9,*) 'Creating OUTFILE name...'
! Create filename and output grouped bounding surface points
      select case(grp)
      case(1:9)
        write(rnum,'(I1)') grp
      case(10:99)
        write(rnum,'(I2)') grp
      case(100:999)
        write(rnum,'(I3)') grp
      case(1000:)
        write(*,*) 'Max rows exceeded. Program terminated.'
        STOP
      End Select
      write(OUTfile,25) 'Region',adjustr(trim(rnum)),'.txt'
      write(*,*) OUTfile
      write(9,*) OUTfile
25   FORMAT(3A)
      Open(unit=7,file=OUTfile,status='replace',action='write')
c     EndIf
      EndIf

```

!!

```
Do m = 1,a
write(9,'(A,2I3) ') 'Region matches: ',regrow(m,1),regrow(m,2)
EndDo
write(9,*) ' --- Initialization Parameters --- '
write(9,*) 'a,regrow(1,2),grp: ',a,regrow(1,1),regrow(1,2),grp
b = 0
do n = regrow(1,1),regrow(a-1,1)
write(9,*) '*** n check ***'

b = b + 1
write(9,*) n,regrow(b,2)
reg = regrow(b,2)
c IF (regrow(n,1) .ne. 0) then
do j = 1,ny
do k = 1,nz

If (bnds(n,j,k,4) .eq. reg) then
bnds(n,j,k,5) = 1
bnds(n,j,k,3) = grp

If (intermit) then
c If ((grp .eq. 1) .or. (grp .eq. 2) .or.(grp .eq. 3)) then
If ((k .lt. nz) .and. (bnds(n,j,k+1,4) .ne. bnds(n,j,k,4))) then
write(4,*) n,j,k,grp, bnds(n,j,k,5)
write(7,*) n,j,k,grp, bnds(n,j,k,5)
c EndIf
EndIf
EndIf

EndIf
EndDo
EndDo
c EndIf
EndDo
grp = grp + 1
If (intermit) then
c If ((grp .eq. 1) .or. (grp .eq. 2) .or.(grp .eq. 3)) then
close(7)
c EndIf
EndIf

write(9,*) '*** CURRENT RUN NUMBER: ',grp
write(9,*) 'Deallocating region-row array with cnt = ',a
deallocate(regrow)
If (allfull) then
write(*,*) 'Program finished...I think'
STOP
EndIF
```

EndDo ! Master Do loop ends here

```

deallocate(aspect)

706  write(*,*) '** Calling TSIM filling routine **'

c    write(*,*) nx,ny,nz
c    STOP
c    write(*,*) 'Enter maximum region number:'
c    read(*,*) n
c    write(*,*) 'Testing max ',grp-2
c    STOP
    Do      SR = 1,(grp - 2)  !5
    write(*,*) "
    write(*,*) '--> Processing group: ',SR
    call TSIMfill(nx,ny,nz,bnds,region,grp,SR,Facies)

    EndDo

    write(*,*) 'Program finished. Outputting selected format...'

c    If
c    Open(unit=6,file='TstCk.txt',action='write',status='replace')
c
c    close(6)
c    EndIf
    TPROGS = 0  ! 0,1,2,4,5
    idim = 3
    If (TPROGS .eq. 0) then
! Chunk compatible TPROGS row order
    Open(unit=6,file='Output.asc',action='write',status='replace')
    write(6,'(3I5)') nx-1,ny-1,nz-1
    Do k = 1,nz-1
    Do j = ny-1,1,-1
    Do i = 1,nx-1
    write(6,'(I3)') facies(i,j,k)
    EndDo
    EndDo
    EndDo
    close(6)

    Open(unit=6,file='Output.bgr',action='write',status='replace',
+form='unformatted')
    write(6) 3
    write(6) (nx-1),(ny-1),(nz-1)

    write(6) (((facies(i,j,k),i=1,nx-1),j=ny-1,1,-1),k=1,nz-1)

    close(6)

    elseif (TPROGS .eq. 1) then
! MODFLOW row numbers
    Open(unit=6,file='OutputMOD.txt',action='write',status='replace')
c    write(6,*) nx-1,ny-1,nz-1
    Do k = nz-1,1,-1
    Do j = 1,ny-1
    Do i = 1,nx-1

```

```

write(6,*) facies(i,j,k)
EndDo
EndDo
EndDo
close(6)

elseif (TPROGS .eq. 2) then
! x,y,z and facies coordnates
Open(unit=6,file='OutputXYZ.txt',action='write',status='replace')
Do i = 1,nx - 1
Do j = 1,ny
Do k = 1,nz
If ((bnds(i,j,k,3) .eq. 1) .or. (bnds(i,j,k,3) .eq. 2) .or.
+(bnds(i,j,k,3) .eq. 3) .or. (bnds(i,j,k,3) .eq. 4) .or.
+(bnds(i,j,k,3) .eq. 5)) then
write(6,*) i,j,k,Facies(i,j,k)
EndIf
EndDo
EndDo
EndDo
close(6)

elseif(TPROGS .eq. 4) then
! Output MODFLOW and TPROGS files
Open(unit=6,file='Output.asc',action='write',status='replace')
write(6,*) nx-1,ny-1,nz-1
Do k = 1,nz-1
Do j = ny-1,1,-1
Do i = 1,nx-1
write(6,*) facies(i,j,k)
EndDo
EndDo
EndDo
close(6)

c
Open(unit=6,file='OutputMOD.txt',action='write',status='replace')
write(6,*) nx-1,ny-1,nz-1
Do k = nz-1,1,-1
Do j = 1,ny-1
Do i = 1,nx-1
write(6,*) facies(i,j,k)
EndDo
EndDo
EndDo
close(6)

elseif (TPROGS .eq. 5) then
! Export ALL three formats
! TPROGS
Open(unit=6,file='Output.asc',action='write',status='replace')
write(6,*) nx-1,ny-1,nz-1
Do k = 1,nz-1
Do j = ny-1,1,-1
Do i = 1,nx-1
write(6,*) facies(i,j,k)
EndDo

```

```

        EndDo
        EndDo
        close(6)
! MODFLOW row numbers
    Open(unit=16,file='OutputMOD.txt',action='write',status='replace')
c    write(16,*) nx-1,ny-1,nz-1
        Do k = nz-1,1,-1
        Do j = 1,ny-1
        Do i = 1,nx-1
        write(16,*) facies(i,j,k)
        EndDo
        EndDo
        EndDo
        close(16)
! XYZ and facies values
    Open(unit=16,file='OutputXYZ.txt',action='write',status='replace')
    Do i = 1,nx - 1
    Do j = 1,ny
    Do k = 1,nz
    If ((bnds(i,j,k,3) .eq. 1) .or. (bnds(i,j,k,3) .eq. 2) .or.
+(bnds(i,j,k,3) .eq. 3) .or. (bnds(i,j,k,3) .eq. 4) .or.
+(bnds(i,j,k,3) .eq. 5)) then
        write(6,*) i,j,k,Facies(i,j,k)
        EndIf
        EndDo
        EndDo
        EndDo
        close(16)

    else
    write(*,*) 'No valid output conditions selected.'

    EndIf
    close(6)

    close(4)
    Call FDATE(dandt)

    write(9,*) 'Routine finished at ',adjustl(trim(dandt))

    close(9)
    end program

! -----
Subroutine CentroidAR(bnds,nx,ny,nz,cnt,row,
+centZ,centY,AR,region)
! -- Computes Y and Z centroid for the current region --
integer,intent(IN) :: nx,ny,nz,row,region
integer,intent(IN),dimension(nx,ny,nz,6) :: bnds
integer,intent(OUT) :: centY,centZ,cnt
real,intent(OUT) :: AR
integer ty,tz,maxZ,maxY,minY,minZ,count,n,m
ty = 0; tz = 0; count = 0;
maxZ = 0; minZ = 0; maxY = 0; minY = 0;

do n = 1,ny

```



```

do m = 1,nz
!! Region specific If condition
  If (bnds(row,n,m,4) .eq. region) then
! Check for minimum Y and Z values
  If (minY .eq. 0) then
    minY = n
  ElseIf (n .lt. minY) then
    minY = n
  Endif
  If (minZ .eq. 0) then
    minZ = m
  ElseIf (m .lt. minZ) then
    minZ = m
  Endif
! check for maximum Y and Z values
  If (maxY .eq. 0) then
    maxY = n
  ElseIf ((n .gt. maxY) .and. (n .le. ny)) then
    maxY = n
  Endif
  If ((maxZ .eq. 0) .and. (m .le. nz)) then
    maxZ = m
  ElseIf (m .gt. maxZ) then
    maxZ = m
  Endif
! Add counts to centroid totals
  ty = ty + n
  tz = tz + m
  count = count + 1
  Endif
!! End of region specific If condition
  EndDo
  EndDo
c   write(9,*) 'checking aspect ratio parameters: '
c   write(9,*) maxZ,minZ,maxZ - minZ,minZ,maxZ - minZ
c   write(9,*) real(maxZ - minZ) / real(maxY - minY)
c   write(9,*) real(maxY - minY) / real(maxZ - minZ)
c   cnt = count
c   write(*,*) 'Count = ',count

centY = anint(real(ty) / real(count))

centZ = anint(real(tz) / real(count))
If (bnds(row,centY,centZ,4) .ne. region) then
n = 1
do while (bnds(row,centY,n,4) .ne. region)
n = n + 1
EndDo
c   If (n .eq. nz) then
c   write(*,*) 'Error in centroid (1)'
c   write(9,*) 'Centroid error 1 at:',row,centY,n
c   STOP
c   endif
m = 1
do while (bnds(row,centY,(n + m),4) .eq. region)
m = m + 1

```

```

EndDo
If (n+m .eq. nz) then
write(*,*) 'Error in centroid (2)'
write(9,*) 'Centroid error 2 at:',row,centY,n+m
STOP
endif
centZ = anint(real(n + (n+m)) / 2)
EndIf

AR = real(maxY - minY) / real(maxZ - minZ)
c AR = real(maxZ - minZ) / real(maxY - minY)

write(9,*) "
write(9,*) 'Centroid processing run for (row,region):',row,region
write(9,*) '-----'
write(9,*) ' * TOTAL CELLS IN REGION: ',count
write(9,*) 'MaxZ,AvgZ = ',MaxZ,(real(maxZ + minZ)/2)
write(9,*) 'MaxY,AvgY = ',maxY,(real(maxY + minY)/2)
write(9,*) 'Aspect ratio of unit is: ',AR
write(9,*) 'CentY,CentZ: ',centY,centZ
write(9,*) '-----'

End Subroutine

!
! -----
!
! #####
! #####

Subroutine StartPoint(bnds,i,j,k,nx,ny,nz,allfull)
integer,intent(IN) :: nx,ny,nz
integer,intent(OUT) :: i,j,k
logical,intent(OUT) :: allfull
integer,intent(IN),dimension(nx,ny,nz,6) :: bnds
integer xi,yi,zi
xi = i
yi = j
zi = k

c i = row
Do i = 1,nx
Do j = 1,ny
Do k = 1,nz

If ((bnds(i,j,k,5) .ne. 1)) then !.and.(bnds(i,j,k,4).ne.0) then
allfull = .false.
go to 501
EndIf

EndDo
EndDo
EndDo
allfull = .true.

501 xi = i; yi = j; zi = k

```

End Subroutine

```
! -----  
  
Subroutine TSIMfill(nx,ny,nz,bnds,grp,region,SR,Facies)  
integer,intent(in) :: nx,ny,nz,region,grp,SR  
integer,intent(in),dimension(nx,ny,nz,6) :: bnds  
integer(1),intent(INOUT),dimension(nx,ny,nz) :: Facies  
integer, allocatable :: ISIM(:,,:)  
character(len = 40) :: root,ext,TSIM  
integer sims,xmin,xmax,ymin,ymax,zmin,zmax,yshf,xshf,zshf  
integer TsN,reg,regs,cnt,x,y,z  
real yoff,xoff,zoff  
allocate(ISIM(nx,ny,nz))  
  
! This should correct for overcounting in the main routine  
regs = region - 2  
write(*,'(A,F6.2)') 'TSIM fill called, percent complete = ',  
+100*(real(SR)/real(regs))  
! Select number of possible realizations  
root= 'tsim_GPR'  
ext = '.asc' ! base filename extension  
Sims = 13 ! number of TSIM realizations available  
  
! -----  
! Master loop control  
! -----  
  
write(9,*) 'Calling Random TSIM.....'  
call RandN(TsN,Sims)  
write(*,*) '<< RandN selected >>',TsN  
call TSIM_num(TSIM,TsN,Sims,root,ext)  
write(9,*) 'TSIM: ',adjustl(trim(TSIM))  
write(9,*) 'Attempting to read selected TSIM.....'  
write(*,*) 'Reading TSIM'  
call ReadTSIM(TSIM,Isim,nx,ny,nz)  
write(*,*) '-- Done reading TSIM --'  
xshf = 0  
yshf = 0  
zshf = 0  
zoff = 0  
yoff = 0  
xoff = 0  
! These next lines force conditioned data to be from the same region in TPROGS  
Do i = 1,nx  
Do j = 1,ny  
Do k = 1,nz  
If ((bnds(i,j,k,3) .eq. SR) .and. (Isim(i,j,k) .lt. 0))then  
write(9,*) '-----'  
write(9,*) SR, ' Zone is conditioned by Geostats'  
write(9,*) '-----'  
go to 526  
EndIf  
EndDo
```

```

EndDo
EndDo

write(9,*) 'Selecting random numbers for internal shift...'
Call Random_Number(zoff)
Call Random_Number(xoff)
Call Random_Number(yoff)

xmin = 0
xmax = 0
ymin = 0
ymax = 0
zmin = 0
zmax = 0
cnt = 0
Do i = 1,nx
Do j = 1,ny
Do k = 1,nz
! Make sure the current location is the correct group then do stuff
  If (bnds(i,j,k,3) .eq. SR) then
! check for min/max values on all parameters
  If ((xmin .eq. 0) .and. (ymin .eq. 0)) then
    xmin = i
    xmax = i
    ymin = j
    ymax = j
    zmin = k
    zmax = k
    go to 550
  EndIf
  If (j .gt. ymax) then
    ymax = j
  EndIf
  If (j .lt. ymin) then
    ymin = j
  EndIf
  If (i .gt. xmax) then
    xmax = i
  EndIf
  If (i .lt. xmin) then
    xmin = i
  EndIf
  If (k .gt. zmax) then
    zmax = k
  EndIf
  If (k .lt. zmin) then
    zmin = k
  EndIf

! add point to region count
550   cnt = cnt + 1
      EndIf
      EndDo
      EndDo
      EndDo
! Min andMax Dimensions are now known for selected region

```

```

zshf = ANINT(0.8*(zoff*(real((nz-1) - (zmax - zmin))))))
yshf = ANINT(yoff*(real((ny-1) - (ymax - ymin))))
xshf = ANINT(xoff*(real((nx-1) - (xmax - xmin))))

If (zshf .lt. 0) then
zshf = 0
EndIf
If (yshf .lt. 0) then
yshf = 0
EndIf
If (xshf .lt. 0) then
xshf = 0
EndIf

write(*,*) 'Offset dims: ',xshf,yshf,zshf
write(9,*) 'Set Interior region shift: ',xshf,yshf,zshf
write(9,*) 'Currently processing: ',SR
write(*,(A,3I4)) ' Max: ',xmax,ymax,zmax
write(*,(A,3I4)) ' Min: ',xmin,ymin,zmin
write(*,(A,3I4)) ' Height: ',xmax-xmin,ymax-ymin,zmax-zmin
write(*,*) (xmax-xmin + xshf .lt. nx),(ymax-ymin + yshf .lt. ny)
+,(zmax-zmin + zshf .lt. nz)

write(*,*) '<< Beginning replacement >>', SR
Do i = 1,(nx - 1)
Do j = 1,(ny - 1)
Do k = 1,(nz - 1)
If (bnds(i,j,k,3) .eq. SR) then

Facies(i,j,k) = Isim(xshf+(i-xmin),yshf+(j-ymin),zshf+(k-zmin))

EndIf
EndDo
EndDo
EndDo
write(*,*) 'Processing OK'
go to 333

526 write(*,*) '<< Beginning replacement >>', SR
Do i = 1,(nx - 1)
Do j = 1,(ny - 1)
Do k = 1,(nz - 1)
If (bnds(i,j,k,3) .eq. SR) then

Facies(i,j,k) = abs(Isim(i,j,k))

EndIf
EndDo
EndDo
EndDo

```

```

333      n = SR

! -----
! -----
      End Subroutine
!
! -----
!
      Subroutine TSIM_num(TSIM,TsN,Sims,root,ext)
! Selects TSIM file to use based on TsN: Number of selected realization
! Routine verified
      character (len=40),intent(INOUT):: TSIM
      character (len=40),intent(INOUT) :: ext, root
      character (len=40) :: num
      integer,intent(INOUT) :: TsN,Sims

550      Call RandN(TsN,Sims)
      If ((TsN .ge. 1) .and. (TsN .le. Sims)) then
      Else
      GoTo 550
      EndIf

      Select Case(TsN)
      Case(1:9)
      Write(num,'(I1)') TsN
      Case(10:99)
      Write(num,'(I2)') TsN
      Case(100:999)
      Write(num,'(I3)') TsN
      Case(1000:)
      write(9,*) "
      write(9,*) 'TsN limit exceeded. Routine terminated.'
      STOP
      End Select

      write(TSIM,63) adjustl(trim(root)),adjustl(trim(ext)),
+adjustl(trim(num))

63      FORMAT(3A)
      End Subroutine
!
! -----
!
      Subroutine RandN(TsN,Sims)
! Picks a random number to use for the TSIM selection, TsN
! Routine verified
      integer, intent(INOUT) :: TsN,Sims
      real randnum,tnum

      If (Sims .gt. 1) then
      Call Random_Seed()

      Call Random_Number(randnum)

```

```

tnum = randnum * REAL(Sims)
TsN = ANINT(tnum)

ElseIf (Sims .lt. 1) then
write(9,*) 'Error, not enough available TSIMs. Check P-file'
STOP

ElseIf (Sims .eq. 1) then
TsN = 1
EndIf

End Subroutine

!
!-----
!

Subroutine ReadTSIM(TSIM,Isim,nx,ny,nz)
character (len=40), intent(IN) :: TSIM
integer,intent(IN) :: nx,ny,nz
integer,dimension(nx,ny,nz) :: Isim
integer,allocatable :: TIsim(:,,:)
integer i,j,k,val,IO,x,y,z

open(unit=10,file=TSIM,action='read',status='old')
read(10,*) x,y,z
go to 556
If ((x .lt. nx) .or. (y .lt. ny) .or. (z .lt. nz)) then
write(9,*) '*****'
write(9,*) 'TSIM dimensions too small. Resimulate and try again.'
STOP
EndIf

556 If ((nx .ne. x) .or. (ny .ne. y) .or. (nz .ne. z)) then
write(9,*) 'Type 1 TSIM read.'
write(*,*) 'Type 1 TSIM read.'
write(9,*) 'Non-fatal exception, inconsistent TSIM dimensions:'
write(9,*) 'Read: ',x,y,z
write(9,*) 'Expected: ', nx,ny,nz
write(9,*) "
allocate (TIsim(x,y,z))
do k = 1,z
do j = 1,y
do i = 1,x
read(10,*,IOSTAT=IO) val
TIsim(i,j,k) = val
enddo
enddo
enddo
do k = 1,nz
do j = 1,ny
do i = 1,nx
Isim(i,j,k) = TIsim(i,j,k)
EndDo
EndDo
EndDo

deallocate (TIsim)

```

```
else
write(9,*) 'Type 2 TSIM read.'
write(*,*) 'Type 2 TSIM read.'
do k = 1,nz
do j = 1,ny
do i = 1,nx
read(10,*,IOSTAT=IO) val
Isim(i,j,k) = val
enddo
enddo
enddo
endif
close(10)

EndSubroutine
```